TASK-DEPENDENT MODULATION OF CORTICOMUSCULAR

COHERENCE DURING DEXTEROUS MANIPULATION

by

Alexander Reyes

A Dissertation Presented to the
FACULTY OF THE USC GRADUATE SCHOOL
UNIVERSITY OF SOUTHERN CALIFORNIA
In Partial Fulfillment of the
Requirements for the Degree
DOCTOR OF PHILOSOPHY
(BIOMEDICAL ENGINEERING)

December 2015

Epigraph

"If you want to find the secrets of the universe, think in terms of energy, frequency and vibration."

- Nikola Tesla

Dedication

To my mother and father.

Acknowledgements

Over the years, there have been many individuals who have helped me pursue the goals I had set out to do many years ago. Their encouragement, guidance and friendship has allowed me to achieve my dreams and without their influence I would not have the strength to overcome the obstacles I have encountered.

First and foremost, I would like to thank Francisco for being my adviser and giving me the opportunity to work in his lab. He has always provided me with the support I needed throughout my PhD. Because of his teachings, I have become a better scientist. I have learned many things from observing his interactions with numerous individuals over the years and the knowledge and influence I have gained from Francisco will not be forgotten.

Jason. Well, Jason has been a great mentor and friend over the years. Witnessing his transition from being a post-doc in Francisco's lab to having a lab of his own provided a great deal of inspiration to me. He has helped shape me into the scientist I am today and has changed my outlook on life. He has been there to make sure that I stay on track with my PhD and has always encouraged me.

I would like to thank Dr. Gerald Loeb for his input on the direction of my PhD. He has challenged me over the years to defend my position on each and every scientific

endeavor. One of the first pieces of advice he gave to me when I started at USC was to go to the library and perform a rigorous literary search before running to the lab to conduct experiments. His advice has saved me from countless hours of unnecessary experimentation. I have the utmost respect for him.

Thanks to Dr. Charles Liu, Dr. Chrisi Heck, Rossana Arreola, and the EEG tech team at the USC Keck School of Medicine for their assistance and guidance in my research.

Over the years, Josh became one of my best friends. When I arrived at USC, he seemed to be the only person in the BME graduate school who shared my love of football. We would watch nearly every sporting event that came on tv. During those those times when there was nothing good on, we would busy ourselves with countless games of chess and weekly poker nights. I learned a lot about how to play poker with Josh, including his tells.

As senior lab members, Manish and Sudarshan helped me to transition into the lab and provided me with invaluable guidance and support. Emily Lawrence has become a very good friend of mine. Our numerous outings of oysters and wine tastings provided relaxing getaways from the stress of research. Sarine Babikian has always been there for me and I am forever grateful. I would also like to thank Akira, Victor (for going easy on me in chess), Brendan (for going easy on me in tennis), Evangelos, Heiko, and Nora. Chris Laine has been a huge help in my PhD. He has helped shape my research into what it is today. Overall, I have to thank all of my present and past lab members for tolerating the outrageous nicknames I came up with for them.

George Tsianos and Matteo have been very good friends from the beginning. Sanna Sundquist has been a dear friend to me over the years and has provided me with lots of

feedback throughout the years. I also would like to thank Dr. Khoo, Mischal Diasanta, Diana Sabogdal for their academic support.

I would like to thank my Texas friends Brian Bowden, Eric Villaseñor, Royce, Meredith, Gary, Cindy, and Brad and Mark Creel, as well as Leslie and Sandy for their endless criticism of the USC football program every year.

My sisters, Melissa and Amy, have always been there to support my efforts, and for that I am eternally grateful. I would also like to thank my nephews and nieces: Andres, Christina, Thalia, Maya, Gabriella, Isaiah, Anthony. Lastly, none of this would be possible without the endless support from my mother and father.

Table of Contents

List Of Tables

List Of Figures

Abstract

This dissertation focuses on characterizing cortical involvement during low force dexterous manipulation. Cortical oscillations in the beta frequency range (15 - 30 Hz) are synchronous with contralateral muscular activity during static precision pinch, indicative of strong cortico-muscular coupling. However, it is poorly understood how the cortex modulates the control of fingertip forces during a time-critical dexterous task. The goal of this research was to examine the functional connectivity between cortex and muscle during a force tracking precision pinch task using a rigid wooden dowel and a compliant unstable spring at two force levels. At the low force level for both objects and at the high force level with the dowel, the difficulty in maintaining a steady compression was minimal. However, at the high force level with the unstable spring, the dexterity requirements to maintain a steady force compression were significantly more challenging and required heightened sensorimotor integration. Using this novel paradigm, we showed that increases in sensory feedback and dexterity demand disrupt consistent descending commands seen in stable grasps and are reflected as a reduction in beta corticomuscular coherence. Despite the fact that the force levels were kept constant for both objects, these findings suggest that for precision force control there exist functionally different cortical circuits that are highly dependent on the temporal demands of the task.

Chapter 1

Introduction

1.1   Background

Human dexterous manipulation is characterized by the ability to precisely control the forces we exert on everyday objects with our fingers and hands. Throughout the day we interact with our surroundings in a variety of ways, ranging from large force production tasks, such as when holding a hammer to strike a nail, to fine manipulation involving low forces, such as typing, playing the piano or buttoning a shirt button. Fine manipulation involving the pads of the index finger and thumb is commonly referred to in literature as a precision pinch. Numerous studies have utilized this paradigm to assess many aspects of hand function including the examination of forces exerted on an object (Johansson & Westling 1984, McDonnell, Ridding, Flavel & Miles 2005), muscle strategies using electromyography (Maier & Hepp-Reymond 1995), the effects of transcranial stimulation (Davare, Lemon & Olivier 2008), cortical power (Murthy & Fetz 1992), and cortical synchrony with hand muscles (Baker, Olivier & Lemon 1997) to name a few. While the

literature is rich with static precision pinch analysis, this encapsulates a small fraction of daily hand-object interactions.

This dissertation focuses on characterizing dexterous function by utilizing well established electrophysiological recordings and force measurements and introducing the element of instability. The goal here was to tax the nervous system with a dexterously demanding task to differentiate between how the brain communicates with peripheral hand muscles when performing simple versus difficult manipulation tasks. Coherence analysis was used to assess these differences by identifying cortical areas with known functional projections onto spinal motor neurons controlling hand muscles and by describing the preferred frequencies of communication.

1.2   Neural Control of Movement

The sensorimotor process involved in performing a motor task is depicted as a three step process as shown in Fig. 1.1. During skilled manipulation, tactile information about the physical properties of the object in hand (e.g., shape, weight, smoothness, etc.) are relayed to the cortex. The brain incorporates this information and subsequently provides an appropriate motor command, thereby changing the state of the task. With this new state, sensory information is updated and the process continues. While this model provides a general conception of the sensorimotor process, the true mechanisms involved are far more intricate.
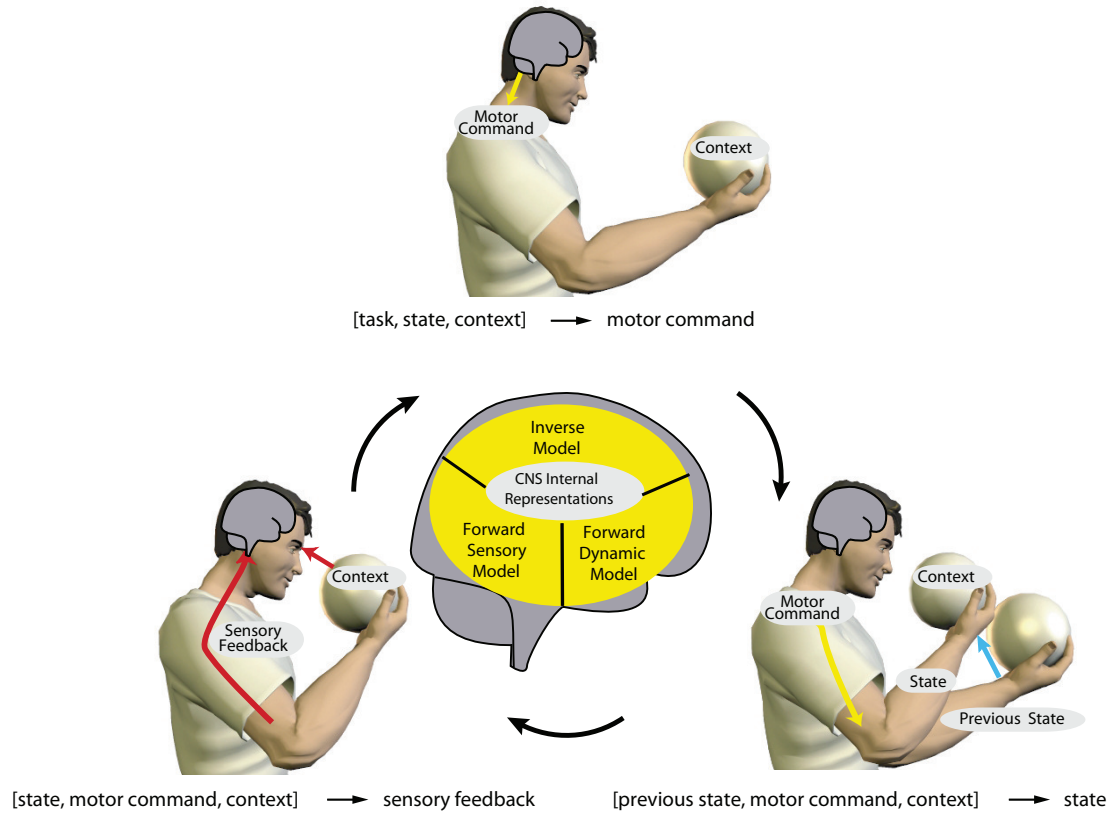
Figure 1.1: Schematic of the sensorimotor process involved in motor control. Initially, sensory information from the object being held is obtained. The demands of the task designate an appropriate motor response to the sensory cortex. Execution of the motor command causes in a change in the state of the task resulting in new sensory information and the process continues.

1.2.1 Sensory Processing

The importance of sensory feedback in manipulation cannot be overstated. This is evident in the large somatotopic representation of the hand in the sensory and motor homunculus.

Indeed, the success of *homo sapiens* is largely due to the co-evolution of cognitive development and the ability to use tools (Faisal, Stout, Apel & Bradley 2010). The abundance of mechanoreceptors in the glabrous (i.e. hairless) skin of the hand which relay critical afferent sensory information such as pressure, vibration, static touch, and proprioception (Johansson & Flanagan 2009) emphasize the importance of sensory feedback in object manipulation.

Mechanoreceptors in the fingers and hands transmit sensory information to dorsal root neurons in cervical segments C6 and C7 through $A\beta$ neurons. The diameter of these heavily myelinated group II axons range from 6 - 12 μm and permit the transmission of cutaneous information at conduction velocities of 35 - 75 meters per second (Bear, Connors, Paradiso, Bear, Connors & Neuroscience 1996), second only in speed to $A\alpha$ neurons for proprioception. Axons from the nuclei in the dorsal root ascend through the dorsal column medial lemniscus pathway, decussate in the medulla and synapse with neurons in the thalamus. These neurons then project onto cells in the primary sensory cortex (S1), secondary sensory cortex (S2) and the posterior parietal cortex.

The methods by which the sensory information is processed is dependent on the specific goals of the task. For example, a feedforward strategy is applied to reach for an object based on an internal model (Kawato 1999) and no sensory integration is necessary. However, when the task requires manipulation, a feedback control strategy must be implemented to integrate sensory information to correct for errors (Desmurget & Grafton 2000). Neurons of the primary sensory area are known to project to areas involved in voluntary movement and the planning of movement, namely the primary motor cortex (M1) and the supplementary motor area (SMA) (Martin 2003).

1.2.2 Motor Control

Cortical areas involved in the execution of motor task have been heavily studied. Gross factors influencing the contributions from specific areas include velocity, force and position (Jancke, Specht, Mirzazade, Loose, Himmelbach, Lutz & Shah 1998, Deiber, Honda, Ibaez, Sadato & Hallett 1999, Ashe 1997, Thickbroom, Phillips, Morris, Byrnes & Mastaglia 1998, Humphrey, Schmidt & Thompson 1970). In a functional magnetic resonance imaging (fMRI) study comparing cortical involvement during power grip versus precision pinch, the researchers showed greater sensorimotor activity when performing a power grip compared to a precision pinch. However the precision pinch task showed higher activation in ventral premotor, posterior parietal and prefrontal cortices (Ehrsson, Fagergren, Jonsson, Westling, Johansson & Forssberg 2000, KuhtzBuschbeck, Ehrsson & Forssberg 2001). In a separate fMRI study, it was shown that maintaining a precision pinch on a small object with just enough force to keep it from slipping activated the supplementary motor area (SMA), whereas stronger isometric forces showed no SMA activation (KuhtzBuschbeck et al. 2001, Haller, Chapuis, Gassert, Burdet & Klarhfer 2009, Galla, de Graaf, Bonnard & Pailhous 2005). Furthermore, self-paced movements of individual fingers revealed prominent blood flow into the SMA (Roland, Larsen, Lassen & Skinhoj 1980). In a positron emission tomography (PET) study, it has been shown that as the difficulty of a task is increased, activation in the premotor, SMA and caudate nucleus was increased (Winstein, Grafton & Pohl 1997). The interpretation from these studies suggests that gross movements and strong contractions can be controlled directly from the primary motor area (M1), however, low force and fine

precision pinch tasks require the additional engagement of the SMA and premotor cortex for critical control of fine manipulation and high level motor planning.

The control of hand function is mediated by direct cortical projections via the lateral corticospinal tract (CST) onto alpha motor neurons in the ventral horn of the spinal cord. The first evidence for direct corticospinal projections onto contralateral muscles was suggested by Bernhard *et al.* in 1953 who investigated skilled hand tasks performed by macaque monkeys (Bernhard, Bohm & Petersen 1953). Anatomical studies have shown that primary motor neurons terminate in the spinal cord (Kuypers 1960, Shinoda, Yokota & Futami 1981). It is now known that, in addition to M1, axons in the CST originate from the dorsal and ventral premotor cortices, SMA, and cingulate motor cortex (Dum & Strick 2005, Dum & Strick 1991). Descending commands from the cortex are highly task specific and the origin, pathway and synaptic input play a role in the execution of movement (Lemon 2008).

1.3 Previous Work

1.3.1 Electrophysiological Studies

The production of static and slow oscillatory precision pinch forces upon an object is a critical aspect of everyday grasping. Several studies have used time series analysis techniques such as spike-triggered averaging, transcranial magnetic stimulation and cross-correlation to assess the relationship between cortical activity and the electromyogram (EMG) (Lemon, Johansson & Westling 1995, Lemon & Mantel 1989, Muir & Lemon 1983). In addition to these techniques, corticomuscular coherence (CMC), has been

used to determine cortical projections from M1 onto spinal neurons (Feige, Aertsen & Kristeva-Feige 2000, Fetz & Cheney 1980, Mima & Hallett 1999, Halliday, Conway, Farmer & Rosenberg 1998). Simply stated, CMC measures the consistency of the phase lag between cortical activity (i.e. EEG) and muscular activity (i.e. EMG). The result is a coherence spectra describing the correlation between the signals for all frequencies of interest. Studies have associated coherence in distinct frequency bands with specific motor tasks. For example, CMC in the alpha frequency range (8 - 12 Hz) has been associated with brief finger movements (Feige et al. 2000, Ohara, Mima, Baba, Ikeda, Kunieda, Matsumoto, Yamamoto, Matsuhashi, Nagamine & Hirasawa 2001) and coherent sigma oscillations (12 - 15 Hz) are associated with the startle reflex (Grosse & Brown 2003).

Perhaps the most studied frequency range for coherence analysis is the beta band which extends from 15 - 30 Hz. Corticomuscular coherence studies have shown that this range is associated with static force production (Murthy & Fetz 1992, Baker et al. 1997, Baker 2007, Conway, Halliday, Farmer, Shahani, Maas, Weir & Rosenberg 1995, Kilner, Baker, Salenius, Hari & Lemon 2000, Kilner, Fisher & Lemon 2004, Kilner, Baker, Salenius, Jousmki, Hari & Lemon 1999, Kristeva, Patino & Omlor 2007). CMC has been used to determine the specific cortical areas and frequencies involved in precision pinch tasks (Kilner et al. 2000, Riddle & Baker 2006, Fisher, Galea, Brown & Lemon 2002, Chen, Entakli, Bonnard, Berton & De Graaf 2013). It has also been shown that beta CMC in the primary motor cortex is modulated by digit displacement (Riddle & Baker 2006) and object compliance (Kilner et al. 2000). Furthermore, these rhythms are absent during movement (Baker et al. 1997, Brown 2000, Kilner et al. 1999, Kilner et al. 2000, Kilner et al. 2004, Feige et al. 2000). Significant coherence in the beta frequency range during

7

sustained muscular contractions suggests that these rhythms are necessary for stability. One study has investigated beta coherence in the supplementary motor area to show that CMC was associated with precision control of fingertip forces (Chen et al. 2013).

Only a handful of groups have investigated the synchrony of gamma oscillations ($>$ 30 Hz) between the cortex and musculature. These studies have shown that gamma CMC is associated with strong muscular contractions (Mima, Simpkins, Oluwatimilehin & Hallett 1999, Brown, Salenius, Rothwell & Hari 1998, Hari & Salenius 1999). In more recent investigations, it was shown that during static force production, peak coherence appeared in the beta frequency range, however, during slow oscillatory force production, the coherence spectra shifted into the gamma range (Omlor, Patino, Hepp-Reymond & Kristeva 2007, Patino, Omlor, Chakarov, Hepp-Reymond & Kristeva 2008).

The limitations of these studies is that they focus primarily on static force production or slow finger movements. As a result, the functional role of M1 and other cortical areas remain relatively unexplored for time-sensitive dynamic manipulation. Largely due to the complex nature involved in the control of the hand, few research efforts have explored the full details of the neuromechanics involved in dynamic force production. Thus, the current body of literature lacks adequate coherence analysis where unpredictable and unstable objects are manipulated.

1.3.2 Measuring Dexterous Ability

Given the ease with which we are able to pick up an object, such as a pen and immediately begin to write, it is easy to underestimate the complex neural strategies involved in controlling the large number of degrees of freedom in the hand. Literally, there exist

an infinite number of muscle coordination patterns that can generate the same force on an object, a problem known as muscle redundancy (Bernstein 1967). The method used by the nervous system to select the appropriate pattern are currently unknown but is of significant interest. Several studies hypothesize that a strategy is selected which maximizes or minimizes a cost function. Optimization functions that have been employed include energy minimization (Alexander 1997), maximizing smoothness of movements (Flash & Hogan 1985) and minimizing torque (Uno, Kawato & Suzuki 1989). Despite the implementation of the multitude of control strategies in state-of-the-art robotic hands, even the most advanced designs pale in comparison to the dexterous capabilities of a toddler.

Multi-finger dexterous manipulation of an object involves rotation, translation, making and breaking of contact surfaces, and adjustments to fingertip endpoint force magnitude and direction (Valero-Cuevas, Smaby, Venkadesan, Peterson & Wright 2003, Westling & Johansson 1984, Loeb, Brown & Cheng 1999). This process requires continuous sensorimotor integration to update muscle coordination strategies to produce accurate hand postures and endpoint finger forces necessary to maintain control of an object. Over the years, many clinical methods have been developed to measure dexterity in humans including the Box and Blocks (Mathiowetz, Volland, Kashman & Weber 1985), 9-Hole Peg (Mathiowetz, Weber, Kashman & Volland 1985), Jebsen-Taylor (Jebsen, Taylor, Trieschmann, Trotter & Howard 1969), and Fugl-Meyer (Duncan, Propst & Nelson 1983) tests. These quantitative measures of dexterous performance suffer from a number of pitfalls: (1) they rely on repetitive tasks which are scored based on time to completion and accuracy, (2) they involve gross upper body movements, effectively taking the focus

away from individual finger movements, and (3) they do not rely on the integration of critical sensory feedback and can be performed based on visual feedback alone.

Valero-Cuevas *et al.* (2003) defines dexterity as the ability to dynamically regulate endpoint force magnitude and direction (Valero-Cuevas et al. 2003). This concrete definition led to the development of the Strength-Dexterity (SD) test (Valero-Cuevas et al. 2003). In this novel precision pinch paradigm, dexterity is measured by asking participants to compress a slender spring prone to buckling to the point of maximal stability. Subject performance is based on their ability to dynamically regulate their endpoint force direction and magnitude to stabilize the spring throughout compression (Valero-Cuevas et al. 2003). **Strength**, the force necessary to bring the spring to solid length (i.e. where all the coils of the spring are touching), and **dexterity**, the ability to dynamically regulate endpoint force direction and magnitude, are paramount to task performance. Given the dynamic nature of the SD test, continuous sensorimotor integration is required to account for variability, small perturbations and increased proprioceptive/sensory feedback from the fingertips. fMRI studies during SD spring compression have found that specific cortical and subcortical areas become active when dexterity demands of the task increase (Mosier, Lau, Wang, Venkadesan & Valero-Cuevas 2011, Holmstrom, de Manzano, Vollmer, Forsman, Valero-Cuevas, Ullen & Forssberg 2011, Talati, Valero-Cuevas & Hirsch 2005).

In precision pinch paradigms where static forces are applied to rigid objects, the predominant muscle strategy is that of co-contraction (Smith 1981). In the SD test, however, the dynamic nature of the task necessitates a more advanced control strategy. Individual control of the index finger and thumb are required to maintain a constant force on

the spring. As a result, the strategy of the muscles controlling the digits operate in a more fractionated pattern (Schieber & Santello 2004, Bennett & Lemon 1996, Kilner et al. 1999). It is known that sensory feedback in precision pinch manipulation is crucial to task performance (Johansson & Westling 1984, Johansson & Flanagan 2009, Westling & Johansson 1984, Westling & Johansson 1987) and given the dynamic nature of the SD test, the sensorimotor loop becomes highly susceptible to neural noise and transmission delays. By taxing the nervous system with a dexterously demanding task, this precision pinch paradigm makes it possible to push the limits of sensorimotor integration to determine how the nervous system controls for instability. Building upon this work and by combining high-temporal electrophysiological recordings, we employ a variation of the SD paradigm to characterize the neural control of the hand in the context of real world dynamic manipulation.

1.4 Prior Lab Work

- A multipurpose data acquisition system was developed to capture force data measured from compressible springs and transmit the information wirelessly. The device was designed with versatility in mind and was able to capture data from a multitude of both passive and active sensors (Reyes & Valero-Cuevas 2013). This device was used in a number of studies including analysis of body movement on a slack line, during running, walking and cutting, and as a rehabilitation gaming device for dexterous manipulation and motor control in children with autism spectrum disorder.

- We successfully showed that the precise location of a fine-wire recording site could be detected in a 3T scanner. Furthermore, spike-triggered averaging was used to develop transfer function models from a fine-wire EMG to surface EMG recordings.

- We recorded electrocorticographic (ECoG) data from a few patients undergoing monitoring for epileptic seizures to investigate the changes in cortical power during simple and dexterous tasks involving static and dynamic force production as well as movements.

- We have developed an experimental paradigm to investigate spatiotemporal corticomuscular relationships between rigid and compliant object manipulation with the hand. Non-invasive EEG was recorded from five healthy subjects during a visuomotor force tracking task. For all data collections, we simultaneously recorded endpoint fingertip force and surface EMG from select muscles that control the index finger and thumb. We utilized signal processing techniques such as coherence and power spectral density analysis to demonstrate that significant differences arise in the frequency domain between cortical and muscular activity during tasks of varying degrees of stability.

1.5   Significance of Research

This research can provide several significant contributions to the scientific, clinical and robotics communities. Scientifically, the ideas presented here will help formulate a new definition of dexterity which includes neurophysiological measurements. The spectral analysis in this dissertation will help further our understanding of how the brain utilizes

specific cortical oscillations to integrate sensory feedback with motor control. From this, it would be possible to determine how and when the brain becomes dissociated during complex movements and assigns the task to subcortical and/or spinal circuits. From a clinical perspective, corticomuscular coherence analysis could provide clinicians with non-invasive methods for the early detection of nerve pathologies and neuromuscular disorders affecting dexterous performance and assist in tracking rehabilitation progress. In the robotics field, this research could be used in the development of hierarchical controllers which track synchronous cortical and muscular oscillations to send commands to robotic and prosthetic limbs based on the desired intent of the user.

This dissertation provides a novel analysis of cortical drive to contralateral hand muscles during dexterous manipulation. Many hand-object interactions throughout the day involve dynamic movements and the readjustment of fingertip forces, however these complex interactions are rarely addressed in literature. The Strength-Dexterity paradigm offers a novel method of investigating cortical involvement during dynamic dexterous tasks. Unfortunately, the investigations utilizing the SD test have been performed under the temporal constraints of functional MRI. The methods presented here utilize a variation of the SD paradigm and bypass the temporal limitations of fMRI by using EEG to characterize the frequency content involved in brain-body communication. Furthermore, this research expands on the corticomuscular literature to incorporate instability and unpredictability in manipulation tasks in an effort to move away from static grasp analysis. The results presented here begin to address how the sensorimotor system utilizes time-sensitive tactile feedback in order to accurately control the muscles of the hand

during dexterous manipulation and helps to further our understanding of how cortical bandwidth is utilized in strategic motor tasks.

1.6 Dissertation Outline

1.6.1 Chapter 2

This chapter presents a custom designed low-cost wireless data acquisition system with user-configurable settings. Originally, the device was designed to capture force data during the Strength-Dexterity test, however several applications are discussed to highlight the devices' wireless capabilities as well as the versatility in acquiring data from several types of active and passive sensors. This work was presented at the 35th Annual American Society for Biomechanics Conference in 2011 and as a podium presentation at the IEEE EMBS Special Topic Conference on Point-of-Care Healthcare Technologies in 2012. Dr. Francisco J. Valero-Cuevas is a co-author.

1.6.2 Chapter 3

This chapter discusses the ability to detect a micro-hematoma formation made during fine-wire electrode placement in a structural MRI. Additionally, transfer function models were developed to relate the propagation of individual motor unit action potentials recorded with a fine-wire electrode to an array of surface electrodes. Part of this work was presented at the 6th International IEEE/EMBS Conference of Neural Engineering in 2013. Dr. Krishna Nayak, Dr. Gerald Loeb and Dr. Francisco J. Valero-Cuevas are co-authors.

1.6.3 Chapter 4

This chapter investigates differences in cortical power in epilepsy patients during tasks of varying difficulty. This pilot work was done in collaboration with the Department of Neurology at the Keck School of Medicine of USC. Part of this work was presented at the 43rd Annual Meeting of the Society for Neuroscience in 2013 and at the 7th World Congress of Biomechanics in 2014. Emily L Lawrence, Sarine Babikian, Dr. Christianne Heck, Dr. Charles Liu and Dr. Francisco J. Valero-Cuevas are co-authors.

1.6.4 Chapter 5

Chapter 5 provides a review of the functional significance of synchronous oscillations in the cortex and in the muscle. The calculation and interpretation of coherence are discussed.

1.6.5 Chapter 6

This chapter examines the effects of modulation of synchronous cortico-muscular oscillations in dexterous tasks. We explore the role of cortical areas other than the primary motor cortex during dexterous manipulation and extends the analysis of corticomuscular coherence into the gamma frequency range and the supplementary motor area. This work was done in collaboration with the Applied Mathematical Physiology Lab (AMPL). This work was done in collaboration with the Applied Mathematical Physiology Lab (AMPL). Dr. Christopher M. Laine, Dr. Jason J. Kutch and Dr. Francisco J. Valero-Cuevas are co-authors.

1.6.6   Chapter 7

Chapter 7 discusses the future direction of this research.

Chapter 2

Data Acquisition Box

Abstract

As electronic components become smaller and cheaper with each passing year, wearable technology is rapidly becoming realizable. The ability to wirelessly transmit data from wearable sensors allows for individuals to perform complex movements and tasks without being tethered to a computer or confined to an indoor laboratory setting. In this paper, we describe a novel wireless data acquisition box (DAB) capable of transmitting data from up to 16 unique sensors to a computer with built-in Bluetooth capabilities. Sample rates, signal gains and filter cutoff frequencies can be preprogrammed as per the requirements of the study. We have been able to receive stable transmissions from over 100 ft. away even as the wearer performs rapid movements. Furthermore, the device is compact enough to fit inside a pocket and has the ability to support both passive and low-power active sensors. Data has been successfully collected with this system on several occasions, a few of which are mentioned here.

2.1   Introduction

The use of wearable wireless systems are an invaluable asset in the laboratory setting as they allow for the acquisition of biological and kinematic data. However, many commercially available systems are typically expensive, require the use of a USB receiver and cannot be used in harsh outdoor environments. Furthermore, many Bluetooth systems cater to a proprietary or specific type or brand of sensor and are application specific, such as ECG monitoring (Andreasson, Ekstrom, Fard, Castao & Johnson 2002, Proulx, Clifford, Sorensen, Lee & Archibald 2006), glucose monitoring and EMG systems. Current wireless systems which allow for the acquisition from different types of sensors are often limited to passive sensors. Without a doubt, sensor versatility, long range acquisition and affordability are paramount for research purposes.

To our knowledge, there does not currently exist a commercially available device which can sample from several sensors at satisfactory sampling rates using Bluetooth technology (Cosmanescu, Miller, Magno, Ahmed & Kremenic 2006). The wireless acquisition system described here circumvents these shortcomings by giving experimentalists the freedom to collect data from active and passive sensors while also incorporating a novel encoding algorithm to maximize sampling rates. We have employed off-the-shelf electronic components to bring low-cost technology to bring versatility and affordability to the laboratory setting. In addition to its wireless capabilities and ease-of-use, the device is small enough to fit into the pocket of the user, giving participants the freedom to explore their environment while data from up to 16 sensors are telemetered to a computer. This first

implementation of the device works in tandem with a custom designed graphical user interface giving testers visual confirmation of data quality.

2.2 Methods

2.2.1 Telemetry Details

The data acquisition box (DAB), shown in Fig. 2.1, supports inputs from up to 16 types of sensors including accelerometers, load cells, temperature transducers, etc. Interfacing connectors provide +3.3 V and +5.0 V to power active sensors. Three of the DAB inputs have been configured in differential mode while the remaining 13 are single-ended. Differential inputs reject common noise with a CMRR of 105 dB before conversion to single-ended inputs. Data are then amplified, filtered and sequentially sampled at an adjustable rate. 12-bit analog-to-digital conversion is achieved with a peripheral interface controller (PIC) microcontroller (Microchip, Chandler, AZ) operating at 30 million instructions per second (MIPS). Each sample is prepended by a 4-bit address to ensure proper decoding by the receiving algorithm. The DAB employs Universal Asynchronous Receiver/Transmitter (UART) protocol to transmit data and address as two 8-bit packets. Each data packet is enclosed within a start (low) and stop (high) bit. These bits indicate to the receiver when a valid data packet is being transmitted. Data that do not contain the correct transmission sequence are discarded. The result is a dual packet serial transmission of 20 bits for single sample and is shown in Table 2.1.
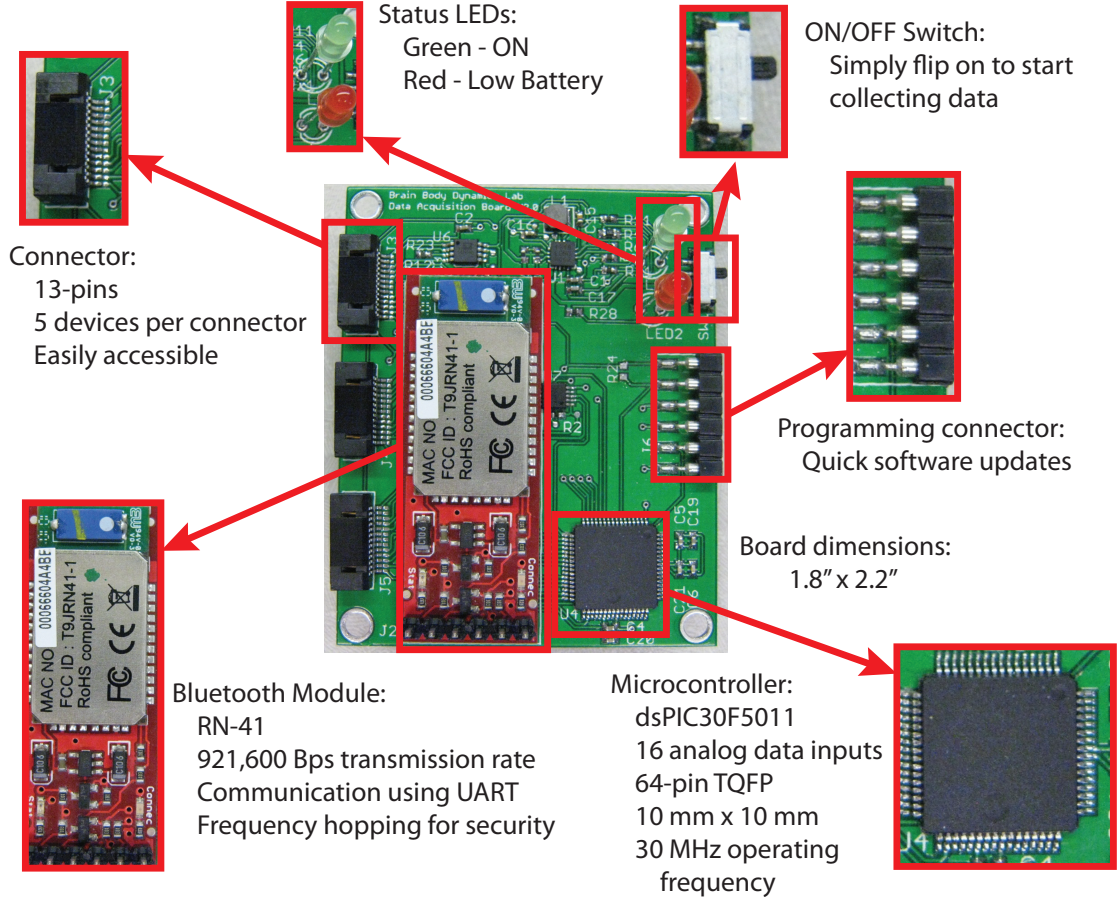
Figure 2.1: Circuit board layout for Data Acquisition Box (DAB) with individual components and description of features. The circuit board measures 1.8 x 2.2 inches.

Although the PIC microcontroller can sample data at high frequencies, the maximal sampling rate per channel is limited by the transmission rate of the Class 1 Bluetooth Module (Roving Networks, Los Gatos, CA), which can achieve stable transmission rates up to 921,600 bps. Given this, the calculated maximal sampling frequency for a channel is $Fs_{max} = 46080/N$ Hz/channel, where N is the number of channels in use. As a result, when only a single channel is in use, the maximal sampling rate is approximately 46 kHz. When all 16 channels are in use, the DAB can sample at 2.88 kHz per channel. While

these are the maximal sampling rates that can be achieved, the user is able to sample at lower sampling rates.

Byte 1									
start	d8	d9	d10	d11	a0	a1	a2	a3	stop
Byte 2									
start	d0	d1	d2	d3	d4	d5	d6	d7	stop

Table 2.1: Serial communication arrangement for transmitted data. Start and stop bits indicate to the receiver when valid data have arrived. Four address bits are used to indicate channel number and 12 data bits correspond to sensor voltage.

2.2.2 Receiving Data

Since many laptop computers and portable devices come with built-in Bluetooth connectivity, we have eliminated the need for receiving hardware (such as a receiving antenna), which may take up a USB port and require the installation of drivers. We take advantage of the widespread use, ease of connectivity and low power consumption associated with Bluetooth technology, making this the ideal choice for the DAB over other wireless standards such as WiFi and RF. Once the device has been paired with the host computer, a virtual communication port is created through which all data are transmitted and received. Using a custom Matlab GUI, users simply push a start and stop button to begin and end data collection. This feature allows users to stream data for an indefinite amount of time, limited only by disk space and battery life.

When the start button is pushed, the algorithm opens Realterm (Broadcast Equipment Ltd., Auckland, New Zealand), an open-source hyper terminal program, to establish the serial communication link. A request for data is sent from the computer to wake the device up from a power-saving sleep mode to begin transmission. After the user has

collected data for the desired time, communication terminates and the device re-enters sleep mode.

For this initial design, incoming data are not displayed in real time, but are instead written to a text file. This was done to reduce computational demands on the receiving unit and minimize potential data bus and CPU conflicts across platforms. Once transmission has completed, the program opens the text file, decodes the data using the address bits and populates the data matrix according to the appropriate channel. The time required to decode the data stream will depend on the recording length and CPU speed. All data are saved as .mat files with subject identification and trial number stored for recall when necessary in the Matlab GUI.

2.2.3 Additional Features

The printed circuit board (PCB) is contained within a custom wearable rectangular enclosure made from acrylonitrile butadiene styrene (ABS) material and manufactured using a 3-D printing machine. The entire device measures 5.08 cm × 5.84 cm × 1.27 cm and weighs less than 100 g, making it smaller and lighter than an average cell phone. It uses a standard low-profile +3.7 V Li-ion rechargeable battery with a capacity of 1000 mAh. The battery is recharged by an external wall charger and takes approximately 30 minutes to complete. Future versions of the device will incorporate a recharging circuit to eliminate the need to remove the battery. Noise and crosstalk on the PCB were minimized by optimizing component placement to create direct signal traces and by incorporating a ground plane layer. Two onboard LEDs indicate status: green when the device is on and red when the battery is low and needs to be recharged. A red LED on the Bluetooth

module lets users know that there is no communication between the device and computer. When communication is established, the red flashing LED ceases and a second greed LED turns on and remains illuminated for the duration of the data transmission. Preliminary tests show that the DAB can receive data from up to 100 ft. away and with a few hours of use every day, the device can operate for two weeks without the need to recharge the battery.

2.2.4 Sensors

Here we describe two types of sensors that have been configured for use by the data acquisition box. To measure fingertip forces exerted upon hand held objects, we used a strain gauge based single-axis load cell (Measurement Specialties, Hampton, VA) capable of measuring up to 10 lbs. of force. This sensor uses a Wheatstone bridge configuration to measure changes in resistance and produces a differential output proportional to the applied normal forces. The circular load cell measures 1.27 cm in diameter and 0.41 cm in height, requires a +5.0 V supply and draws 2.0 mA of current.

For movement analysis, we used a custom designed low-profile tri-axial accelerometer (STMicroelectronics, Geneva, Switzerland) mounted on a custom designed printed circuit board measuring 15 mm in diameter. The miniature accelerometer measures 4 mm $\times$ 4 mm $\times$ 1 mm, has a detection range of ± 2 g, sensitivity of about 1 V/g, powered by either +3.3 V or +5.0 V, and requires approximately 850 μA of current. The load cell and accelerometer in comparison to a U.S. penny are shown in Fig. 2.2.

Figure 2.2: Uni-directional load cell and ti-axial accelerometer next to a US penny for size comparison.

2.3 Results

We first tested the sensitivity and reliability of this device by mounting the tri-axial accelerometer on a sliding tray that moves along a single axis. The sensor was attached using tape and moved back and forth causing the sensor to experience acceleration in a single direction. After a few trial movements, the accelerometer was remounted so that the movement direction aligned with a different acceleration axis. This procedure was repeated for all three axes.

Fig. 2.3 shows data collected from an accelerometer mounted on a moving tray at a sample rate of 400 Hz. Initially, the direction of the movement was aligned with the x-axis of the accelerometer, then moved to align with the y-axis and finally the z-axis. The top, middle and bottom graphs correspond to accelerations along the x, y and z directions, respectively. As expected, the output of the accelerometer is sensitive only to movements along the aligned axis while the other channels produce no activity. At approximately 21 and 42 seconds, the accelerometer was repositioned, causing the sensor to experience

accelerations on all channels. The results obtained in this test illustrate that the device can accurately collect rapid dynamical data from several channels without cross talk.
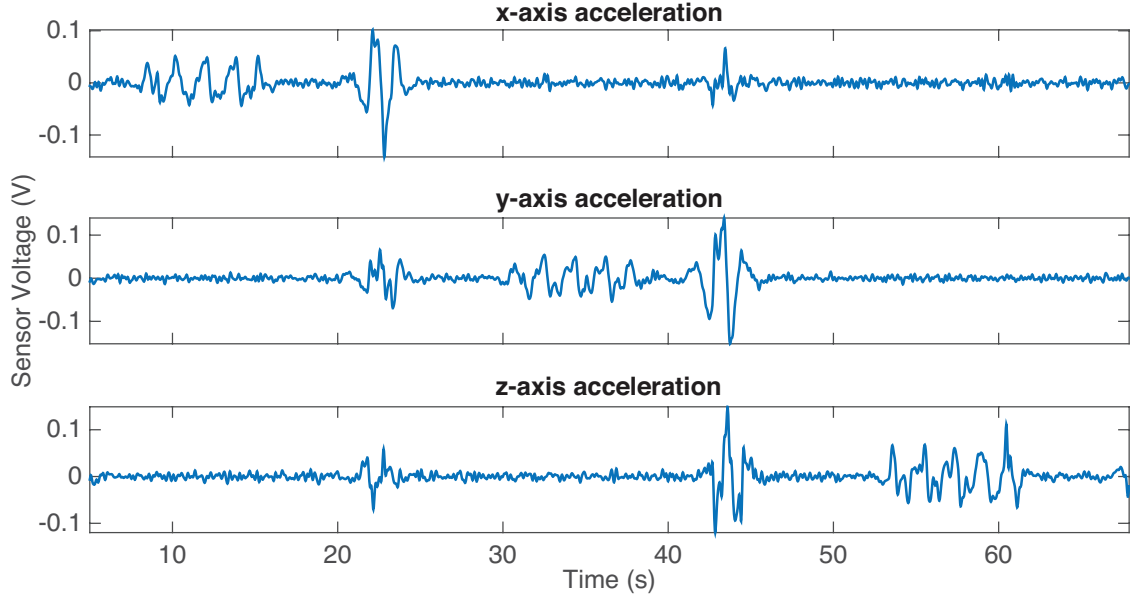
Figure 2.3: Sensitivity of accelerometer to detect accelerations in three perpendicular directions.

Next, we captured fingertip force dynamics during a sensorimotor tasks that measures strength and dexterity during manipulation of a small deformable spring (Valero-Cuevas et al. 2003). The device records from force and acceleration sensors attached to either end of a compressible spring using double-sided tape, as shown in Fig. 2.4. Subjects were asked to squeeze the spring between their thumb and index finger in an attempt to compress it fully without it buckling. Subjects were asked to curl in the remaining three fingers to avoid any contact with the spring. Once they reached a comfortable level of compression, they were asked to maintain that posture for a few seconds.
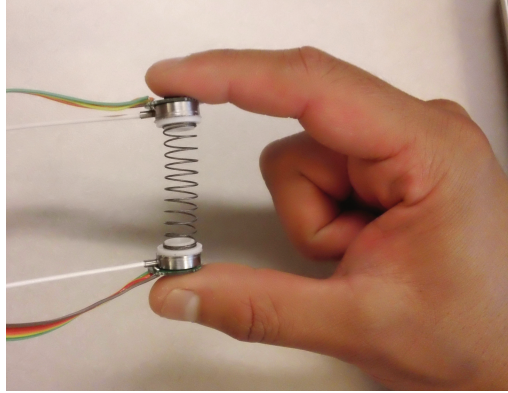
Figure 2.4: Compressible spring with load cells and accelerometers attached at either end.

Fig. 2.5 shows a sample of data collected from two load cells and two tri-axial accelerometers, a total of 8 channels, sampled at 400 Hz for 30 seconds. The top figure shows normal forces applied to a compressible spring squeezed between the thumb and index finger. Sudden drops in the sensor voltage indicate when the spring buckled and finger contact was lost. The bottom figure shows the Euclidean norm of the x, y and z accelerations from accelerometers placed on the ends of the spring. This was performed to show two representative acceleration traces rather than all six channels.
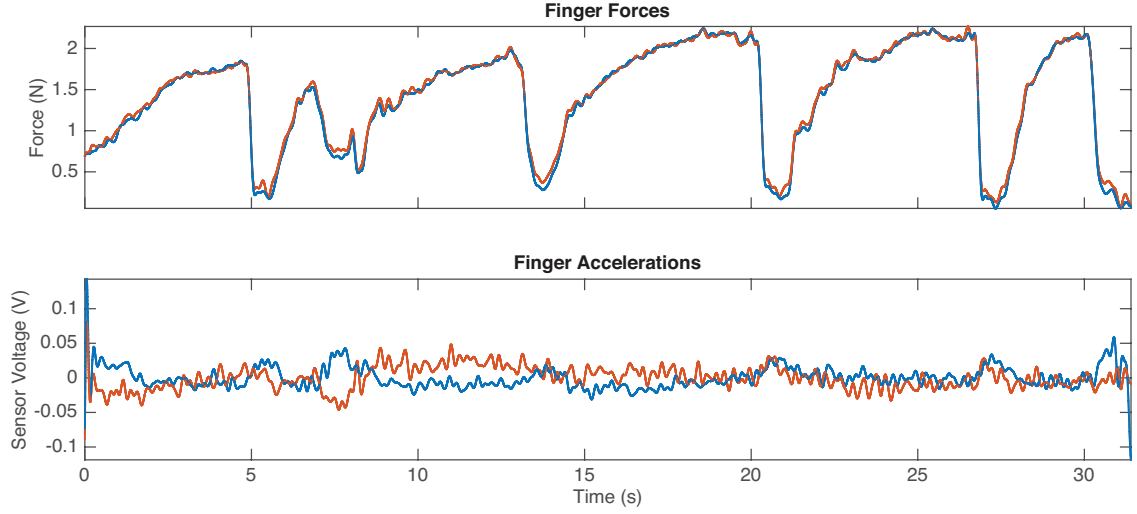
Figure 2.5: Top trace: Force profiles for index finger and thumb during spring compression. Bottom trace: Euclidean norm of index finger and thumb accelerations.

Analysis of the force data can be used to obtain the maximal compression force and the sustained compression, defined as the period in which the compression force is bounded by one standard deviation of the mean force (Dayanidhi, Hedberg, Valero-Cuevas & Forssberg 2013). Using these metrics, a dexterity score can be given to the subject based on their performance (Valero-Cuevas et al. 2003).

To showcase the wearability of the device, five tri-axial accelerometers were attached to a subject as they ran, walked, made cutting maneuvers, and jumped in an open field. Accelerometers were attached using medical tape to the knees, ankles and trunk as shown in Fig. 2.6.

Figure 2.6: Subject wearing five accelerometers attached to the thighs, trunk and ankles.

Fig. 2.7 shows ten seconds of acceleration data captured from a subject who started from rest and then began to jog. Data from 15 channels were captured at a rate of 300 Hz from the subject to show the kinematics involved during a light jog. The time series data show that each channel is independent of the others and there are no indications of erroneous decoding or lost data while collecting from multiple sensors. During our recording session, we were able to receive reliable data transmissions at distances up to 15 m, giving an active collection area of approximately 706 m^2. All data were collected using a PC running Windows 7 and Realterm 2.0.0.70.
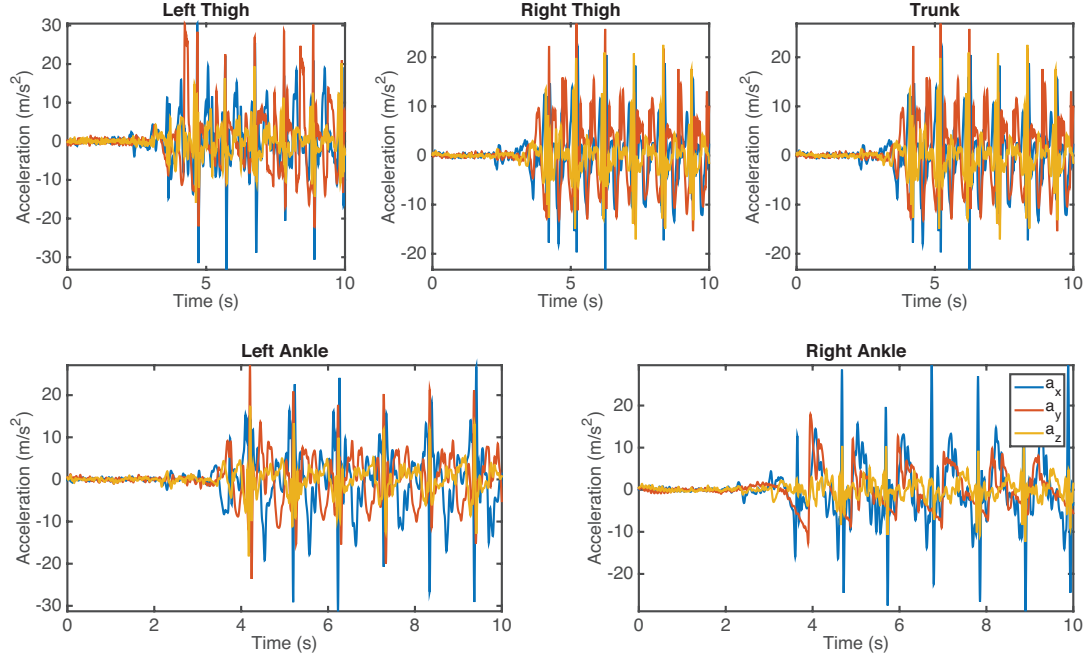
Figure 2.7: Five accelerometers attached to the thighs, trunk and ankles of a subject as they start from rest then perform a light jog.

By analyzing the sensor data during these exercise and movement tasks, it will be possible to compare kinematic data between healthy subjects and individuals at varying stages of rehabilitation from anterior cruciate ligament (ACL) injuries. Deviations from healthy kinematic data will provide physical therapists with a measurement tool to help them gauge the severity of the injury and allow them to develop customized rehabilitation programs for ACL patients.

Lastly, the device was used as a gaming controller to promote gross motor skill development in children with autism spectrum disorder (ASD). The device was attached to the trunk of the child using an adjustable belt and had an accelerometer attached which

would mimic the child's jumping actions to control an on-screen character's vertical position. The side-scrolling game consisted of a character whose goal was to avoid obstacles by jumping over them.

During the prototyping phase of the game, the acceleration captured from the DAB was integrated twice to yield position data. This was then compared to a Kinect gaming system to determine if it was possible to obtain accurate position data from our custom designed accelerometers and DAB. In this test, the subject performed gradually larger jumps within a 10 second interval. Figure 2.8 shows the vertical acceleration, velocity and position of the trunk sensor obtained through the integration of the acceleration captured by the DAB. In the last panel of the figure, the position data captured from the Kinect system is plotted to show the comparison of the true vertical position against our twice integrated acceleration. The offset in the trunk trace of the Kinect data arises from the fact that the Kinect system uses the center hip marker as the datum (i.e. at rest, the trunk marker is approximately 0.15 m above the hip).
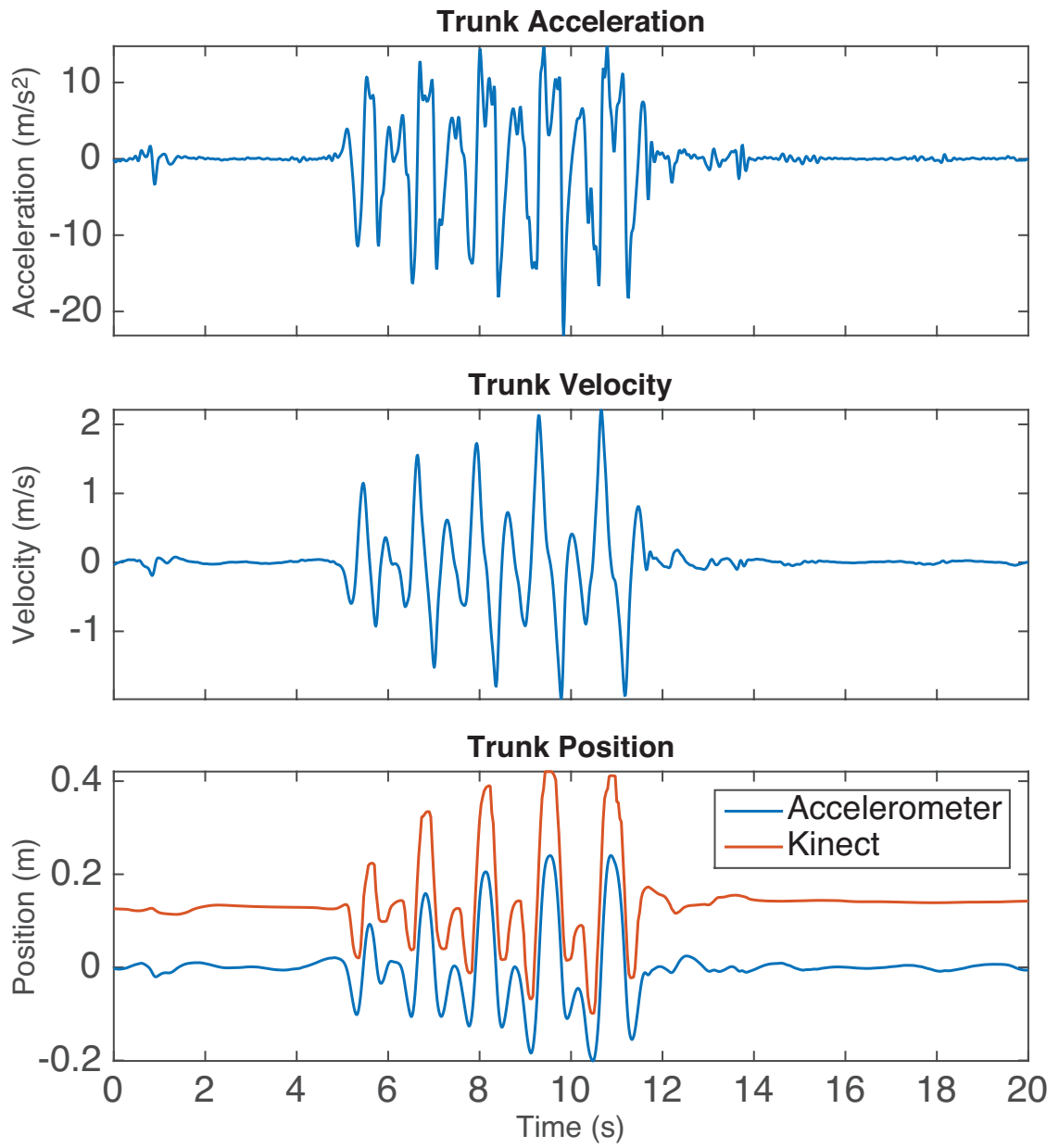
Figure 2.8: A comparison of the position data of the Kinect system to the integrated accelerometer recordings.

2.4 Discussion

The multipurpose wireless data acquisition box presented here is configurable, wearable, robust, low cost, and easy to use. The device can be tailored to collect analog data from a wide variety of active and passive sensors, giving it the potential for use in countless laboratory, clinical and industrial applications. With this device, subjects are permitted to freely move around in their environment while data is reliably transmitting and displaying data on a user-friendly GUI. Aside from being a valuable laboratory device, the system was also designed with clinical and in-home rehabilitation and monitoring applications in mind. Given the economical pricing of the wireless transmitter, we hope to distribute these devices to parents and their children in need of physical therapy for hand function and gross motor skills. Our in-home rehabilitation comes in the form of custom designed video games that use the device and attached sensors as the controlling input. We believe this approach will serve as a fun and effective motivational tool for children to engage in daily rehabilitation. Currently, the system is undergoing several updates to the hardware, GUI and firmware to make the device integratabtle, user-friendly and fully configurable. The device, PCB and enclosure will be upgraded by adding strain relief to the connectors and will incorporate a rechargeable battery circuit. Additionally, the device will undergo a complete redesign of the enclosure to make it more robust and stylish. Firmware will be updated to reduce power consumption for the PIC to give the device a longer battery life. Lastly, the GUI software will be updated to present the data in real time and we will work towards making the device compatible with cell phones, tablets and other Bluetooth enabled devices.

Acknowledgments

Chapter 3

Localization of a Fine-wire Recording Site and its Propagation Characteristics

Abstract

The ability to extract information about muscle activation and control at the scale of individual motor units from surface EMG depends critically on the spatial distribution of the electrodes with respect to the source within the muscle. Despite this importance, few studies have used the precise location of an intramuscular recording site to relate frequency characteristics, such as filtering effects, to those of non-invasive surface recordings. In this study, we recorded from a single fine-wire EMG electrode inserted into the *extensor carpi radialis brevis* (ECRB) of the right forearm arm of a single volunteer along with seven surface electrodes placed equidistantly around the proximal forearm in the same transverse plane as the fine-wire electrode. Following a series of hand and finger manipulation tasks, the fine-wire electrode was removed and each surface electrode was replaced with a fiducial marker. We then acquired structural images of the forearm of the subject with a 3T scanner. The objectives of this study were two-fold: (1) show that,

with a structural MRI, it is possible to locate the exact fine-wire recording site based on the presence of a micro-hematoma formed during needle insertion and (2) characterize transfer function characteristics from fine-wire to surface electrodes using spike-triggered averaging (STA) of individual motor unit action potentials (MUAPs). Our findings indicate hematoma formations showing the path of the needle as it moved deeper and proximally into the muscle of interest. Secondly, we developed input-to-output characteristics and extracted hints of MUAPs buried in the noise floor which would otherwise be overlooked. These results pave the way for the optimization of system identification models, validation of volume conduction models and may lead to methods of solving the inverse problem of source localization.

3.1 Introduction

Intramuscular recordings have long served as the gold standard for obtaining muscular activity from individual motor units (MUs). Fine-wire and needle electrodes have been used in numerous human and animals studies for use in understanding biokinesiology during movement and force production (Cianchetti & Valero-Cuevas 2010, Burgar, Valero-Cuevas & Hentz 1997), assisting in the clinical diagnosis of neuromuscular diseases (Oaube 1991), and the assessment of motor unit conduction velocities (Farina, Arendt-Nielsen, Merletti & Graven-Nielsen 2002) to name a few.

Despite the numerous advantages of intramuscular recordings, many pitfalls exist. Fine-wire recordings are obtained using a hypodermic needle that pierces the skin to insert either one or two thin-gauged stripped wires in the muscle of interest. Once placement

has been carefully validated through either stimulation or visual inspection of the EMG signal, the hypodermic needle is removed leaving the wires embedded within the muscle. Placement of needle electrodes is a similar procedure, however the needle remains within the muscle throughout the duration of the study. Certification is required for insertion of intramuscular electrodes in human subjects. Potential complications associated with intramuscular EMG recordings include muscle spasms, numbness, soreness and may cause the subject to feel faint (Jonsson, Omfeldt & Rundgren 1967).

Surface EMG (sEMG) offers a non-invasive alternative to intramuscular recordings at the cost of limited bandwidth. Bandwidth for sEMG ranges up to approximately 600 Hz whereas invasive techniques range up to 1.0 kHz (Rash & Quesada 2003). Studies have investigated the relationship between sEMG to those of fine wire (Rajaratnam 2014, Semciw, Neate & Pizzari 2014), however the experimentalist is never precisely sure of the exact location of the intramuscular electrode recording site nor the spatial relationship between the target muscle and the surface electrode(s).

An action potential in a motor neuron depolarizes the sarcolemma in all the muscle fibers that it innervates. The action potential enters the innervation zone and travels along the muscle in both direction. The interference pattern of the depolarized muscle cells make up the electromyogram. Many factors influence the quality of the surface EMG, including electrode design, contact impedance and electrode placement (Fuglevand, Winter, Patla & Stashuk 1992). However, even under ideal conditions, one is still faced with the problem of degraded signal-to-noise ratio caused by the spatial low-pass filtering effects of tissues and signal attenuation from muscle to electrode. Understanding the spatio-temporal spectral relationship that exists between intramuscular and surface electrode

recordings would serve as an invaluable tool for describing muscle activation within a volume conductor. To date, signal propagation has often been described with computational models using symmetrical configurations and estimating electromagnetic propagation parameters (Plonsey 1974, Farina, Mesin, Martina & Merletti 2004, Farina 2001, Lowery, Stoykov, Taflove & Kuiken 2002, Gootzen, Stegeman & Van Oosterom 1991, Roeleveld, Blok, Stegeman & Van Oosterom 1997). By knowing the exact location of an intramuscular fine-wire recording site within the muscles of the forearm, we can maximize the information obtained from spatially known surface EMG recordings (Farina 2001).

To our knowledge, there have been no reports which accurately localize an intramuscular recording site within a muscle belly in relation to sEMG sites. We present here, for the first time, the detection of a fine-wire recording site from a structural MRI from the formation of a hematoma created during needle insertion. Secondly, we relate both spatial distances and signal propagation characteristics from the intramuscular recording site to generate accurate transfer functions. These results will be used to fully characterize the electrical parameters of biological tissues to experimentally validate volume conduction models.

3.2 Methods

3.2.1 Ethics

We collected data from a right-handed consenting volunteer (male, 28 years old). The participant had no known history of neurological conditions and had no history of hand

surgery. All aspects of this study were approved by the Institutional Review Board (IRB) at the University of Southern California.

3.2.2 Recordings

A pair of fine-wire electrodes and seven bipolar surface electrodes were used to record EMG from the right forearm of a single consenting volunteer (male, 28 years old) who performed isometric and dynamic force generation manipulation tasks with the hand, wrist and fingers. The seven bipolar surface EMG electrodes (Delsys, Boston, MA) were placed circumferentially around the proximal third at the widest part of the right forearm. The electrodes were arranged equidistantly with no particular objective muscle in mind. Each electrode was labelled with a number from one to seven for reference. A large ground electrode was placed on the right olecranon. The fine-wire electrode was inserted using a 26-gauge needle into the belly of the *extensor carpi radialis brevis* (ECRB) muscle between surface electrodes 3 and 4 at an angle of approximately 25° relative to the surface of the arm. The target muscle was confirmed using structural landmarks, muscle palpation and visual inspection of EMG response. Figure 3.1 shows the placement of the surface electrodes and Fig. 3.1a shows the insertion point for the hypodermic needle used to place the fine-wire electrodes. All EMG recordings were captured at a sample rate of 4 kHz.
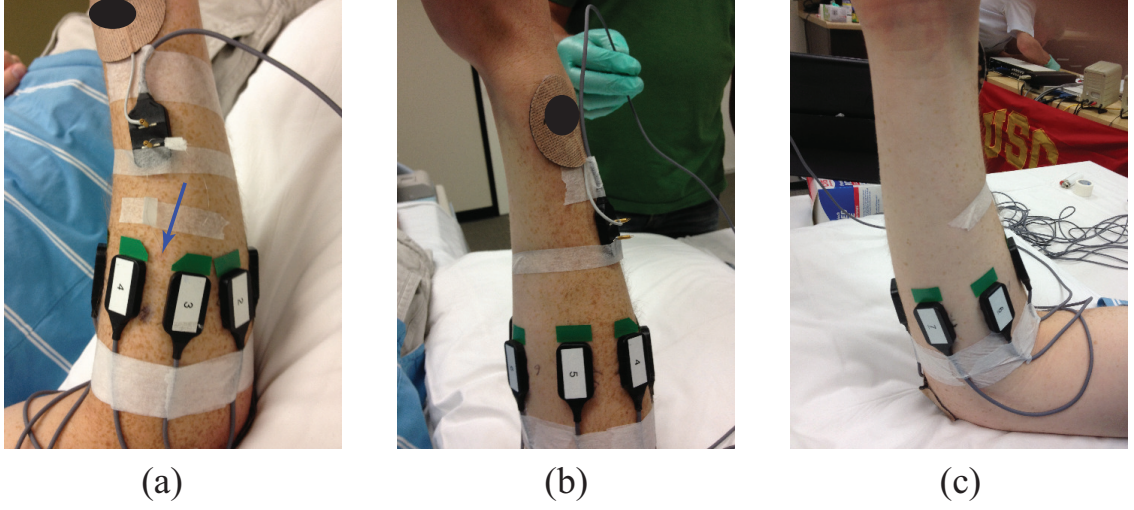
Figure 3.1: Placement of EMG electrodes around forearm. (a) Point of insertion for fine-wire electrode. Surface electrodes 2 - 4 can be seen on the posterior-lateral forearm. (b) Surface electrodes 4 - 6 on the anterior-lateral forearm. (c) Surface electrodes 6 and 7 on the anterior forearm.

3.2.3 Spike-Triggered Averaging

Motor unit action potentials represent the basic driving force for producing full scale muscular contractions. Fine-wire recordings often record from either one or a few individual units. Here, we investigated synchronous time-locked surface EMG activity centered on the peak of each fine-wire MUAP using spike-triggered averaging (STA) (Murthy & Fetz 1996b). In general, the STA can be written as

$$STA\left(\tau\right) = \frac{1}{N}\sum_{i=1}^{N}x\left(t_i - \tau\right) \qquad (3.1)$$

where N is the total number of spikes to average, t_i is the temporal location of event i for signal $x(t)$ and τ is the window size for the average. STA was calculated using the peak height of a detected MUAP over a 30 ms window (5 ms before and 25 ms after peak). EMG data were notch filtered at 60 Hz and high pass filtered from from 2 Hz to remove any slow trends in the data.

To describe the characteristic of signal propagation in biological tissue, a transfer function model was estimated using a 50th order fast transversal least means square (LMS) adaptive filter (Slock & Kailath 1991). For a sample frequency of 4 kHz, a fifty-tap FIR filter will include latencies up to 12.5 ms, allowing deep MUAPs to propagate to surface electrodes.

3.2.4 Imaging of a Hematoma

To determine if it would be possible to image the exact location of the fine-wire recording site, we had made preparations to capture structural MR images immediately following the manipulation portion of the study. Within 30 minutes, the fine-wire electrodes were removed and each surface electrode was replaced by an MR compatible fiducial marker (i.e. vitamin E tablet). We obtained structural MR images of the subject's forearm in a clinical 3T scanner (GE Healthcare, Waukesha, WI) with the arm fully pronated to maintain the same posture and muscle-electrode relationship as during the experiment. The scanner was configured to acquire fast HD 3D spoiled gradient recalled (SPGR) with 1.5 mm slices.

3.3 Results

3.3.1 MR Images

Figure 3.2 shows the progression of the hematoma formation through the muscular tissue as shown by the blue arrows. As the hypodermic needle pierced the skin during fine-wire electrode insertion, small hematoma formations appear along the path. In the scanner, these small blood formations are revealed as dark spots in the MR scan. The left panel shows the hematoma view from the coronal plane moving in the dorsal to volar direction. The right panel shows the progression of the hematoma as viewed in the transverse plane moving deeper into the forearm. Bright dots around the forearm correspond to the fiducial markers representing the locations of the surface electrodes.
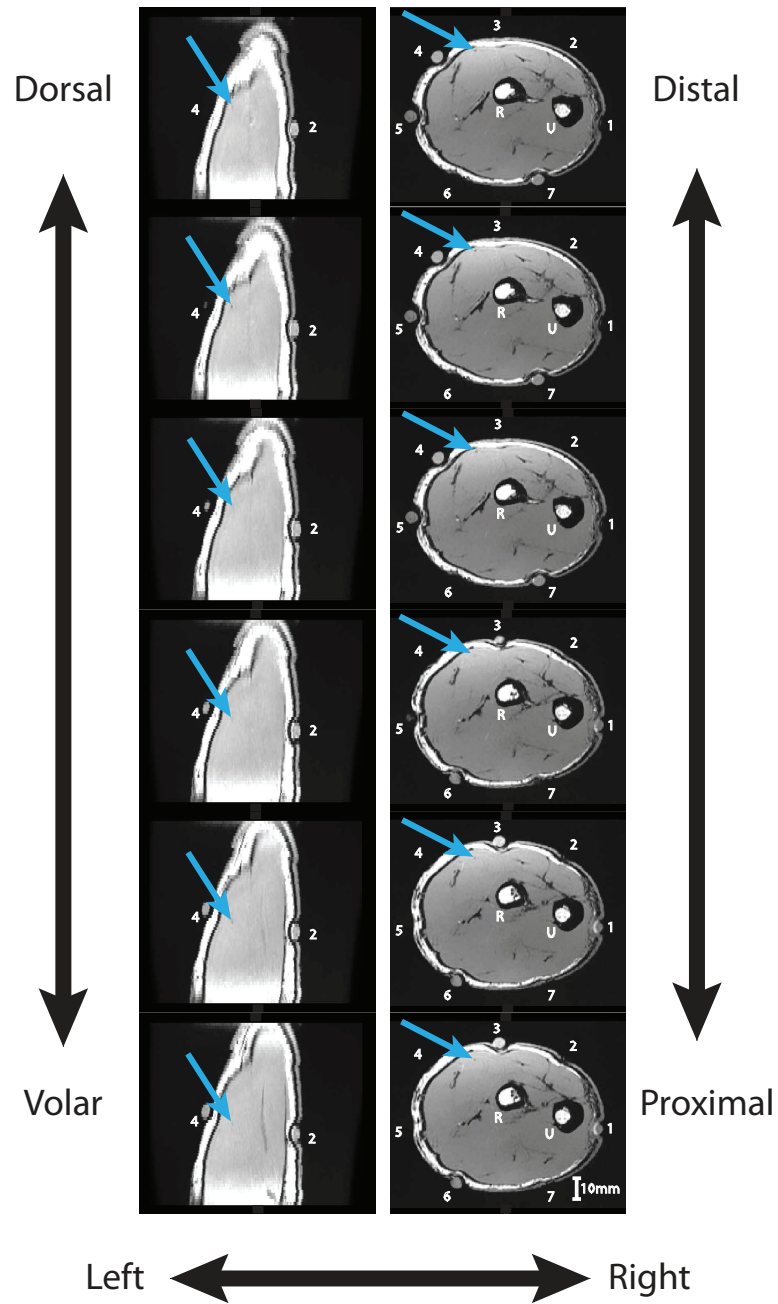
Figure 3.2: Path of hypodermic ned used to insert fine-wire electrodes. The left panel shows the path from the perspective of the sagittal plane. The right panel tracks the path from the transverse plane.

Figure 3.3 shows the sagittal, coronal, and transverse planes that best represent the final detectable location of the micro-hematoma. From the series of images, it was determined that the needle reached a depth of approximately 8 mm into the tissue. These measurements were consistent with measured depth of the needle and video taken during the electrode placement. Cross-validation with anatomical landmarks and similar scans containing clearly labeled muscle groups further confirmed that the micro-hematoma was in the ECRB muscle.
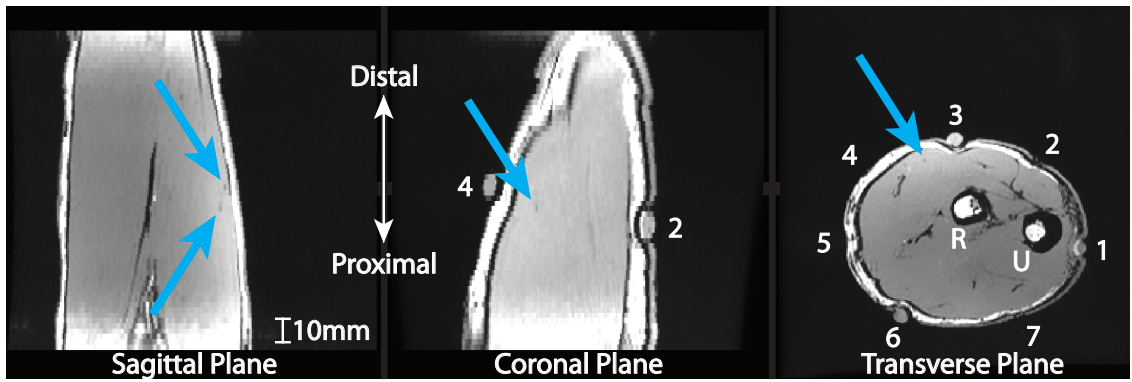
Figure 3.3: Insertion point for fine-wire electrode. Structural MR images of forearm indicating a hematoma representing the location of a fine-wire electrode within the *extensor carpi radialis brevis* muscle.

3.3.2   STA

Following strong muscular contractions during the dexterous tasks, a motor unit action potential (MUAP) train appeared in the intramuscular recording, however there was no visible movement in the hand or wrist. Figure 3.4 shows the spike-triggered average of 840 MUAP events triggered on the peak of the waveform from the fine-wire recording.

Nine separate MUAP bursts appeared throughout the data and consisted of a smaller MUAP with a peak of 0.12 V and a larger MUAP with a peak voltage of 0.4V. The peak detection algorithm to capture the spike times was adjusted to capture both sets of MUAPs.

STA of MUAP

N = 840
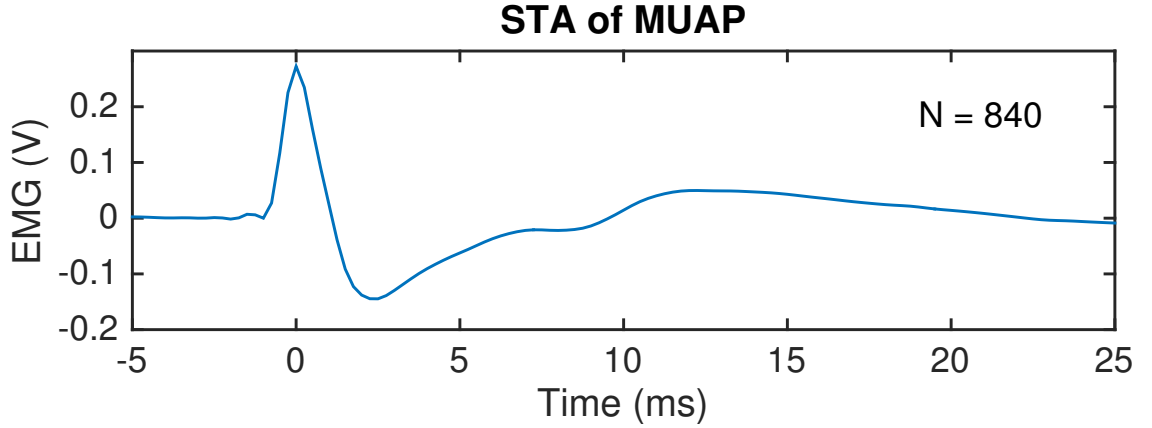
Figure 3.4: Spike-triggered average of 840 individual motor unit action potentials in a fine-wire recording.

Figure 3.5 shows an example transfer function calculated using the LMS method from the fine-wire recording to surface electrode 3 and is represented as the blue discretized trace. Here, the coefficients were normalized to have a maximum value of 1 and the entire trace was inverted from its true transfer function. Inversion of the trace does not affect the cutoff frequency, it merely changes the sign of the resulting waveform. The orange trace in Fig. 3.5 is a 50th-order *sinc* function centered at 25. Convolving a *sinc* function with a time domain signal, $x(t)$, effectively low-pass (LP) filters the signal. For an infinitely long *sinc* function, the frequency domain transform yields a rectangular waveform (i.e. an ideal low-pass filter) as shown in the following Fourier transform pair

$$rect\left(\frac{t}{\tau}\right) \quad \longleftrightarrow \quad \tau sinc\left(\frac{\omega\tau}{2\pi}\right) \tag{3.2}$$

where τ is the width of the rectangle function, and $2\pi/\tau$ is the cutoff frequency. The similarity in shape of these signals demonstrates that the transfer function for this input-to-output relationship assumes the general form of a LP filter.
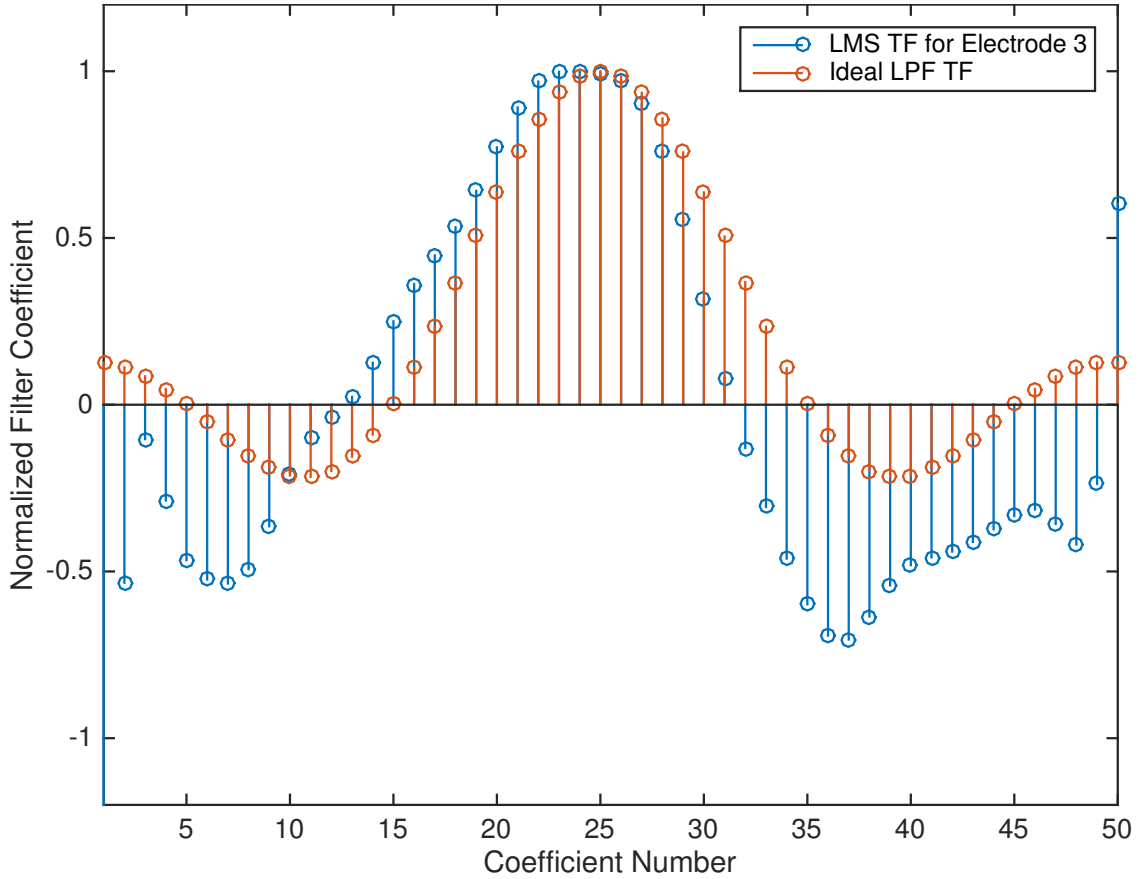
Figure 3.5: Comparison between the calculated transfer function coefficients from fine-wire to electrode 3 (blue trace) and an ideal low-pass filter (orange trace).

Table 3.1 describes the relative locations of the surface and fine-wire electrodes according to the scanner coordinate system. The last column of Table 3.1 indicates the muscle(s) directly under the surface electrodes as determined using anatomical landmarks. Electrodes 1 through 7 are the surface electrodes labelled in 3.1 and electrode 8 is the fine-wire recording. The proximity of the fine-wire recording sight to surface electrode 3 and the fact that the surface electrode was at least in part recording from the ECRB helps to explain the relative cleanliness of the transfer function estimation.

Electrode	Coordinates (mm)			Muscle
	x	y	z	
1	-87.36	-41.92	43.21	*flexor digitorum profundus* (FDP)
2	-78.58	-7.76	25.14	*extensor digiti minimi* (EDM) and *extensor carpi ulnaris* (ECU)
3	-54.25	-0.30	6.91	*extensor carpi radialis brevis* (ECRB) and *extensor digitorum* (ED)
4	-24.57	-10.03	-2.74	*brachioradialis* (BR)
5	-17.48	-38.62	-14.09	*brachioradialis* (BR)
6	-37.59	-67.35	-4.74	*palmaris longus* (PL) and *flexor carpi radialis* (FCR)
7	-66.75	-68.45	28.29	*flexor carpi radialis* (FCR)
8	-44.33	-8.95	1.04	*extensor carpi radialis brevis* (ECRB)

Table 3.1: Coordinates of each recording electrode with respect to MRI coordinate system.

Electrode	Distance from fine-wire electrode (mm)
1	68.68
2	41.91
3	14.41
4	20.15
5	42.78
6	59.04
7	69.18

Table 3.2: Distance from fine-wire electrode to each surface electrode in millimeters.

Figure 3.6 shows the computed STAs shown as white traces for each surface (Electrodes 1 - 7) and the fine-wire (Electrode 8) channels overlaid on the transverse view of the right forearm.

The yellow traces in each surface electrode subfigure are the result of convolving the fine-wire STA of the 50 LMS adaptive filter coefficients calculated from each input-to-output relationship. Each subplot is arranged to appear next to its respective electrode around the arm, indicated by the numbered red dots. The red 'x' labeled as number 8 indicates the location of the fine-wire recording and its trace is shown at the bottom of the figure.
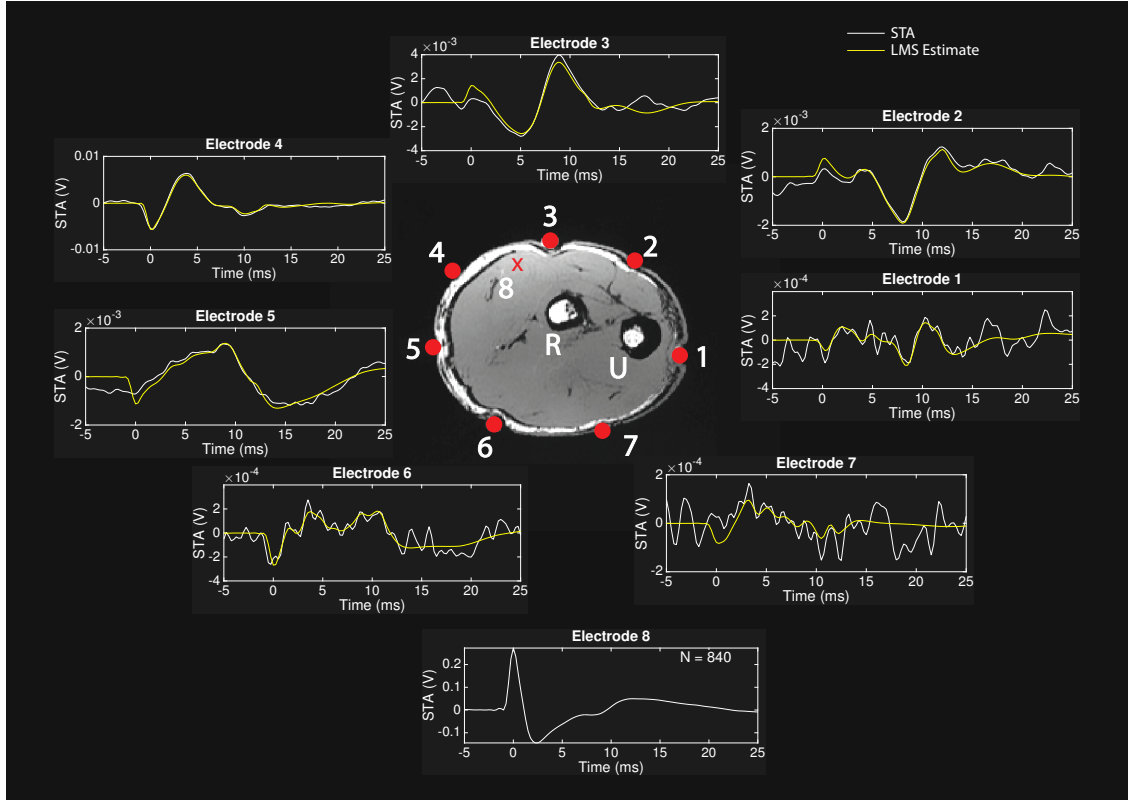
Figure 3.6: Spike-triggered average of fine wire and surface electrodes with approximate location. Peak of fine wire MUAP used as trigger. White traces indicate STA. Yellow traces are estimates of STA. Electrode 8 is the STA of the fine-wire channel.

3.4   Discussion

In this, the first study of its kind, we combined magnetic resonance imaging with precision electrophysiological recordings to detect the precise location of an invasive EMG electrode and map its spatial relationship within the muscle. We then continued to investigate signal transformations that occur when MUAPs propagate through biological tissue to surface electrodes. While invasive electromyography will likely remain the sole method

of recording high quality MUAPs, these results make it possible to begin to tease apart electrical parameters of skin, fat, muscle and bone.

The location of the recording electrode relative to the source of the fine-wire recording site is separated by a so-called volume conductor made up of biological tissues. It is well known that these tissues act as a spatial low-pass filter to both attenuate and spread the frequency of the signal (Day 1997). The extent of the filtering effects are dependent on the electrical properties of the medium (i.e conductivity and prematurity), distance from source to recording site, muscle fiber size, etc. (Roth, Gielen & Wikswo 1988, Blok, Stegeman & van Oosterom 2002, Farina et al. 2004).

In an anisotropic and inhomogeneous medium, such as skeletal muscle, factors such as fiber direction, appellation angle and frequency dispersion play an important role in how signals are conducted (Lowery, Stoykov, Dewald & Kuiken 2004, Roth et al. 1988, Roeleveld et al. 1997). In our analysis, system identification was best estimated for Electrodes 2-5 in Fig. 3.6. The waveforms for these electrodes were preserved in these channels due to their relative proximity to the fine-wire recording site. Peak latencies in these channels were consistent with values obtained from conduction velocity studies (Farina et al. 2002).

Low-pass filtering effects of the tissues becomes evident as the width of the action potential gradually widens at surface electrodes farther away, with the most prominent effect seen at electrode 5. The magnitude of the STAs for electrodes 2 - 5 are buried deep within the noise floor and are not detectable in the raw traces. In Electrodes 1, 6 and 7, the surface electrodes appear to be too far from the fine-wire site, resulting in poor estimates of the STAs for those channels. However, by the number of events used in the

STA will improve both the SNR and temporal resolution (Farina et al. 2002). In this study, we averaged 840 action potentials to generate the averages, but with thousands of events, it could be possible to expose faint underlying signals in distant electrodes.

With the addition of high-resolution MR images, piecewise linear models incorporating boundary conditions between two media can be developed to increase the accuracy of the invasive recording site as well as the spatial distribution of tissues and surface recording sites. Higher density surface EMG arrays would only further enhance the ability to quantify electrical parameters such as conductivity and permittivity for each tissue (i.e muscle, bone, skin, and fat). Signal processing techniques such as system identification, independent components analysis and equalization techniques can be used to recover an accurate representation of a single MUAP from a weighted combination of surface electrode recordings as depicted in Fig. 3.7. Invasive recordings, $X(s)$, pass through system identified FIR filters, $H(s)$, to an array of surface recordings, represented as $Y(s)$. From the forward transfer models, an inverse model, $H(s)$, is attainable. Statistical processing techniques such as independent components analysis, blind deconvolution and Bayesian inference can be integrated to undo the filtering effects and triangulate a muscles and obtain its activation level.
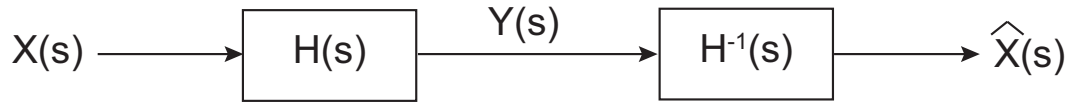
Figure 3.7: System identification and equalization for use in source localization.

The ability to locate the source of ground-truth MUAPs within a muscle along with transfer function fitting enables the optimization of system identification, validation of

volume conduction models and provides information regarding electrical properties of biological tissue. Analysis of this data may lead to methods of source localization and the decomposition of individual muscle activation levels during low isometric force production, slow finger movements, and motion-to-force transitions leading to improvements in the dexterous capabilities of robotic and prosthetic hands.

Acknowledgments

Chapter 4

Power Spectral Density Analysis in Phase II Epilepsy Patients with Implanted Subdural Electrodes

Abstract

The ability of the human hand to precisely control the direction and magnitude of fingertip endpoint force during a dynamic manipulation task serves as indication of dexterous ability. However, the classification of cortical rhythms into its constituent frequency bands as they relate to dexterity demand has been relatively unexplored. In this study, cortical activity was recorded from a grid of subdural electrocorticographic (ECoG) electrodes implanted in two patients undergoing monitoring for intractable epileptic seizures prior to epilepsy surgery. Subject 1 performed a series of three tasks with each successive task increasing in dexterity demand. They first held a rigid object at three points of contact using their thumb, index and middle fingers with just enough force to prevent the object from slipping. Secondly, the object was rotated back and forth in a twisting motion as if tightening and loosening a bottle cap at a frequency of approximately 1 Hz. Lastly, they performed the Strength-Dexterity (SD) test, a measurement of dexterity involving the

compression of an unstable spring between the index finger and thumb. Subject 2 also performed the SD test, but not the other two tests. Power spectral density (PSD) was calculated when the subjects were fully engaged in the task to eliminate any extraneous effects. PSD was referenced to a quiescent period when the subjects were relaxed with no movements or distractions. Preliminary results reveal task-dependent spectral shifts in the motor and sensory cortices based on task difficulty. A firm understanding of the changes that occur in these cortical rhythms may pave the way to understanding how the brain controls for dynamic force production and instability.

4.1   Introduction

Surgical implantation of subdural electrodes is the primary method of successfully local-izing and excising epileptogenic zones (Wyler, Ojemann, Lettich & Ward Jr 1984, Stefan, Quesney, AbouKhalil & Olivier 1991, Weinand, Wyler, Richey, Phillips & Somes 1992). In some cases, large subdural electrode arrays placed over the temporal lobe, a common location of seizure foci, overlap with the hand areas of the primary motor cortex per-mitting the analysis of cortical rhythms involved in manipulation. Functional MRI has been used to investigate dexterous manipulation (Mosier et al. 2011), however due to its poor temporal resolution, the characterization of frequency activity during these complex sensorimotor tasks remains largely unexplored. It is known that cortical oscillations in specific frequency bands are present in motor tasks (Murthy & Fetz 1992). The phys-iological relevant cortical oscillations are often classified into distinct frequency bands, these are delta (0 - 4 Hz), theta (4 - 8 Hz), mu (8 - 12 Hz), sigma (12 - 15 Hz), beta (15

- 30 Hz), and gamma (> 30 Hz). Positive increases in power when in a frequency band are a result of synchronous firing of underlying neurons and is referred to as event-related synchronization (ERS). Conversely, a decrease in power is attributed to randomized firing of underlying neurons and is referred to as event-related desynchronization (ERD) (MacKay 2005, Pfurtscheller & Lopes da Silva 1999). Many studies use these time-locked measurements to associate motor function with cortical rhythms. For example, ERS in the theta range is associated with preparation of movement (Popivanov, Mineva & Krekule 1999) and rhythmic movement (Turak, Louvel, Buser & Lamarche 2001), ERD in the alpha range is associated with hand and finger movements (Pfurtscheller & Lopes da Silva 1999) and tactile stimulation (Chatrian, Petersen & Lazarte 1959), and ERS in the beta frequency range during fast finger tapping and ERS during slow finger tapping and weak muscle activity (Toma, Mima, Matsuoka, Gerloff, Ohnishi, Koshy, Andres & Hallett 2002).

Currently, there have been no ECoG studies which investigate cortical power during dynamic dexterous manipulation. Here, dexterity is defined as the ability to dynamically control the direction of the applied force at the fingertip (Valero-Cuevas et al. 2003). In this study, we challenged participants to perform a variety of manipulation tasks varying in dexterity demand to investigate cortical oscillations associated with simple versus difficult motor tasks. We found that cortical area and bandwidth increased with more difficult tasks and that the beta frequency range provided the most information regarding task difficulty. Work in this area may lead to advancement in understanding the neural control strategies employed by the nervous system during object manipulation.

4.2 Methods

4.2.1 Ethics

We obtained ECoG recordings in two male patients (34 and 43 years old) who were being continuously monitored in the ICU for epileptic seizures. The participants gave written consent prior to data collection and the protocol was approved by the Institutional Review Board at the University of Southern California.

4.2.2 Experimental Paradigm

In this study, the first subject performed three tasks manipulation tasks. In the first, they was instructed to small object weighting approximately 300 g with a three fingered grasp (thumb, index, and middle fingers) statically as shown in Fig. 4.1a for 30 seconds with just enough force to keep it from slipping. In the second task, they rotated the same object for 30 seconds in a twisting motion back and forth twisting motion as if tightening and loosening a bottle cap at a rate of approximately 1 Hz (Fig. 4.1b). In the third task, both subjects compressed a small slender spring between the index finger and thumb as much as possible while trying to prevent the spring from buckling to the points of maximal compression (Fig. 4.1c), a paradigm known as the Strength-Dexterity test (Valero-Cuevas et al. 2003). In all tasks, normal forces were recorded from a uni-axial load cell (Measurement Specialties, Hampton, VA) at the points where the fingertips came into contact with the objects. Due to the placement of the subdural electrodes, the subject performed the motor tasks with their left (non-dominant) hand.

(a)
Task 1: Static
Three-fingered Grasp

(b)
Task 2: Three-fingered
Rotation

(c)
Task 3: Unstable
Spring Compression

~1Hz

Increasing Dexterity Demand
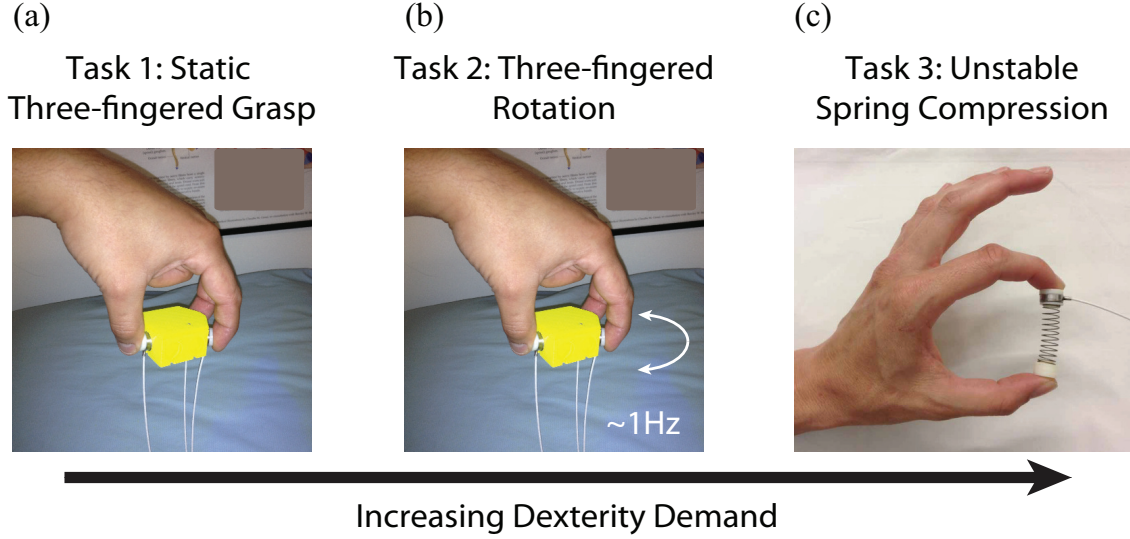
Figure 4.1: Manipulation tasks performed during electrocorticographic recordings. Normal forces at the point of contact were recorded using a uni-axial load cell. From left the right the tasks increase in dexterity demand from static hold to slow movements and finally to unstable object manipulation. (2) Three-fingered static grasp of a 300 g object using the thumb, index and middle fingers. (b) Three-fingered rotation using the 300 g object which was oscillated back and forth in a twisting motion at a rate of approximately 1 Hz. (c) Strength-Dexterity test in which the subject compressed a slender spring as much as possible using a precision pinch.

4.2.3   Electrocorticography (ECoG)

Neurophysiological monitoring was achieved using a 128-channel head box (EMU 128FS, XLTEC). Subject 1 had an 8×8 array of subdural electrodes implanted in the right hemisphere overlaying the sensorimotor cortex and portions of the prefrontal, premotor and posterior parietal cortices as shown in Fig. 4.2a. Subject 2 was implanted with a 6×8 grid covering the right sensorimotor cortex as shown in Fig. 4.2b. The platinum subdural electrodes had a with 1 cm center-to-center spacing with a contact diameter of 2.5 mm. Data for Subject 1 were sampled at 500 Hz and at 1 kHz for Subject 2 with

open filters. Prior to analysis data were filtered from 5 - 100 Hz and notch filtered at 60 Hz and harmonics up the Nyquist frequency.
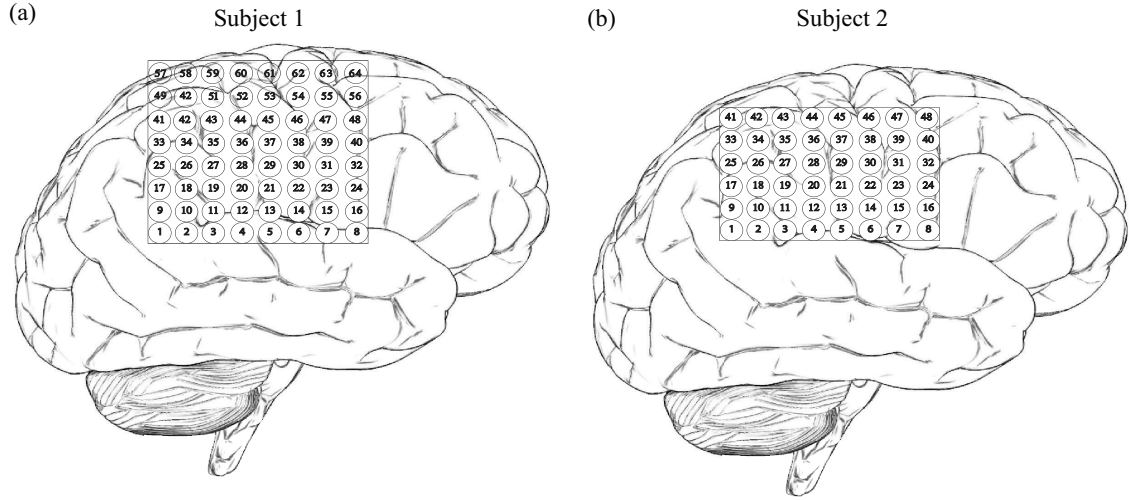
Figure 4.2: Approximate electrode grid layout for Subjects (a) 1 and (b) 2.

4.2.4 Spectral Analysis

The average power spectral density (PSD) was calculated during each task and further separated into the delta, theta, mu, and beta frequency bands. All data were compared to a quiescent time when the patient performed no movements. Three-second long epochs of data were analyzed during which the subjects were well into the task.

4.3 Results

Figure 4.3 shows the changes in PSD in Subject 1 over the entire grid as compared to a resting period. Cortical areas experiencing ERS are shown in dark red, indicating an increase in power requirements for the specified task than during rest. ERD is shown in

blue and indicates that there was more power in rest than in the task being performed. For Task 1, the only increase in power during is confined to the beta frequency, which is consistent with literature regarding static force production (Murthy & Fetz 1992, Fetz & Cheney 1980, Baker et al. 1997, Kilner et al. 1999). For Task 2, there were large increases in power in the delta, theta and mu frequency ranges over the primary motor area, which is also consistent with findings in literature that have investigated slow rhythmic movements (Turak et al. 2001, Pfurtscheller & Lopes da Silva 1999) and increases power over the in the medial cortex in the mu and and beta frequency range. In the primary motor area however, beta frequency range was abolished. During Task 3, there were increases in power only in the medial cortex in the mu and beta range and increased power in M1 in the beta frequency range. The spectral plots for Task 2 suggest that both cortical area and bandwidth requirements increase with steady rotation movements. Tasks 2 and 3 involve active moment which seems to be correlated with increases in power in the medial cortex towards the supplementary motor area (SMA). For the tasks that required a steady force production (i.e. Task 1 and 3), beta range power increased in the motor cortex.
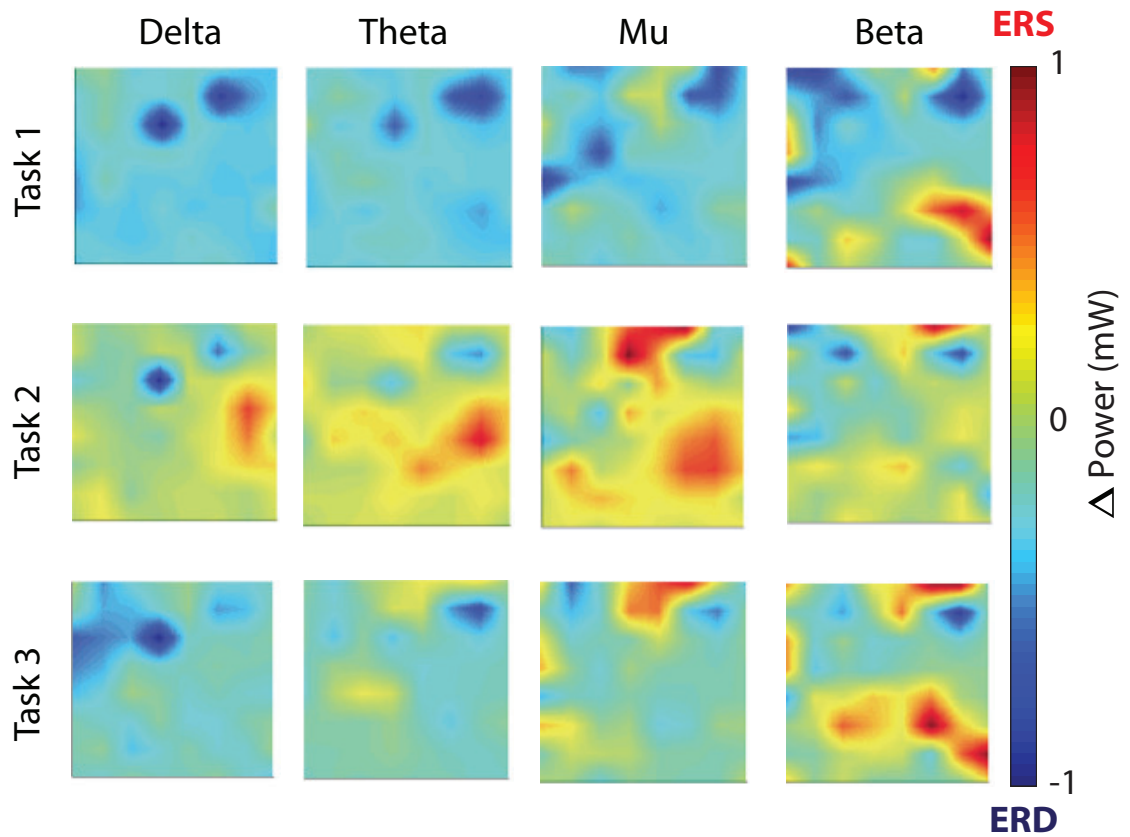
Figure 4.3: ERS and ERD.

The changes in power as compared to rest in the beta frequency range for Subject 2 is shown in Fig. refECoGBetaPower.eps. This subject only performed the SD test (i.e. Task 3 in Subject 1). During the SD test, beta power increased slightly in the most posterior part of the sensorimotor area, however beta power decreased anterior to this section while the other areas remained relatively unchanged from rest.
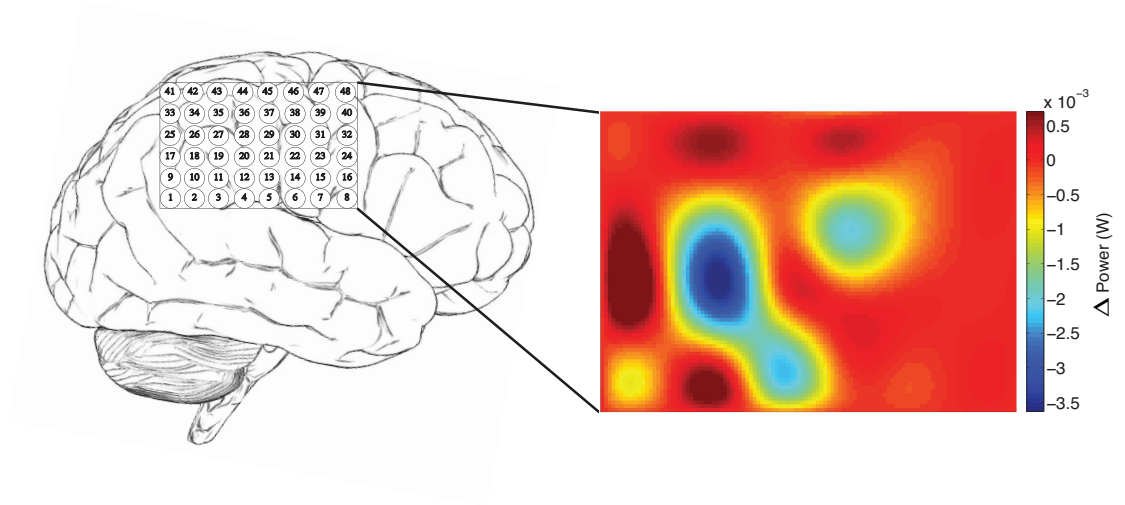
Figure 4.4: Electrocorticographic power associated with dexterity.

4.4 Discussion

We were given a unique opportunity to collect cortical activity from arrays of subdural ECoG electrodes implanted in two subjects who underwent monitoring for intractable epilepsy prior to epilepsy surgery. Subject 1 performed tasks that varied in dexterity requirement. Subject 2 only performed the most dexterous task. The aim of this study was to determine whether spectral analysis of cortical activity in the motor and sensory cortices could provide information about spatiotemporal relationships in the brain during manipulation of unstable objects.

Subject 1 showed an increase in beta power over the sensorimotor cortex (Fig. 4.3) which was in direct contrast to Subject 2, who showed that the hand area of the sensory cortex exhibits a large decrease in power during spring compression (Fig. 4.4). This difference in power changes is likely due to the fact that Subject 1 was squeezing the

spring well within the stable domain. The compression force on the spring for which the PSD was calculated was relatively low, suggesting that this subject was not incorporating increased sensory feedback. Instead, they were squeezing the spring at low enough levels that mimics stable force production. It has been shown that beta range oscillations in the cortex are associated with the maintenance of stable forces (Murthy & Fetz 1992, Fetz & Cheney 1980, Baker et al. 1997, Kilner et al. 1999). Subject 2, on the other hand, was performing the SD test correctly and was squeezing the spring to nearly the point at which the spring would fly out of the hand. Because this subject made dynamic updates to the forces applied to the ends of the spring, beta rhythms in the sensorimotor cortex attenuated. It has been shown in literature that dynamic movements cause beta rhythms to disappear (Toma et al. 2002, Baker et al. 1997, Brown 2000, Feige et al. 2000).

These preliminary data suggest that differences in task complexity are detectable using ECoG electrodes and are reflected as changes in the power spectral density. Continued data collected will assist in the development of cortical maps that relate cortical activity during during the production of static and dynamic. We will also begin recording data kinematic data to relate moment variability to changes in the PSD. Furthermore, electromyographic recordings will be added with the goal of detecting relationship between cortical activity to muscle activity for simple and difficult tasks as well as measure conduction delays from cortex to endpoint movement and force. Future work in this area may lead to advancement in brain-computer interfaces that allow for the control of higher degrees of freedom and real-time classification of finger function.

Acknowledgements

Chapter 5

Introduction to Coherence

Abstract

Understanding the cortical control of voluntary movements is an important topic in neuroscience. One method of assessing this control is through coherence analysis. In this chapter, the development, calculation and implications of coherence are discussed. We begin with a description of cortical oscillations, current ideas on their generating mechanisms and how they are measured. Next, the motor associations of specific frequency bands are discussed followed by a brief description of the connectivity between cortex and muscles. Lastly, coherence is introduced as a tool for measuring the functional connectivity between the cortex and peripheral muscles.

5.1 Introduction

In healthy humans, electroencephalography (EEG) and magnetoencephalography (MEG) serve as the predominant methodology for non-invasive measurements of the temporal dynamics of the active cortex. The ability to record high temporal activity enables

experimentalists and clinicians to subdivide the power spectra of cortical oscillations into discrete frequency bands and begin to associate changes the in rhythms activity with motor actions. Positive increases in the power spectra of underlying neurons in a frequency range is referred to as event-related synchronization (ERS). Conversely, decreases in power at a frequency is referred to as event-related desynchonization (ERD) (MacKay 2005, Pfurtscheller & Lopes da Silva 1999, Pfurtscheller & Neuper 1994, Leocani, Toro, Manganotti, Zhuang & Hallett 1997). For example, ERS of sigma oscillations of approximately 14 Hz are associated with concentration and suppression of a motor response (Rougeul-Buser & Buser 1997, Nashmi, Mendona & MacKay 1994), whereas ERD of beta rhythms coincide with slow finger tapping and weak muscular activity (Toma et al. 2002).

Measuring the power in the brain gives a general idea of the role of oscillations in motor control, however, in order to truly understand the cortical control of the hand, a relationship between the rhythms of the cortex and of the musculature must be established. It has long been known that the primary motor cortex (M1) projects directly onto the motor neurons in the dorsal column of the spinal cord (Bernhard et al. 1953). As a result, descending commands from M1 have been shown to exhibit synchronous oscillations with spinal motor neurons which can be detected in the electromyogram (EMG) (Conway et al. 1995, Baker et al. 1997, Brown 2000). Corticomuscular coherence (CMC) assess the strength of the temporal correlation between EEG and EMG. CMC has been heavily investigated in the beta frequency range (15 - 30 Hz) for static force production (Murthy & Fetz 1992, Baker et al. 1997, Baker 2007, Conway et al. 1995, Kilner et al. 2000, Kilner et al. 2004, Kilner et al. 1999, Kristeva et al. 2007, Chen et al. 2013), yet recent work has shown that

gamma CMC is present during slow oscillatory force production (Omlor et al. 2007, Omlor, Patino, Mendez-Balbuena, Schulte-Mnting & Kristeva 2011, Patino et al. 2008), strong muscular contractions (Mima et al. 1999, Brown 2000, Hari & Salenius 1999) and movement (Brown 2000, Hari & Salenius 1999).

In several studies, precision pinch tasks have been used to detect corticospinal projections from the primary motor cortex to contralateral muscles(Baker, Pinches & Lemon 2003, Lemon et al. 1995, Lemon & Mantel 1989, Muir & Lemon 1983). However it is known that, in addition to M1, the corticospinal tract (CST) is comprised of neuron originating from the supplementary motor area (SMA), the dorsal and ventral premotor cortices, and the cingulate cortex (Dum & Strick 1991, Dum & Strick 2005, He, Dum & Strick 1995), yet the functional coupling in the prefrontal cortex has been relatively unexplored. Only one study, to our knowledge, has demonstrated high beta-range CMC in the SMA for a fine precision pinch task (Chen et al. 2013).

Excluding gross movements of the arms, CMC has been investigated during static grasps, slow and fast finger movements, and slow oscillatory force production. Needless to say, there is still much research to be done, specifically in the domain of dynamic dexterous manipulation, such as when typing, writing, or playing an instrument. Further coherence studies will undoubtedly serve as an invaluable tool for understanding the neural control of the hand.

5.2 Oscillations in the Cortex

The universe is filled with oscillatory systems: planetary orbits, electromagnetic radiation such as light, the pendulum of a clock, and even sound is vibration of the air. Therefore, it's not surprising that the nervous system also possess oscillatory characteristics. The first human electroencephalographic recordings of cortical oscillations in the 8 - 12 Hz frequency range were recorded by Hans Berger in 1929 (Berger 1929). Since then, numerous clinical and research studies have investigated the functional significance of these oscillations.

Studies have shown that individual cortical neurons possess the inherent ability to fire over wide frequency ranges (Llins 1988, Hutcheon & Yarom 2000), however, models describing the generating mechanisms of these oscillations have yet to be developed. It has been suggested that the rhythm of cortical oscillations is the result of pyramidal neurons discharging during post-inhibitory rebound excitation following the discharge of large populations of inhibitory neurons joined through gap junctions (Jasper & Stefanis 1965, Pauluis, Baker & Olivier 1999). Another theory hypothesizes that intrinsic cell properties and cortico-thalomocortical networks serve as the main underlying generator of cortical oscillations (Steriade 1997).

The parallel arrangement of long dendritic branches of pyramidal neurons act as neural dipoles creating time-varying field potentials that can be recorded through the scalp using electroencephalography (EEG) and magnetoencephalography (MEG) (MacKay 2005). This accumulation of electrical activity from large populations of neurons is comprised of several frequencies summed together and is best viewed in the frequency domain. Changes

in the power spectral density (PSD) of EEG and MEG recordings can be characterized into two categories: event-related synchronization (ERS) and event-related desynchronization (ERD). During ERS, the underlying neuron population fires synchronously which is seen as an increase in the PSD at the firing frequency. Conversely, during ERD, the neuron population are firing in a more randomized pattern causing the PSD to decrease at that particular frequency (MacKay 2005). In both of cases, the change in the PSD must be measured relative to a reference period, typically the time prior to a stimulus event (Pfurtscheller & Lopes da Silva 1999, Da Silva & Pfurtscheller 1999).

Spectral analysis of EEG and MEG signals over the sensorimotor cortex have enabled the association of specific frequency bands with motor tasks. Physiologically relevant oscillations have been observed up to 80 Hz and have been classified into five distinct bands: theta (4 - 8 Hz), alpha (8 - 12 Hz), sigma (12 - 15 Hz), beta (15 - 30 Hz), and gamma (>30 Hz). Table 5.1 provides an overview of the motor associations for each frequency band as it relates to changes in sensorimotor PSD.

Inspection of Table 5.1 clearly indicates that oscillations in the cortex are an important factor in motor control. Yet the underpinnings surrounding the reasons why the brain operates in a specific frequency band for a motor task and switching to another range for a different task is currently unknown. Without a concrete explanation of how and why the brain oscillates in the way that it does, research is limited to identifying consistencies in PSD changes observed prior to and after a stimulus. Additional problems arise due to the definition of what constitutes a certain frequencies band. For example the 'beta' frequency range is 13 - 24 Hz according to Gross *et al.* (Gross, Pollok, Dirks, Timmermann, Butz & Schnitzler 2005) whereas Conway *et al.* extends this range by another 11 Hz to include

Name	Frequency Range (Hz)	Motor Association
theta	4 − 8	ERS: preparation of movement (Popivanov et al. 1999), rhythmic movement (Turak et al. 2001)
alpha	8 − 12	ERS: relationship to finger tremor (Jasper & Andrews 1938) ERD: hand and finger movements (Pfurtscheller & Lopes da Silva 1999); tactile stimulation (Chatrian et al. 1959); task complexity and attention (Boiten, Sergeant & Geuze 1992, Dujardin, Derambure, Defebvre, Bourriez, Jacquesson & Guieu 1993)
sigma	12 − 15	ERS: attentive preparation/concentration, suppression of motor response (Rougeul-Buser & Buser 1997, Nashmi et al. 1994) ERS: fast finger tapping (Toma et al. 2002)
beta	15 − 30	ERS: fast finger tapping (Toma et al. 2002) ERD: slow finger tapping, weak muscle activity (Toma et al. 2002), slow and brisk finger movements (Stanck Jr & Pfurtscheller 1996)
gamma	30 − 50	ERS: during (rigorous) muscle activity and attention, onset of movement (Popivanov et al., 1999)

Table 5.1: Event-related synchronization (ERS) and event-related desynchronization (ERD) in the cortical motor areas in association with specific motor tasks.

13-35 Hz (Conway et al. 1995). Those researchers working in the lower gamma frequency range may feel that they are being infringed on. Overall, the investigation of power spectral changes in EEG and MEG provides us with a view of one side of the coin. The nervous system is a complex interaction between brain and body and as such, it is necessary to investigate the transmission of cortical information to the periphery.

5.3 Correlation

To understand coherence and its derivation, we begin with the mathematical definition of Pearson's correlation coefficient between two variables x and y, which is given as:

$$\rho_{xy} = \frac{cov\,(x, y)}{\sigma_x \sigma_x} \tag{5.1}$$

where cov is the covariance and σ_x and σ_y are the standard deviations of x and y, respectively. The correlation coefficient is counted between -1 and +1. A correlation of +1 indicates a perfect relationship (e.g. the signal area basically the same, but may have different amplitudes), a -1 would indicate that the signals are anti-correlated (e.g. out of phase by 180°), and a 0 suggests that there is no relationship between the two (e.g. both signals are white noise).

Correlation is a bivariate analysis, meaning that this can only be performed with two signals, unlike Fourier transform or evaluating the mean, which can be performed on a single signal. This raises problems which are demonstrated using the following examples. Consider the signals $x_1\,(t) = cos\,(2\pi 15 t)$ and $x_2\,(t) = 0.5 \cdot cos\,(2\pi 15 t)$ shown in Fig. 5.1a and their Fourier domain transformations shown in Fig. 5.1b. These signals are

pure cosine waves with different amplitudes and no difference in phase. This results in a perfect linear correlation of $+1$. Notice in this example that, regardless of the amplitudes of the oscillations, the correlation coefficient is unaffected.

(a)

(b)
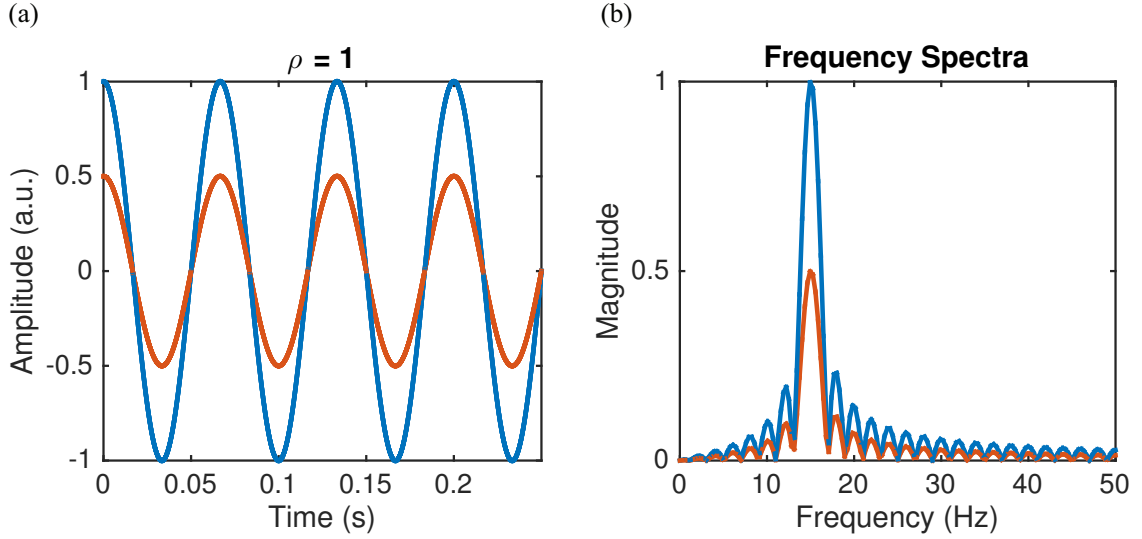
Figure 5.1: Two cosine signals and frequency representation with a perfect linear correlation. (a) The blue trace is a pure cosine wave with a frequency of 15 Hz and an amplitude of 1. The red trace is a 15 Hz cosine wave with an amplitude of 0.5. The correlation between the two signals is $\rho = 1$. (b) Frequency domain representation of the cosine signals in (a). The peak frequency is at 15 Hz for both traces and their magnitude directly relate to the amplitude of their respective cosine waves.

In the next example, signals $x_3(t) = cos(2\pi 15t - \pi/5)$, $x_4(t) = 0.5 \cdot cos(2\pi 15t - \pi/2)$ and $x_5(t) = 0.5 \cdot cos(2\pi 15t - \pi)$ have been added and are shown in Fig. 5.2a and their frequency domain transformations are shown in Fig. 5.2b. Here, it can be seen that although the frequency of oscillations remains the same for all signal, phase shifts of $\pi/5$, $\pi/2$ and π result in correlation coefficients of $\rho_{x1x3} = 0.81$, $\rho_{x1x4} = 0$ and $\rho_{x1x5} = -1$.

70

The frequency spectra for the additional signals $x_3(t)$, $x_4(t)$ and $x_5(t)$ are the same. The critical problem with simple correlation begins to arise. The correlation between these signals is now dependent of the phase shift. The magnitude of the correlation should not depend on the phase shift as this can often happen in real data recordings due to transmission delays.

(a)

(b)
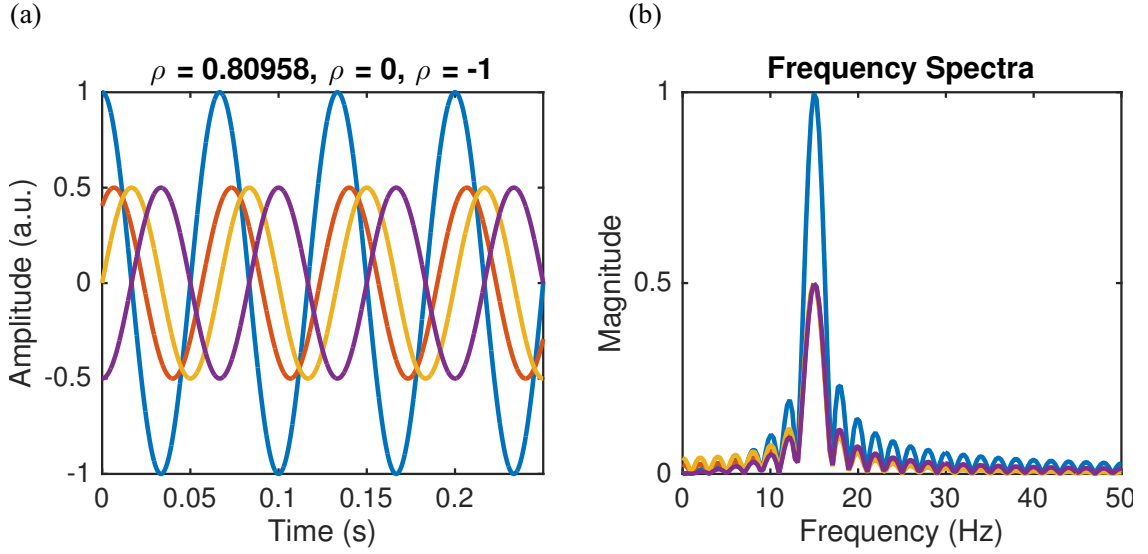
Figure 5.2: The effects of phase shifting a signal on correlation. (a) The primary signal (blue trace) is a cosine with an amplitude of 1 and frequency of 15 Hz. The next three signals share the same frequency but are shifted by $\pi/5$ (red trace), $\pi/2$ (yellow trace) and π (purple trace), resulting in correlation coefficients of $\rho = 0.81$, $\rho = 0$ and $\rho = -1$. (b) Frequency domain representation of the cosine signals in (a). The main trace is represented in blue with magnitude 1 and the three shifted waves overlap each other and have magnitude 0.5 at 15 Hz.

One final example demonstrates the problems with correlation coefficients. Consider two signals, each with two distinct frequencies, $x_1(t) = cos(2\pi 15t) + 0.01 \cdot cos(2\pi 250t)$ and $y_1(t) = 0.5 \cdot cos(2\pi 15t - \pi/2) + 0.03 \cdot cos(2\pi 250t)$. These are shown in Fig. 5.3a. Both signals contain the same two frequencies, however they differ in amplitude. The frequency spectra in Fig. 5.3b shows large peaks for the signals at 15 Hz and almost unseen peaks at 250 Hz. The correlation coefficient for this signal pair is $\rho_{x1y1} = 6 \cdot 10^{-4}$ (i.e. nearly zero). Now, if we multiply the 250 Hz component in both signals by 100, effectively replacing x_1 with $x_2(t) = 0.5 \cdot cos(2\pi 15t - \pi/2) + \cdot cos(2\pi 250t)$ and replacing y_1 with $y_2(t) = 0.5 \cdot cos(2\pi 15t - \pi/2) + 3 \cdot cos(2\pi 250t)$, we obtain the signals in Fig.5.3c and frequency transform in Fig. 5.3d. The resulting correlation coefficient is now $\rho_{x2y2} = 0.7$, a much different value than before.
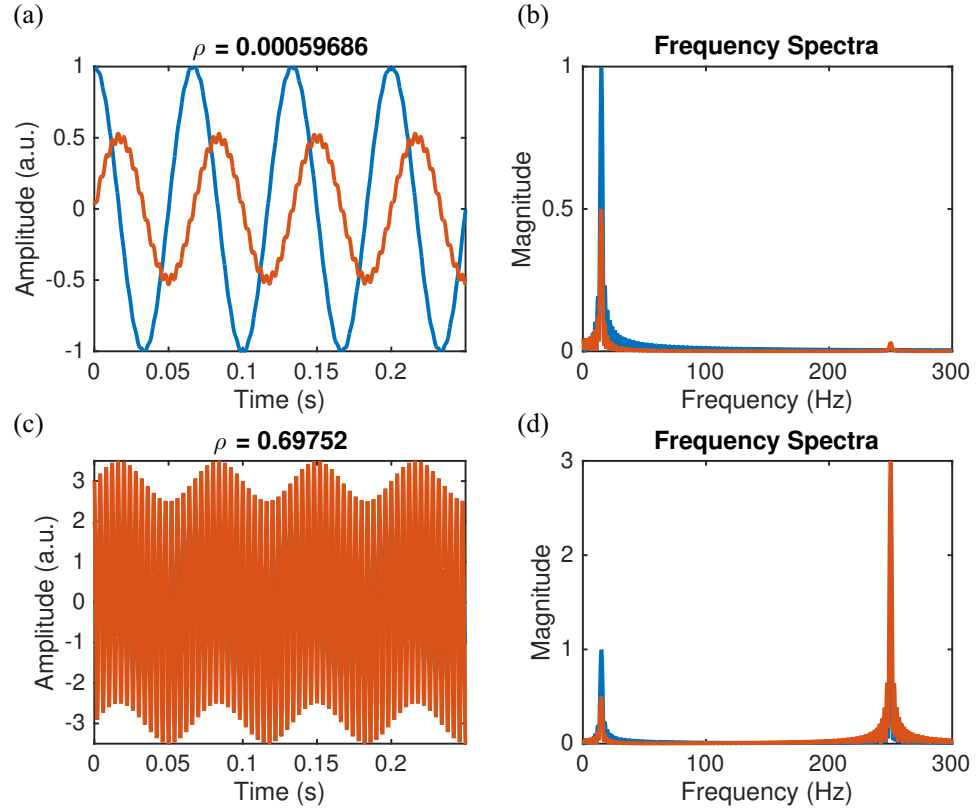
Figure 5.3: Effect of frequency component magnitude on correlation. (a) The primary wave (shown in blue) consists of two frequencies: a 15 Hz component with unit amplitude and a 250 Hz component with amplitude 0.01. The second signal consists of the same frequency components, however the 15 Hz component has an amplitude of 0.5 and a 250 Hz component of 0.03. The correlation between the signals is nearly 0 (b) Frequency domain representation of signals in (a). The 15 Hz components for both signals are much larger than the 250 Hz components. (c) The two signals have similar frequency components as in (a) however, the 250 Hz components have been amplified by 100. The correlation is now $\rho = 0.7$. (d) Frequency spectra of the signals in (c). The 250 Hz components now dominate the 15 Hz components.

These examples demonstrate that initially, when one frequency component was shared between the two signals, the phase dominated the magnitude of the correlation coefficient while amplitude had no effect. However, as the complexity of the signal increases by adding more tones, both phase and amplitude of the signal components had drastic effects on the correlation coefficient. In real world electrophysiological signals, we are not afforded the luxuries of pure sine and cosine waves, therefore it seems a shame to describe the relationship between two complex signals using a single coefficient, such as correlation. Instead, it is necessary to describe the relationship between two signals on a per frequency basis. This is the basis of coherence.

5.4   Calculation of Coherence

Briefly, coherence is a measure of the temporal correlation between two signals (Nunez, Srinivasan, Westdorp, Wijesinghe, Tucker, Silberstein & Cadusch 1997). The concept of coherence can be described with the following example. Imagine that we were observing a wave traveling down the length of a rope as one end is moved up and down and arrives at the other end some time later. We can clearly see that the two ends are physically connected and the peak of the wave at one end always appears at a fixed time later at the other end. However, imagine now that we were unable to see the length of the rope, but we could oscillate one end at a desired frequency and amplitude and observe the response at the other end. After a few trials, it could quickly be concluded that if an oscillation at a particular frequency occurring at the end we control always occurs at a constant time later at the other end, there likely exists a relationship between the two systems.

Continued experimentation would only strengthen the argument that the systems are functionally connected and by extending this relationship to include all frequencies, we could develop a correlation spectrum. This is the basic underlying principle of coherence.

For the time-series variable $x(t)$, let the auto spectral density be defined as

$$P_{xx}(f) = \frac{1}{L} \sum_{i=1}^{L} X_i(f) \cdot X_i^*(f) \tag{5.2}$$

where $X(f)$ is the Fourier transform of $x(t)$ of the current segment $(i = 1 \ldots L)$ and $*$ denotes the complex conjugate. Similarly, for $y(t)$,

$$P_{yy}(f) = \frac{1}{L} \sum_{i=1}^{L} Y_i(f) \cdot Y_i^*(f). \tag{5.3}$$

The auto spectral density of a signal represents the power of the signal. The cross spectrum of the signals $x(t)$ and $y(t)$ is represented as

$$P_{xy}(f) = \frac{1}{L} \sum_{i=1}^{L} X_i(f) \cdot Y_i^*(f) \tag{5.4}$$

Coherence is calculated by normalizing the square of the cross-spectral density between two signals by the product of their individual auto spectral densities (Rosenberg, Amjad, Breeze, Brillinger & Halliday 1989, Farmer, Bremner, Halliday, Rosenberg & Stephens 1993, Baker et al. 1997, Nunez et al. 1997) as indicated in Eq. 5.5. This gives the equation for coherence as

$$C_{xy}(f) = \frac{|P_{xy}(f)|^2}{P_{xx}(f) \cdot P_{yy}(f)} \tag{5.5}$$

Notice the similarity in the equation of coherence with that of Eq. 5.1 for correlation. The difference is that coherence is bounded between 0 and 1 (rather than -1 and +1) and is a function of frequency. Hence for each frequency of interest, a correlation coefficient is assigned. For a coefficient of 1 at a particular frequency, there exists a perfect linear relationship between the two signals, while a 0 indicates linear independence (Farmer et al. 1993).

As with any study, it is necessary to compare across conditions and subjects. Therefore an appropriate transform which accounts for differences in trial length and number of samples. A Z-transformation provides an adequate technique for handling these unavoidable differences. The Z-transformation for coherence is given as

$$Z(f) = \frac{tanh^{-1}(C_{xy}(f)) - \frac{1}{2T-2}}{\sqrt{\frac{1}{2T-2}}} \tag{5.6}$$

where C_{xy} is the coherence between two signals, T is the number of sections used in the spectral estimation, and $tanh^{-1}$ is the hyperbolic arctangent.

In physiological measurements, coherence between cortical activity and muscular activity is given the name corticomuscular coherence (CMC). Before getting into the interpretation of CMC in literature, it is important to know that coherence is a measurement that relies on spectral power estimation (i.e. P_{xx}, P_{xy} and P_{xy}). The topic of power spectral estimation is discussed next.

5.5 Multitaper Power Spectral Density Estimation

Thousands of books and articles have been written on the subject of estimating the power content in a time series signal, and justifiably so, as this is a topic of immense importance. While numerous methods exist for calculating PSD of a signal, this section focuses on the multitaper method (Thomson 1982, Percival & Walden 1993).

Perhaps the most widely known (and used) spectral estimation technique is the periodogram. In this method, the power spectral density of a time-series signal, $x(t)$, is measured within a within a fixed time window of length Δt. This is often referred to as a rectangular window or, due to its resemblance to that of a railroad car on a train, a boxcar. The boxcar window is shifted (with or without overlap) N times over the length of the signal $x(t)$. The estimate of the PSD is found by averaging the N power calculation. Overlapping the windowed section of data window helps to reduce variance in the PSD estimation. The periodogram is biased and does not provide a an accurate estimation of the PSD. Furthermore, the sharp edges of the boxcar window causes spectral leakage. Spectral leakage occurs when the true power of a frequency leaks into nearby frequencies. The frequency representation of the boxcar shows shows side lobes that allow power from nearby frequencies to leak into the power estimation. To overcome this problem, windows that taper off at the ends have been developed, these include the Hann, Hamming, and Gaussian windowing functions to name only a few. The frequency domain representations of these window functions are designed to have smaller side lobes to reduce the influence of nearby frequencies in the spectral estimation.

In each of these functions, a single estimate of the power spectral density in a calculated by multiplying the time-series data by the tapers. However, multiple measurements of the spectral content within a time window will help produce an unbiased estimate of the PSD. This method is represented mathematically in Eqs. 5.7 and 5.8 (Pesaran 2008). In these equations, S_{MT} is the multitaper spectral estimate of the individual segment estimation $\widetilde{x}_k(f)$ with K tapers of length N and $w_t(k)$ is the window function operated on time segment x_t.

$$S_{MT}(f) = \frac{1}{K} \sum_{k=1}^{K} |\widetilde{x}_k(f)|^2 \tag{5.7}$$

$$\widetilde{x}_k(f) = \sum_{t=1}^{N} w_t(k) x_t e^{-2\pi i f t} \tag{5.8}$$

A special class of orthogonal window functions, known as the discrete prolate spheroidal sequences (DPSS) or Slepian tapers (Slepian & Pollack 1961, Thomson 1982), provides an optimal method of maximizing the spectral concentration properties within a specified bandwidth (Pesaran 2008). The first three Slepian tapers are shown in Fig. 5.4. With each successive taper sequence, the function has one more zero crossing and works to accurately estimate higher frequencies within the time segment. The goal of these sequences is to maximize the frequency estimation in the bandwidth $[-W, W]$, where W is the half-bandwidth parameter. For a taper length of N, $K = 2NW - 1$ sequences are created.
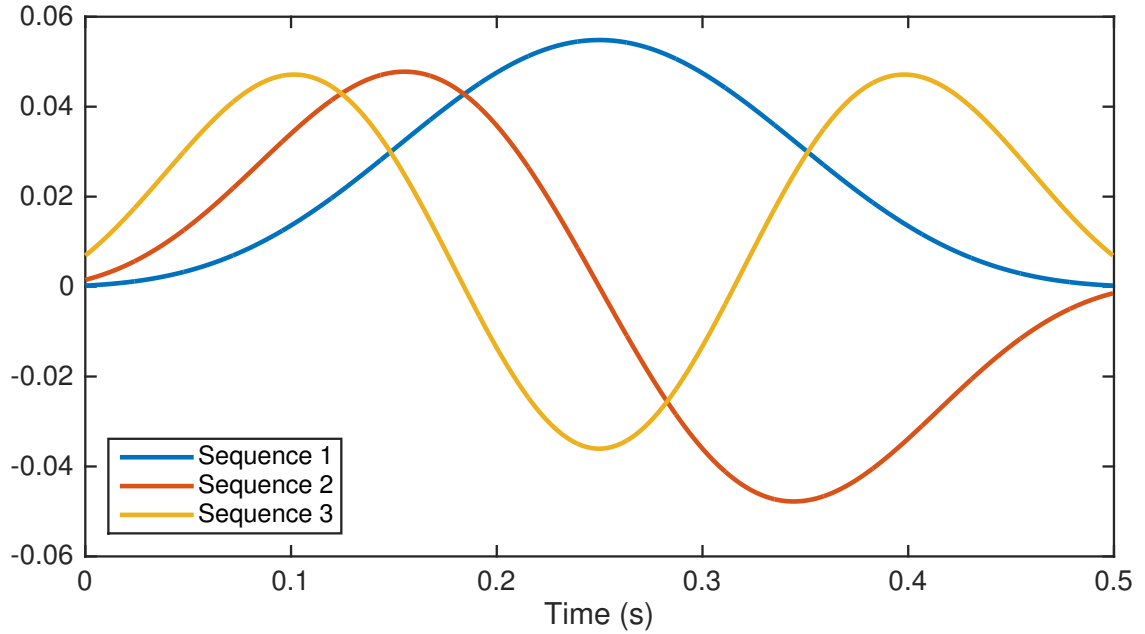
Figure 5.4: First three Slepian multitapers.

The selection of the half-bandwidth parameter and length is dependent on the requirement of the experimenter and determines how smooth the spectral estimate will be. Narrow bandwidths will produce noisy spectral estimations, while a large half-bandwidth parameter will prohibit the detection of specific frequencies in the signal of interest. In physiological signals, it can be assumed that oscillations specific frequency are shared with nearby frequencies. Increasing the number of beyond K will only provide worse spectral estimation (Pesaran 2008).

5.6   Data Preprocessing

Numerous factors impact the calculation of coherence which can lead to erroneous coherence spectra. Therefore, it is important to take the necessary care in the preprocessing of electrophysiological data and consider methodological influences such as EEG reference, EMG rectification, epoch normalization, and frequency spectra estimation to name a few. The choice of reference for electroencephalographic data is a topic of much debate. Re-referencing schemes commonly used are Laplacian (Zhou 2012, Nunez, Silberstein, Cadusch, Wijesinghe, Westdorp & Srinivasan 1994, McFarland, McCane, David & Wolpaw 1997, Peters, Pfurtscheller & Flyvbjerg 2001), common average reference (CAR) (Bertrand, Perrin & Pernier 1985), linked earlobe reference, and Hjorth transformation (Hjorth 1975, Hjorth 1980). The choice of reference can be used to detect the effects of the underlying electrodes while removing the influence of distance sources. Normalization of data epochs in EEG is recommended for coherence analysis in order to remove sections of data that favor larger amplitudes (Halliday & Rosenberg 2000). Electrophygiolocal data is typically non-stationary, therefore smaller sections are also preferred so as to assume quasi-stationarity in shorter time windows. Relevant EEG has been reported up to 100 Hz (Ohara et al. 2001, Marsden, Werhahn, Ashby, Rothwell, Noachtar & Brown 2000, Crone, Miglioretti, Gordon, Sieracki, Wilson, Uematsu & Lesser 1998), and thus EEG data are typically low-pass filtered below 200 Hz.

Rectification is a standard procedure for EMG data prior to coherence analysis. This enables the detection of grouped firing rates of rates (Mima & Hallett 1999, Myers, Lowery, O'malley, Vaughan, Heneghan, Gibson, Harley & Sreenivasan 2003). The literate

debates on the necessity of rectifying EMG and some argue for (Yao, Salenius, Yue, Brown & Liu 2007, Myers et al. 2003) and against it (McClelland, Cvetkovic & Mills 2012). As with EEG, normalization of EMG is recommended for the same purposes mentioned earlier.

5.7   Corticomuscular Coherence Review

Specifically, the analysis of coherence between cortical activity (e.g. EEG, MEG, ECoG, and LFP) and muscular activity (e.g. sEMG and fine-wire) is termed corticomuscular coherence (CMC). Unlike, fMRI, coherence cannot be calculated during a resting period since at least some amount of muscular activity is required. Table 5.2 lists several examples of CMC findings across several cortical frequency bands.

As is evident in Table 5.2, the beta frequency range is heavily studied. The main finding in these studies is that beta CMC is found mostly during isometric force contractions (Murthy & Fetz 1992, Baker et al. 1997, Baker 2007, Conway et al. 1995, Kilner et al. 2000, Kilner et al. 2004, Kilner et al. 1999, Kristeva et al. 2007) and gamma CMC engages cortico-spinal coupling during dynamic force production (Omlor et al. 2007, Omlor et al. 2011, Patino et al. 2008, Chakarov et al. 2009). It can be concluded that beta and gamma CMC are an essential part of object manipulation, however further studies are required to truly understand how the cortex and periphery utilize synchronous frequencies in the control of movement.

Name	Frequency Range (Hz)	Motor Association
theta	4 − 8	N/A
alpha	8 − 12	brief finger movements (Feige et al. 2000, Ohara et al. 2001)
sigma	12 − 15	during startle reflex (Grosse & Brown 2003)
beta	15 − 30	static force production (Murthy & Fetz 1992, Baker et al. 1997, Baker 2007, Conway et al. 1995, Kilner et al. 2000, Kilner et al. 2004, Kilner et al. 1999, Kristeva et al. 2007), attention (Kristeva-Feige, Fritsch, Timmer & Lcking 2002, Safri, Murayama, Igasaki & Hayashida 2006, Safri, Murayama, Hayashida & Igasaki 2007), performance (Witte, Patino, Andrykiewicz, HeppReymond & Kristeva 2007, Kristeva et al. 2007)
gamma	30 − 50	strong muscular contractions (Mima et al. 1999), slow oscillatory force production (Omlor et al. 2007, Omlor et al. 2011, Patino et al. 2008, Chakarov, Naranjo, Schulte-Mnting, Omlor, Huethe & Kristeva 2009)

Table 5.2: Corticomuscular coherence studies across the different frequency bands.

5.8   Separation of Power and Coherence

Lastly, an important distinction must be between power measured in the cortex and coherence between these oscillations and muscular activity. Measures of cortical power provide experimentalists with a view of one side of a multi-dimensional coin. In order to understand how the brain controls the body, it is necessary to observe the transmission of oscillations throughout the nervous system. To state it boldly and succinctly: power does not equal coherence. Despite the fact that coherence relies on spectral power estimation its calculation, it has been shown in numerous studies that reductions and/or increases in cortical power in a specific frequency range, do not necessarily affect coherence magnitude. For example, intravenous injections of diazepam, a known enhancer of beta cortical activity, were given to healthy subjects. Cortical activity in the beta frequency range increased significantly, however, corticomuscular coherence remained relatively unaffected (Riddle, Baker & Baker 2004, Baker & Baker 2003).

As an important reminder, coherence is a measure of the temporal correlation between two signals. The strength of coherence depends on the synchronous activity of two measurement, as determined by the phase relationship of the two signals. A prime example of this was demonstrated by Nunez *et al.* (Nunez et al. 1997). In this example, two signals comprised of the same three frequency components (5, 12 and 20 Hz) with unequal amplitudes (5, 12 and 1), as shown in Fig. 5.5a, were generated with each having different consistencies in their phase relationships. In each signal the phase would randomly change every second. In the 5 Hz component, the phase would vary between

$\pm18°$, the 12 Hz signal would change vary by $\pm180°$ and the 20 Hz signal had a consistent phase throughout the entire duration.

The power in each of the frequency components was directly related to the amplitude, hence the power in 5 Hz component was the lowest of the three components, the 20 Hz component had the greatest power, and the 20 Hz component had the least power. The signal with the most chaotic change in phase shift from one second to the next was the 12 Hz component. As a result, even though it had the highest power, the coherence, as shown in 5.5b is non-existent. The signal with relatively small changes in the phase consistency, (i.e. the 5 Hz component), retained a strong measure of coherence between the two signals. For the 20 Hz signal which had the lowest power (Fig. 5.5a), exhibited the highest coherence (Fig. 5.5b) due to the unchanging phase relationship with each passing second.
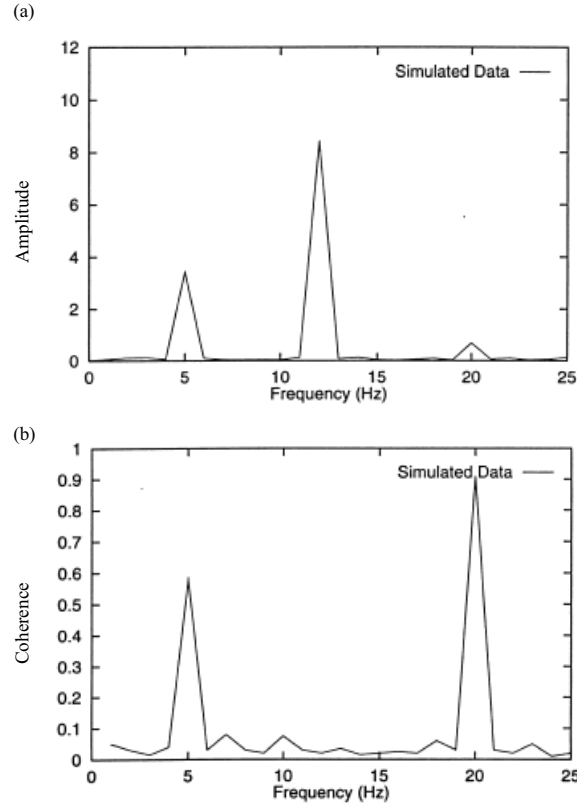
Figure 5.5: Effect on the randomization of signal phase on coherence. (a) Two signals which share frequency components at 5, 12 and 20 Hz are created, each with phase relationships that vary after each second. (a) The amplitude of the 5, 12 and 20 Hz components are 5, 12 and 1, respectively. The phase of the 5 Hz component is randomly varied between $\pm 18°$, the 12 Hz component varies by $\pm 180°$ and the 20 Hz component contains an unchanging phase with each passing second. (b) Since the phase of the 5 Hz components was bounded within a small range, the coherence at this frequency remains relatively strong. Because the phase of the 20 Hz component varies drastically from second to second, the coherence is extremely low. Lastly, the 20 Hz signal, although it had the smallest amplitude, had the strongest coherence due to the consistency in the phase throughout the duration of the signals. Taken from Nunez *et al.* (1997).

In summary, this chapter provided an overview of the range of physiologically relevant cortical oscillations and discussed their possible generating mechanisms. The problems with correlation as a measure of the relationship between two complex physiological systems was discussed. Coherence was introduce was a measure that provides a quantitative analysis of the likelihood that two signals are either physically or functionally related. Over repeated measures of the consistency of the phase relationship, the conclusion that there is indeed a relationship is only strengthened. A review of the studies which have used coherence were presented. It was shown that the beta and gamma frequency ranges are of the greatest interest and high beta corticomuscular coherence is present during sustained muscular contractions while gamma CMC is present during more dynamic motor tasks. Lastly, it was shown that changes in the power of a signal do not provide an indication of how the coherence will be affected, but instead is dependent on the temporal correlation between the two signals.

Chapter 6

Synchronous Corticomuscular Oscillations During Dynamic Unstable Manipulation

Abstract

The control of fingertip forces is essential for dexterous manipulation. However, the functional role of the primary motor cortex and other cortical areas remains relatively unexplored for dynamic manipulation. In this study, we investigated corticomuscular coherence in the beta (15 - 30 Hz) and low gamma (30 - 45 Hz) frequency ranges to quantify the functional connectivity of the cortex to hand musculature during the production of precision pinch forces on a rigid object (a wooden dowel) and a compliant and unstable object (a slender spring prone to buckling). For both objects, 15 right-handed participants produced and held force levels set to 40% and 80% of the greatest compression force they could sustain with the spring. This produced four unique conditions: spring-low (SL), dowel-low (DL), spring-high (SH), and dowel-high (DH). We used EEG to calculate corticomuscular coherence (CMC) with the *first dorsal interosseous* (FDI) and *abductor policies brevis* (APB) muscles during steady hold periods. In the DL and

DH conditions, significant CMC appeared over the sensorimotor cortex, however, their magnitudes were not significantly different. The highest beta CMC was found in the sensorimotor cortex during the SL task, however, in the SH condition, beta range coherence in M1 was abolished. A linear mixed-effects model was used to investigate the effect of task condition on beta range coherence in M1. The results showed that there were no significant differences in effect for low force compressions for either object on beta coherence. However, there was a clear difference in effect for the DH and SH conditions ($p < 0.001$). Our investigations of gamma range CMC showed significant increases over the supplementary motor area (SMA) during the SH task. We speculate that the presence of gamma coherence in the SMA during the most dexterously demanding task supports the notion that higher frequencies may be an indication of rapid sensorimotor integration and strategic motor planning. Overall, these findings suggest that for precision force control, cortical drive to contralateral hand muscles is modulated by dexterity demand and there exist context-sensitive cortical circuits involved in the control of stable and unstable manipulation.

6.1 Introduction

Beta range (15 - 30 Hz) oscillations in the sensorimotor cortex of humans and non-human primates have been frequently observed (Sanes & Donoghue 1993, Donoghue, Sanes, Hatsopoulos & Gal 1998, Witham, Wang & Baker 2010, Murthy & Fetz 1992, Murthy & Fetz 1996a, Murthy & Fetz 1996b, Conway et al. 1995, Lebedev & Wise 2000, Mima

et al. 1999, Stanck Jr & Pfurtscheller 1996). Similar oscillations recorded in the electromyogram (EMG) have been shown to be phase-locked to these cortical rhythms, specifically around 20 Hz, during the maintenance of static forces (Baker et al. 1997, Conway et al. 1995, Murthy & Fetz 1992, Salenius, Portin, Kajola, Salmelin & Hari 1997). The functional connectivity between cortical and muscular activities can be quantified using corticomuscular coherence (CMC), which measures the strength of the phase relationship between two spatially separated systems (Conway et al. 1995, Rosenberg et al. 1989, Farmer et al. 1993). While the neural mechanisms generating these synchronous oscillations are poorly understood, research suggests that CMC magnitude reflects both efferent commands and afferent sensory feedback (Fisher et al. 2002, Riddle & Baker 2005, Baker, Chiu & Fetz 2006).

It has been shown that factors such as applied force level, fatigue, muscle cooling, movement preparation, and learning largely influence beta CMC magnitude (Witte et al. 2007, Mendez-Balbuena, Huethe, Schulte-Mnting, Leonhart, Manjarrez & Kristeva 2011, Tecchio, Porcaro, Zappasodi, Pesenti, Ercolani & Rossini 2006, Riddle & Baker 2005). Other studies which show the disappearance of beta CMC during movement provide further evidence for the association of static force production with beta rhythms (Baker et al. 1997, Brown 2000, Feige et al. 2000, Kilner et al. 2000, Kilner et al. 2004, Kilner et al. 1999). Low force (< 5.0 N) precision pinch paradigms have been used to study cortico-spinal interactions (Baker et al. 2003, Lemon et al. 1995, Lemon & Mantel 1989, Muir & Lemon 1983, Lemon, Baker, Davis, Kirkwood, Maier & Yang 1998). Other studies have found that CMC is modulated by digit displacement (Riddle & Baker 2006) and object compliance (Kilner et al. 2000).

The beta range CMC literature tends to focus heavily on static force production, however the manipulation of objects involves far more dynamical interactions, thereby mandating the exploration of CMC in other frequency ranges. Gamma (30 - 45 Hz) CMC has been shown to be associated with moderate (Brown et al. 1998) and maximal muscular contractions (Brown et al. 1998, Mima et al. 1999). Gamma CMC has also been reported in preparation of wrist movement prior to a go cue (Schoffelen, Poort, Oostenveld & Fries 2011, Schoffelen, Oostenveld & Fries 2005). More recently, dynamic movement investigations have shown that peak coherence shifts from beta into the gamma frequency range (30 - 45 Hz) during slow predictable (Omlor et al. 2007, Patino et al. 2008, Brown et al. 1998) and unpredictable (Omlor et al. 2011) oscillatory force tracking tasks.

Anatomical studies have shown that, in addition to M1, axons of the corticospinal tract originate in the dorsal and ventral premotor cortex and SMA (Dum & Strick 1991, Dum & Strick 2005, Kuypers 1960, Shinoda et al. 1981). In one study, it was shown that during a fine uni-manual manipulation task, beta CMC extended into the SMA (Chen et al. 2013). This evidence suggests that context-sensitive cortical circuits are engaged based on dexterity demand.

From these studies, it is clear that cortico-muscular coupling in the beta range regulates static force while gamma coherence presides during dynamic movements and forces. However, dexterous precision pinch manipulation involves both static and dynamic elements, therefore, it is necessary to investigate the entire coherence spectrum when performing a task that requires the continual adjustment of fingertip forces. In this study, we expand on these previous findings to investigate the role of synchronous cortico-muscular oscillations during a dexterously demanding paradigm in which the precise control of

endpoint finger force is paramount to task performance. Dexterity is defined here as the ability to precisely control the magnitude and direction of fingertip endpoint force (Valero-Cuevas et al. 2003). Based on this definition, the Strength-Dexterity (SD) test was developed to quantify dexterous ability by asking participants to squeeze a slender spring with unstable characteristics as much as possible before buckling (Valero-Cuevas et al. 2003). This paradigm has been used in fMRI studies to reveal context-sensitive cortical areas involved in the control of unstable springs (Mosier et al. 2011, Holmstrom et al. 2011, Talati et al. 2005).

Based on the promising results of these findings, we developed a visuomotor force tracking version of the SD test to assess the modulation of coherence during matched force compression of an unstable compressible spring as compared to the compression of a rigid dowel. We found that beta CMC was present in the primary motor area during low and high force compressions with the wooden dowel and at the low force compression with the spring. Furthermore, we found that, despite matched force levels, beta range CMC during the high compression levels with the spring was significantly reduced in comparison to the high force dowel task in the primary motor cortex. In this dexterously demanding task, we observed a spatial shift of CMC into the SMA and a spectral shift into the gamma frequency range. These findings suggest that the extinction of beta CMC in the sensorimotor cortex in favor of gamma in the SMA for the most unstable and dynamic task may indicate concentration, rapid sensorimotor integration, and strategic motor planning.

6.2 Methods

6.2.1 Subjects

15 healthy participants (30.3 ± 4.6 years, 6 females) who were self reported as right-handed took part in this study. There were no known neurological conditions in any of the participants, nor did they report any prior hand injuries or surgeries. Subjects were consented prior to the experiment and the protocol was approved by the Institutional Review Board (IRB) at the University of Southern California.

6.2.2 Experimental Paradigm

6.2.2.1 Task 1: Strength-Dexterity (SD) Test

We obtained a measure of each participant's dexterous performance by employing a paradigm known as the Strength-Dexterity (SD) test (Valero-Cuevas et al. 2003). The SD test provides a quantitative measure of hand dexterity by challenging participants to use a precision pinch to compress a slender spring prone to buckling to the point of maximal stability. Performance during this task is based on two key components: **strength** and **dexterity**. Here, **strength** is defined as the ability to produce a sufficient amount of force to compress the spring to solid length (i.e. where all of the spring coils are touching); and **dexterity** is defined as the ability to dynamically regulate endpoint force direction and magnitude to stabilize the spring throughout compression (Valero-Cuevas et al. 2003).

Subjects rested their arm on a table and compressed the spring using a posture that was comfortable for them. They were given four attempts (90 seconds each) to try to

compress the spring as much as possible before it slipped out of their hand. During the task, we asked participants to ensure that their 3rd-5th fingers did not assist in the task. The average maximal compression force reached prior to spring buckling was taken as a normalized measure of their dexterous performance. We rounded this value to the nearest tenth and defined this as the subject-specific F_{max}. From this, we calculated 40% and 80% of the subject-specific F_{max} to be used in the second phase of the study.

6.2.2.2 Task 2: Visuomotor Force Tracking

In the visuomotor force tracking portion of the experiment, subjects were seated comfortably in front of a computer monitor with their arm resting on a table with the spring in their hand. When the trial began, subjects were given real-time visual feedback of their applied compression force and instructed to squeeze the spring to match on-screen force levels displayed as a horizontal red line. Breaks were given in between trials when necessary to reduce fatigue effects. In each trial, ten randomized target forces of 40% and 80% of their F_{max} were presented in 30 second intervals with five seconds of rest in between. During the resting periods, the subjects would hold the object with just enough force to prevent it from dropping. Each target level was presented five times per trial and was performed over three trials for a total presentation of 450 seconds per target level. Subjects then repeated the procedure with a rigid wooden dowel for the same duration and matched force levels. This two-by-two factorial design yielded four manipulation conditions: spring-low (SL) , spring-high (SH), dowel-low (DL), and dowel-high (DH).

6.2.3 Compliant and Rigid Object Characteristics

Subjects manipulated two objects: a compliant spring and a rigid wooden dowel.

Spring: The spring used in this study is shown in Figure 6.1. The force required to bring the spring to solid length was approximately 3.7 - 3.8 N. We specifically chose a spring with a low strength requirement (< 15 % maximal precision pinch force) to focus primarily on cortical drive involved in dexterity demand rather than applied force. The spring alone measured 4.2 cm long, weighed approximately 2 grams and had a spring constant of 0.86 N/cm. Custom designed 3-D printed acrylonitrile butadiene styrene (ABS) plastic end caps were glued to both ends of the spring to create flat surfaces on which to attach a force transducer. Additional ABS end caps were attached on top of the sensor for two purposes: (1) to provide a place for subjects to grasp the object and (2) to serve as a thermal barrier to prevent body heat from adding a bias to the temperature sensitive transducer. With the addition of the end caps and sensor, the effective length of the uncompressed compliant object was 5.7 cm as shown in Figure 6.1b.
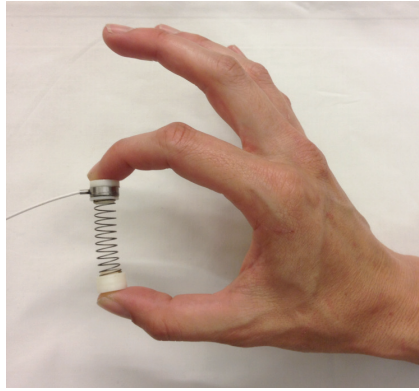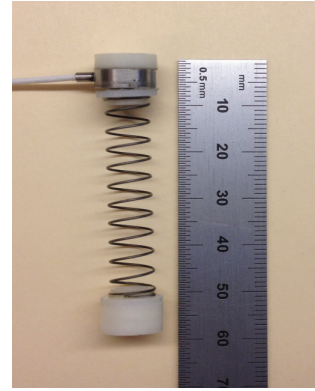
(a)   (b)

Figure 6.1: Spring used in the quantification of hand dexterity. (a) Typical precision pinch hand posture used in the Strength-Dexterity test. Endcaps at either end with a load cell attached to the index finger side of the spring. (b) Close-up of spring and force sensor next to a ruler.

Dowel: Subjects also manipulated a rigid wooden dowel measuring 3.8 cm in length and a diameter of 0.12 cm as shown in Fig. 6.2. With the load cell and ABS end caps, the effective length of the rigid object was 5.2 cm (Fig. 6.2b). This object was chosen for its similarity in length, shape, and weight to the spring. The resting length of the spring was 0.5 cm greater than that of the dowel. A compression force of 0.4 N would be need to be applied to the spring to match the resting length of the dowel.
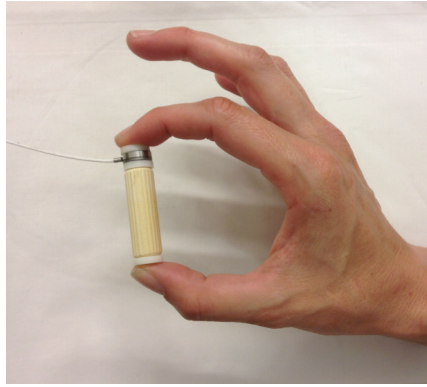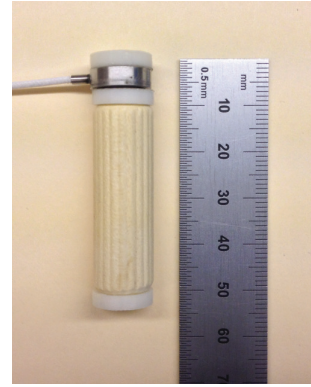
Figure 6.2: (a) Wooden dowel with uni-axial load cell attached. (b) Dowel with load cell and end caps next to a ruler.

6.2.4 Recordings

6.2.4.1 Force

Throughout the SD test and visuomotor force tracking task, normal compression forces were measured by affixing a uni-axial load cell (Measurement Specialties, Hampton, VA) with double-sided tape to the index finger side of the compliant spring. The circular load cell measured 0.41 cm in height and 1.27 cm in diameter and aligned perfectly with the diameter of the objects. Signals from the sensor were differentially amplified with a custom designed circuit set to operate in the range of 0 to 5 N. Data were captured using a USB Data Acquisition (DAQ) system (National Instruments, Austin, TX) sampling at a rate of 2048 Hz. Prior to data collection the sensor voltage was converted to Newtons by removing the DC offset and calibrating the load-cell using a four-point linear regression

with fixed weights. The offset and gain of the load cell were corrected periodically to ensure accurate force recordings.

6.2.4.2 Electromyography (EMG)

Bipolar surface EMG were collected using a Delsys Bagnoli desktop system (Delsys, Natick, MA) from the *first dorsal interosseous* (FDI) and the *abductor pollicis brevis* (APB). Data were amplified from 1000 - 10000 and sampled at a rate of 2048 Hz. The reference electrode for the recordings was placed on the olecranon of the right arm. Recording locations were identified by palpating the muscle during force production in the direction of mechanical action for that particular muscle.

(a) (b)
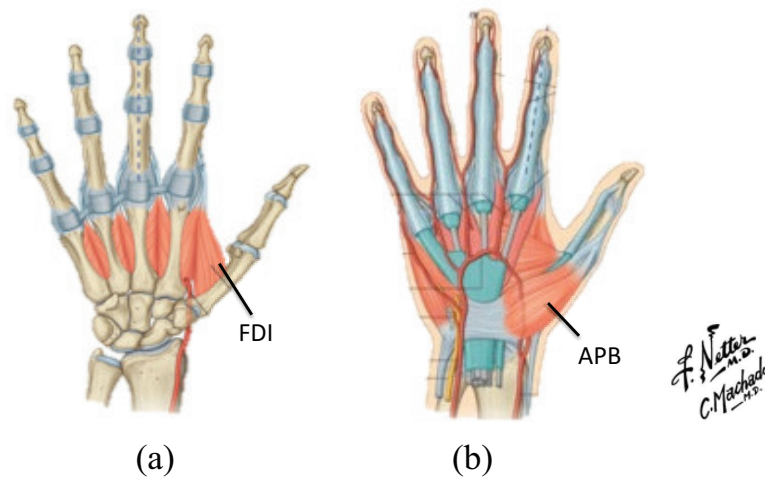
Netter, F. Atlas of Human Anatomy, 3rd Edition.

Figure 6.3: Intrinsic muscles of the hand that were recorded. (a) *First dorsal interosseous.* (b) *Abductor policis brevis.*

6.2.4.3 Electroencephalography (EEG)

64 channels of EEG were recorded at a sampling rate of 2048 Hz (ANT Neuro, Enschede, The Netherlands). The recording sites remained fixed within a flexible cap according to the international 10-20 system for scalp electrode placement. We ensured repeatable recordings of cortical areas across subject by taking skull measurements to place electrode Cz at the cross section of the midway point between the nasion and inion and the midway point between the left and right tragi of the ear. Electrode impedances were kept below 10 kΩ with respect to the reference electrode CPz.
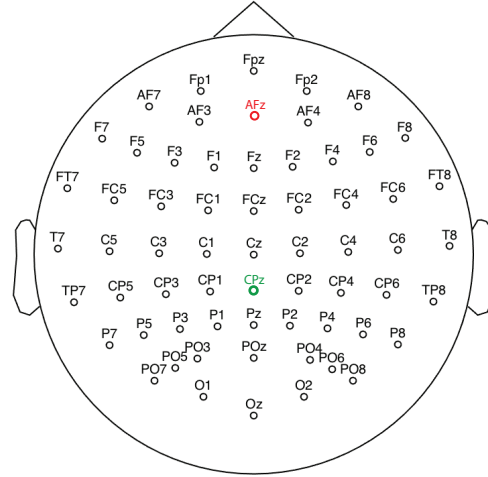
Figure 6.4: *eegosports* EEG cap. (a) Front view. (b) Left view. (c) Top view. (d) 2-D layout of all channels. The ground electrode, AFz, is shown in red and the reference electrode, CPz, is shown in green.

Electrophysiological data were band pass filtered from 10 to 500 Hz and notch filtered at 60 Hz and its harmonics up to 500 Hz using a 4th order Butterworth filter implemented

in MATLAB (Mathworks, Natick, MA) and FieldTrip, a software package for EEG and EMG analysis (Delorme & Makeig 2004, Oostenveld, Fries, Maris & Schoffelen 2011). Subsequently, EMG were rectified to extract group activity of motor units (Halliday, Rosenberg, Amjad, Breeze, Conway & Farmer 1995, Mima & Hallett 1999). Data formats collected from two separate systems were synchronized by configuring the NI-DAQ to send a trigger pulse to the EEG and EMG systems via a split BNC cable. Custom scripts were created to read in trigger events and synchronize all data.

6.2.5 Trial Selection

The start of a trial is defined as the time when the on-screen target transitioned from a resting value to either 40% or 80% of F_{max} and its end is defined as the time when the target value returns back to rest. Trial windows were 30 seconds in duration with a five second inter-stimulus interval. Force data during these steady hold phases were visually examined to determine if the task was performed correctly. Our requirement was that the hold phase must be within a ±15% tolerance of the target force value and be held within this range for at least five seconds; force profiles not meeting these criteria were excluded from analysis. Synchronized EEG and EMG from each condition that satisfied the steady-state criteria were pooled across conditions and subjects and further divided into five second long epochs and normalized prior to coherence analysis (Amjad, Halliday, Rosenberg & Conway 1997). Partitioning the data in this fashion has the overall effect of weighing each trial equally to overcome problems of non-stationary electrophysiological recordings in lengthy trials by assuming the data to be quasi-stationary over smaller time windows. Additionally, this method effectively eliminates coherence bias that favors

sections with high EMG amplitude (Amjad et al. 1997, Laine, Yavuz & Farina 2014, Laine, Negro & Farina 2013, James, Halliday, Stephens & Farmer 2008, Schoffelen et al. 2011).

6.2.6   Coherence Analysis

Synchronous oscillations between cortical activity and EMG indicate functional connectivity which can be assessed through coherence analysis (Mima & Hallett 1999, Nunez et al. 1997). Coherence describes the relationship between two signals through the strength of their consistent phase lag as a function of frequency. The result is a coherence spectrum bounded between 0 and 1 for each frequency of interest. A value of 1 indicates a perfect linear relationship, while a 0 indicates independence. For a given time series, $x(t)$, let the auto spectra be represented as

$$P_{xx}(f) = \frac{1}{L} \sum_{i=1}^{L} X_i(f) \cdot X_i^*(f) \tag{6.1}$$

where $X_i(f)$ represents the Fourier transform of the signal of segment i of L, and $*$ indicates the complex conjugate. A similar spectrum exists for the signal $y(t)$, represented as $P_{yy}(f)$. The cross spectrum between the signals $x(t)$ and $y(t)$ is defined by

$$P_{xy}(f) = \frac{1}{L} \sum_{i=1}^{L} X_i(f) \cdot Y_i^*(f) \tag{6.2}$$

Corticomuscular coherence (CMC) is calculated by normalizing the square of the cross-spectral density between an EMG and an EEG signal by the product of their individual auto spectral densities (Baker et al. 1997, Nunez et al. 1997) as indicated in Eq. 6.3.

$$C_{xy}\left(f\right) = \frac{|P_{xy}\left(f\right)|^2}{P_{xx}(f) \cdot P_{yy}\left(f\right)} \qquad (6.3)$$

CMC was computed for each EEG-EMG electrode pair using FieldTrip, an open-source toolbox in MATLAB for the analysis of EEG and MEG data (Oostenveld et al. 2011). We used discrete prolate spheroidal sequences (DPSS) or Slepian tapers (Slepian & Pollack 1961) for the calculation of the auto and cross spectra. The multitaper method provides several measures of the spectral estimation by multiplying the data series by a series of orthogonal tapers prior to calculating the Fourier transform (Pesaran 2008). Three tapers were used in our analysis, providing a spectral bandwidth of ± 5 Hz (Schoffelen et al. 2011, Maris, Schoffelen & Fries 2007).

6.2.7 Selection of EEG Electrodes

To restrict our statistical analysis to a subset of the electrodes, we selected only those electrodes which showed coherence over the 99% confidence limit in the DL task. Our confidence limit for electrode selection set according to Eq. 6.4 (Rosenberg et al. 1989), where α is our desired confidence level and N is the total number of tapers used in the analysis (Schoffelen et al. 2011, Maris et al. 2007).

$$CL\left(\alpha\right) = 1 - (1 - \alpha)^{\frac{1}{N-1}} \qquad (6.4)$$

We then obtained a difference statistic of standard Z-scores to compare coherence spectra calculated across conditions and subjects to account for differences in the number

of segments (Schoffelen et al. 2011, Kilner et al. 1999, Baker et al. 1997, Laine et al. 2013, Laine et al. 2014). The transformation is given in Eq. 6.5,

$$Z\left(f\right)_n = \frac{tanh^{-1}\left(C_{xyn}\left(f\right)\right) - \frac{1}{2T_n-2}}{\sqrt{\frac{1}{2T_n-2}}}$$

(6.5)

In Eq. 6.5, C_{xyn} is the coherence, T_n is the number of tapers used in condition n and $tanh^{-1}$ is the inverse hyperbolic tangent function.

6.2.8 Linear Mixed-Effects Model

A linear mixed-effect (LME) model provides a method of describing a relationship for a measurable quantity as a function of the sum of weighted independent variables (Winter 2013b, Winter 2013a). We investigated the effects of task condition on mean beta coherence, using a LME model with the following format:

$$CMC_\beta \sim \beta_0 + \beta_1 \cdot Condition + \beta_2\left(1|Participant\right) + \epsilon$$

(6.6)

where CMC_β is the average beta range coherence, $Condition$ is the fixed-effect term, $Participant$ is the random-effect term, the β_n terms are the coefficients for the independent variables, and ϵ is the error. The random-effects term was inserted to account for subject variability since there were several measurements taken for each condition. Two models were generated to estimate FDI-EEG and APB-EEG beta coherence.

103

6.3 Results

6.3.1 SD Test Performance

A typical force profile during the SD test for a single trial in a representative subject is shown in Figure 6.5. Sudden drops in the force trace indicate where the spring buckled and slipped out of their hand. Each subject was given four 90 second attempts to reach their maximal compression force. For this subject, their average maximal compression force prior to spring bucking was calculated to be 2.6 N, shown as the red dotted line. This resulted in $0.4 \cdot F_{max} = 1.04$ N and $0.8 \cdot F_{max} = 2.08$ N, however rounding these values to the nearest tenth gave target low and high forces of 1.0 N and 2.1 N, which are shown as the purple and green dotted lines, respectively. These values were presented to the subject for the visuomotor force tracking task.
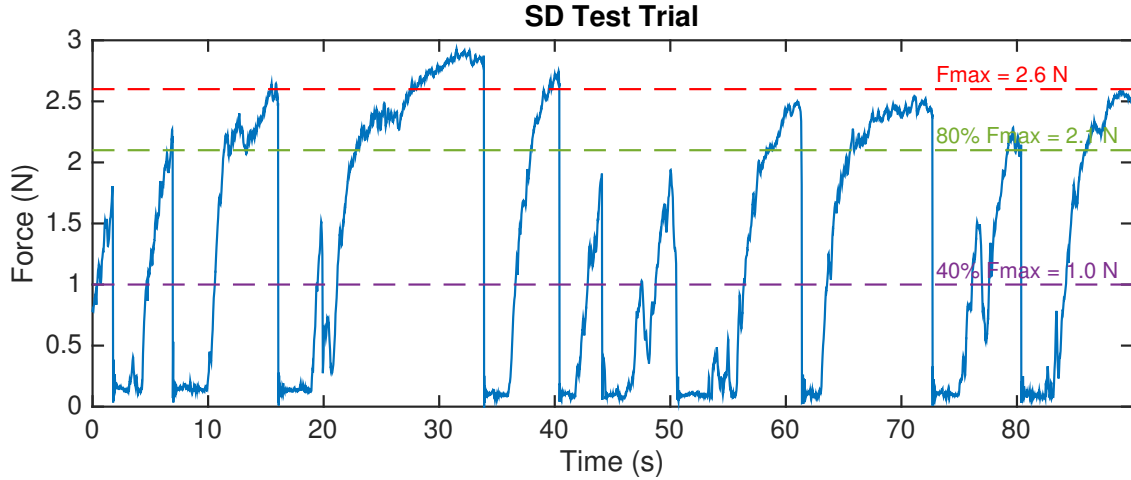
Figure 6.5: Sample force profile during the Strength-Dexterity test. The average maximal compression force for this subject was 2.6 N (red dotted line). As the spring is compressed, it becomes unstable and difficult to control, resulting in the subject dropping the spring. These drops are clearly shown as sudden decreases in the force profile. 40% and 80% of F_{max} were calculated to be 1.0 N and 2.1 N, respectively, and shown as the purple and green dotted lines.

Table 6.1 shows the maximal SD compression force measured for each subject. The last two columns show the calculated 40% and 80% target values that were used for the visuomotor force tracking portion of the study. The average compression force was 2.2 N with a range of 1.8 - 2.8 N and a median of 2.2 N.

Figure 6.6a demonstrates the precision pinch paradigm with the spring. Figure 6.6b shows a single trial of the visuomotor task for a single representative subject consisting of five randomized presentations of each force level. Subjects were asked to match the target force, which is represented as the black dashed line. The trials are classified into spring high (SH) and spring low (SL) conditions. The low and high forces, for this

Subject Identifier	Gender	Age (years)	F_{max} (N)	$0.4 \cdot F_{max}$ (N)	$0.8 \cdot F_{max}$ (N)
P001S002	M	36	2.8	1.1	2.2
P002S002	M	40	2.0	0.8	1.6
P003S001	M	27	2.2	0.9	1.8
P004S001	M	36	1.8	0.7	1.4
P005S001	F	26	2.2	0.9	1.8
P006S001	M	26	2.6	1.0	2.1
P007S001	F	33	2.2	0.9	1.8
P008S001	F	32	2.0	0.8	1.6
P009S004	M	32	2.7	1.1	2.2
P010S003	M	32	2.5	1.0	2.0
P011S002	F	27	2.2	0.9	1.8
P012S001	F	26	2.1	0.8	1.7
P013S001	M	31	1.8	0.7	1.4
P014S001	F	26	1.8	0.7	1.4
P015S001	M	25	2.4	1.0	2.0

Table 6.1: F_{max} values for each subject. 15 right-handed subjects participated in this study, six of which were female. Mean age was 30.3 ± 4.6 years. Mean F_{max} was 2.2 N, median was 2.2 N and range was $1.8 - 2.8$ N.

subject, corresponded to 1.0 and 2.1 N, respectively. The red dashed lines indicate the performance criteria threshold values set to $\pm 15\%$ of the target value. Only those sections which were within threshold for a minimum of five seconds were used for the analysis, which is shown as the grey shaded areas. In Fig. 6.6c, the same paradigm as in Figure 6.6a is repeated with the spring replaced with a stable wooden dowel. Figure 6.6d shows the force tracking profile for the dowel. Low and high force levels are the same as those in Fig. 6.6b. A qualitative comparison between the force variability in the DH and SH conditions illustrates the difficulty in maintaining a steady force with the spring despite the force levels being identical. Furthermore, it can be seen that the force compression of the spring dropped outside of the threshold level in the second to last hold phase (high target). Force compressions with the rigid dowel are clearly distinguished from the

compliant spring by the overshoot following the onset of the target force, which did not

appear in the spring condition.

Figure 6.6: Visuomotor paradigm and force profiles (a) Spring-low precision pinch task. Subjects squeezed a small spring between their index finger and thumb. Normal index finger forces and bipolar surface EMG from several muscles of the hand were recorded (only FDI shown here). (b) Typical force trace for a representative subject during the visuomotor task. Black dashed line is the target force, which, for this subject are 1.0 N and 2.1 N for the low and high target forces, respectively. Red lines indicate tolerance limits of ±15 N. The grey area represents valid hold data. The criteria were that the force had to be within the tolerance limits and be held within that range for a minimum of five seconds. In the last SH condition, it can be seen that the force fell out of range and thus this data was not included in the analysis. (c) The spring object is replaced by a wooden dowel. (d) Force profiles for the visuomotor force tracking task with the same force level performance criteria as in (b).

6.3.2 Muscle Activation

The activation pattern of the intrinsic hand muscles (FDI and APB) for each task is shown in Fig. 6.7. The activation for a particular muscle was obtained by dividing the average value of the rectified EMG during a trial by the mean EMG for that muscle over all trials and conditions. For the FDI muscle, there was steady increase in the activation with force applied for both objects. The FDI becomes more involved in the task during the SH condition than the DH condition despite the force levels being equal. For the APB, the activity was not significantly different for compression of the dowel, however there is a trend towards decreasing activation with applied force. This inverse relationship has been described in literature as the trade-off synergy (Sirin & Patla 1987, Maier & Hepp-Reymond 1995, Maier & Hepp-Reymond 1994, Huesler, Maier & Hepp-Reymond 2000). Tasks with the spring show an overall increase in muscle activity as compared to the dowel.

Figure 6.8 shows a scatter plot indicating the muscle activations across all subjects and tasks to show the relative contribution of the intrinsic hand muscles for each condition. The first principal component (PC) is shown for each condition as a line through the scatter points which aligns with the direction of the most variance. Figure 6.8a compares the resting conditions for the spring and dowel. The first PCs for each task are aligned during the resting condition. In Figure 6.8b, the slope of the PCs have decreased for each condition. In the high conditions, depicted in Fig. 6.8c, the PC for the dowel task shows that there is little APB activation required for this task, however, the PC for the spring

task has a slope of approximately one, suggesting equal contribution for both muscles despite the normal force being the same.
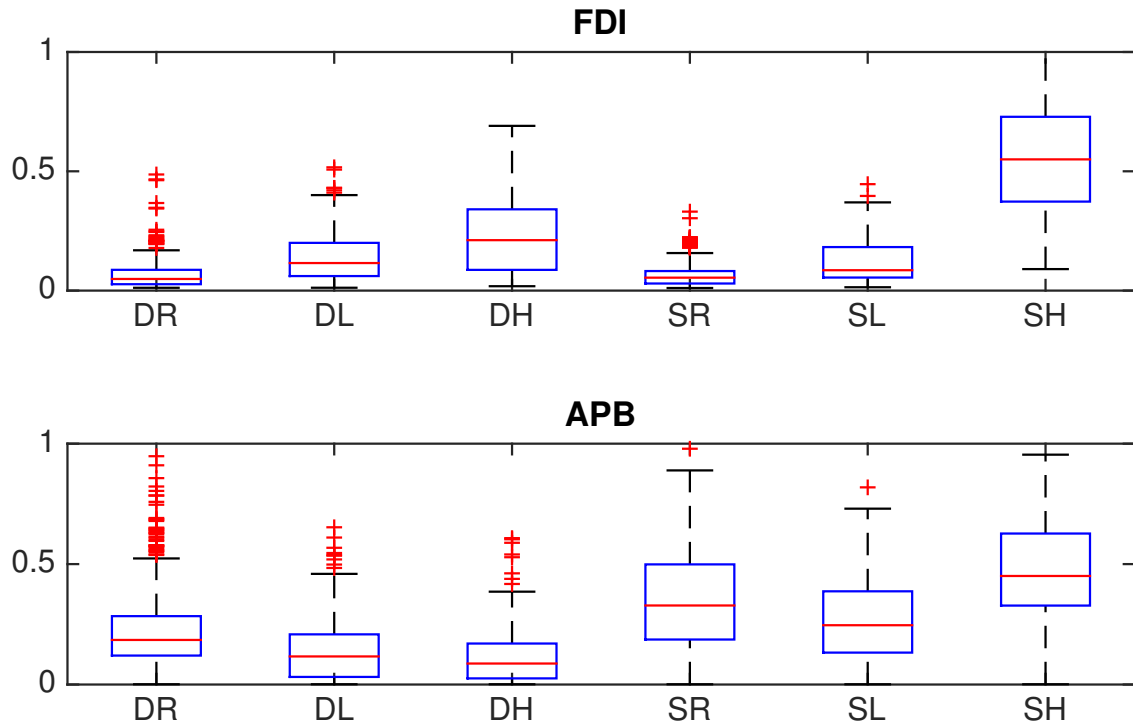
Figure 6.7: Muscle coordination patterns for the FDI and APB across all conditions.
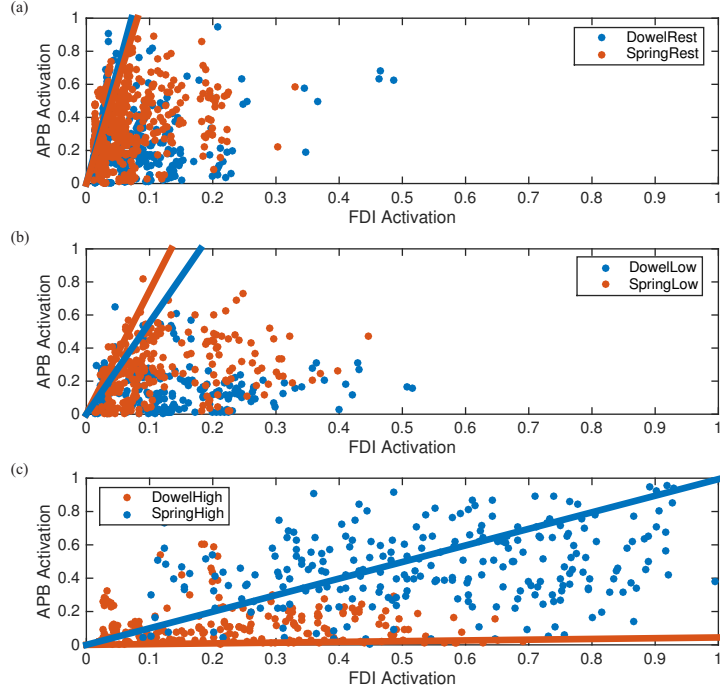
Figure 6.8: Scatter plots showing the muscle activation for the FDI and APB for matched force levels of the objects. The first principal component for each condition is shown to capture the direction of the maximum variance. (a) Rest condition. During the period between the 40% and 80% $F_{m}ax$ target force compressions, the activation the muscles were calculated. The PCs corresponding to the spring and dowel objects are aligned in this task demonstrating that the FDI and APB muscle are activated similarly during rest. (b) Low force condition. As in the resting condition, the first PCs for each object are aligned, but with a slightly lower slope than in (a). (c) High force condition. During high compression with the dowel, the activation of the APB muscle is minimal and is dominated by FDI activity. Compression at the high force of the spring object shows a slop approximately equal to one, suggesting that there is an equal contribution from both muscles in order to maintain a constant force on the spring.

6.3.3 FDI-EEG Coherence

Figure 6.10a shows a head map of the grand average of the spatial Z-transformed cortico-muscular coherence between the FDI and all EEG channels during the DL condition. The map shows only those electrodes which exceeded a 99% Bonferroni corrected threshold based on the number of EEG electrodes. Four significant electrodes over the primary motor cortex (C3, C1, CP3, and CP1) remained after thresholding. Figure 6.10b shows the average Z-transformed coherence of the four electrodes in Fig. 6.10a. The peak coherence of the average appeared in the beta range (grey area of Fig. 6.10b) at 18.15 Hz with a value of 6.7. Figure 6.10 shows the coherence spectra for the electrodes that were above significance for each of the four conditions. The same general trend was present in these four electrodes for all conditions. The highest beta coherence exists for the SL condition, while the DL and DH conditions have comparable coherence spectra, and the SH consistently has the lowest beta CMC.
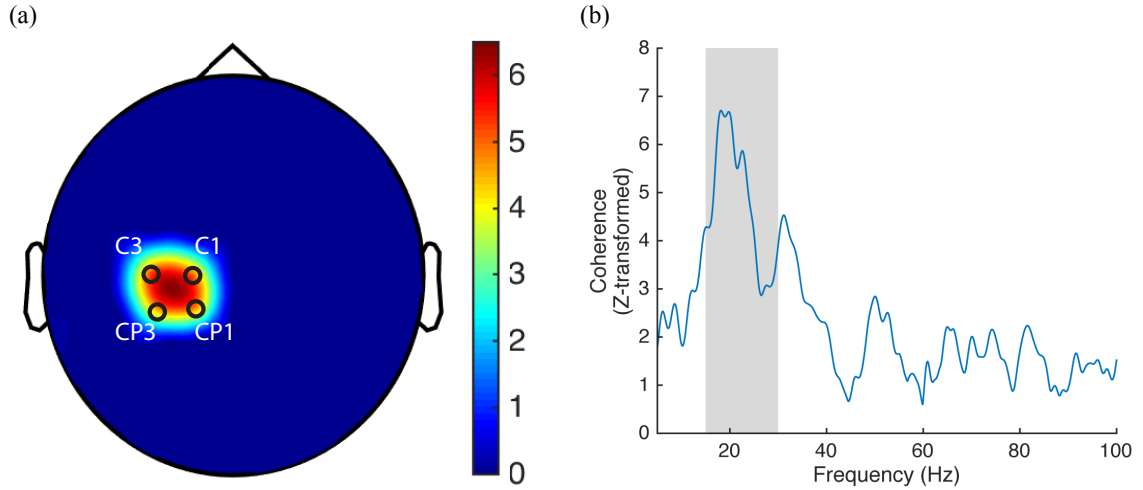
Figure 6.9: Results for the dowel-low task. (a) Grand average Z-transformed coherence head map for the FDI muscle to all EEG electrodes for the DL task. A 99% Bonferonni corrected Z-score threshold was applied to the head map to account for multiple comparisons based on the number of EEG channels. The four electrodes with significant coherence above the threshold were C1, C3, CP1, and CP3 with respective Z-transformed coherence values of 4.81, 5.26, 4.66, and 4.54. (b) Average coherence spectra for the four electrodes shown in (a). The beta frequency range (15 - 30 Hz) is shown as the grey shaded area. Peak coherence for the average was 6.7 at a frequency of 18.15 Hz.
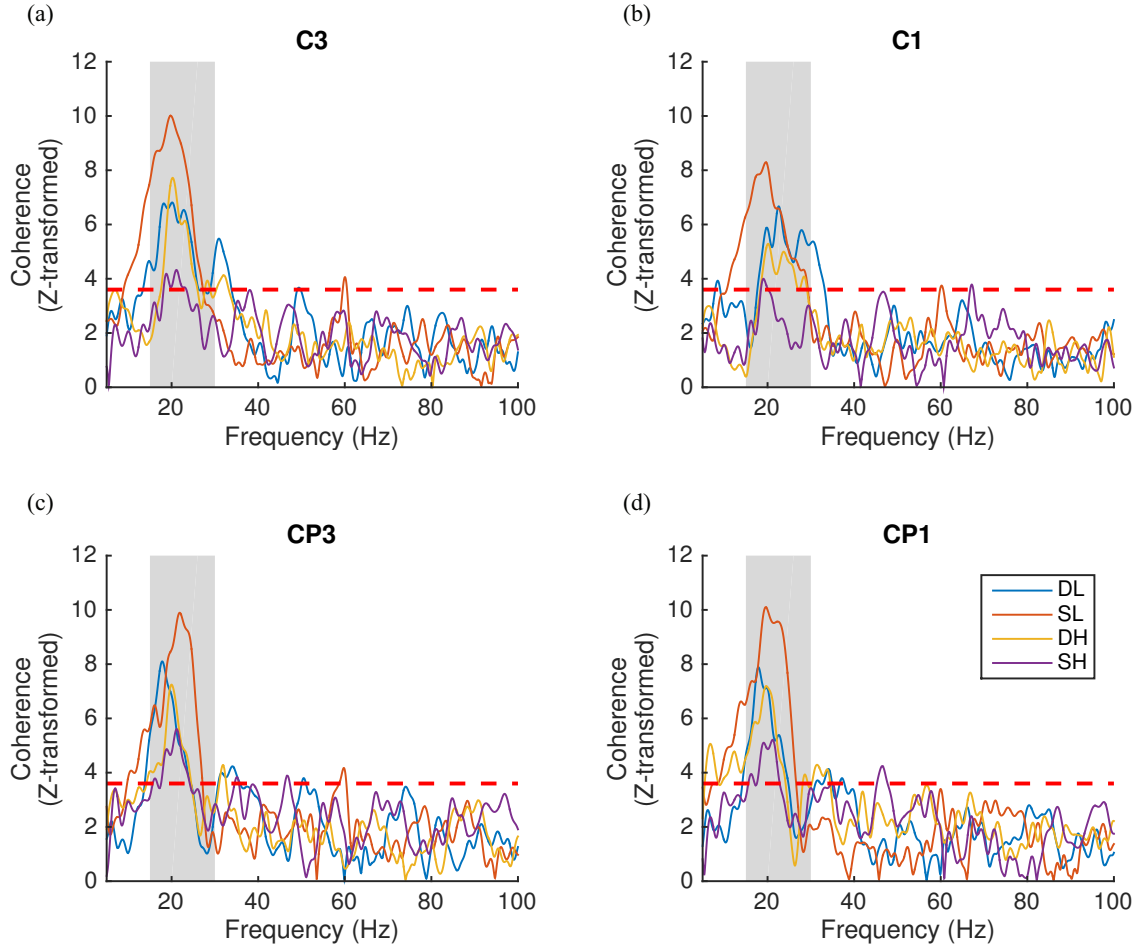
Figure 6.10: Coherence spectra for the four EEG electrodes with average beta range coherence values over the threshold limit. In each plot, all four conditions. The respective condition and trace color are as follows: DL - blue, SH - red, DH - yellow, and SH - purple. Red dashed line in each figure corresponds to the 99% Bonferroni corrected threshold value and the grey shaded areas indicate the beta frequency range (15 - 30 Hz). Individual coherence spectra for each condition for electrode (a) C3, (b) C1, (c) CP3, and (d) CP1.

6.3.4 LME Model

Figure 6.11 shows the effects of each condition on FDI-EEG (Fig. 6.11a) and APB-EEG (Fig. 6.11b) beta range coherence. Using an F-test, we compared the coefficients for the effects of the SL and DL conditions on beta CMC and found that there was no statistical difference in the effects of the low conditions in either FDI-EEG ($p = 0.24502$) or APB-EEG ($p = 0.2357$) coherence. A comparison between the coefficients for the DH and SH tasks, however, showed a clear significance in effect of beta CMC in FDI-EEG ($p = 6.859 \cdot 10^{-8}$) and APB-EMG ($p = 1.6889 \cdot 10^{-5}$).
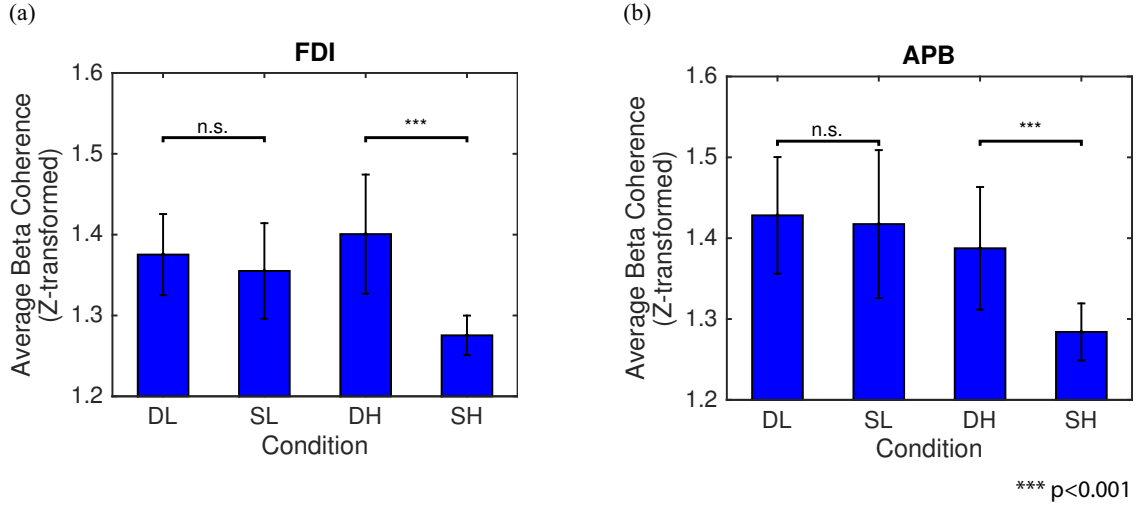
Figure 6.11: Results of the linear mixed-effects model. The model was constructed to predict mean beta range coherence using *Condition* as the fixed-effect and *Participant* as the random effect. In each bar graph, the mean beta range CMC is shown on the vertical axis and condition is on the horizontal axis. Standard error bars are included for each condition and the indicators above the bars represent the statistical difference in the linear mixed effects coefficients as determined using an F-test. n.s. indicates that there was no significant difference in effect between two conditions and $***$ indicates that the p-value was less than 0.001. Linear mixed-effect models for the prediction of (a) FDI-EEG beta coherence and (b) APB-EEG beta coherence.

6.3.5   Power

We investigated the individual EMG beta power for the intrinsic hand muscles and the EEG electrodes of interest. Figure 6.12 shows the average beta power in the the FDI and APB muscles. There is a large increase in beta FDI (Fig. 6.12a) and APB (Fig. 6.12b) power during the SH task compared to all other tasks. There is a highly significant

difference in the effect of the SH vs. the DH task on EMG power (p<0.001) in both intrinsic hand muscles. The firing rates of the motor unit action potentials as well as their shape during compression of the spring at the high force levels could influence spectral content in the beta frequency range leading to the significant increase in the beta range power for the FDI and APB.
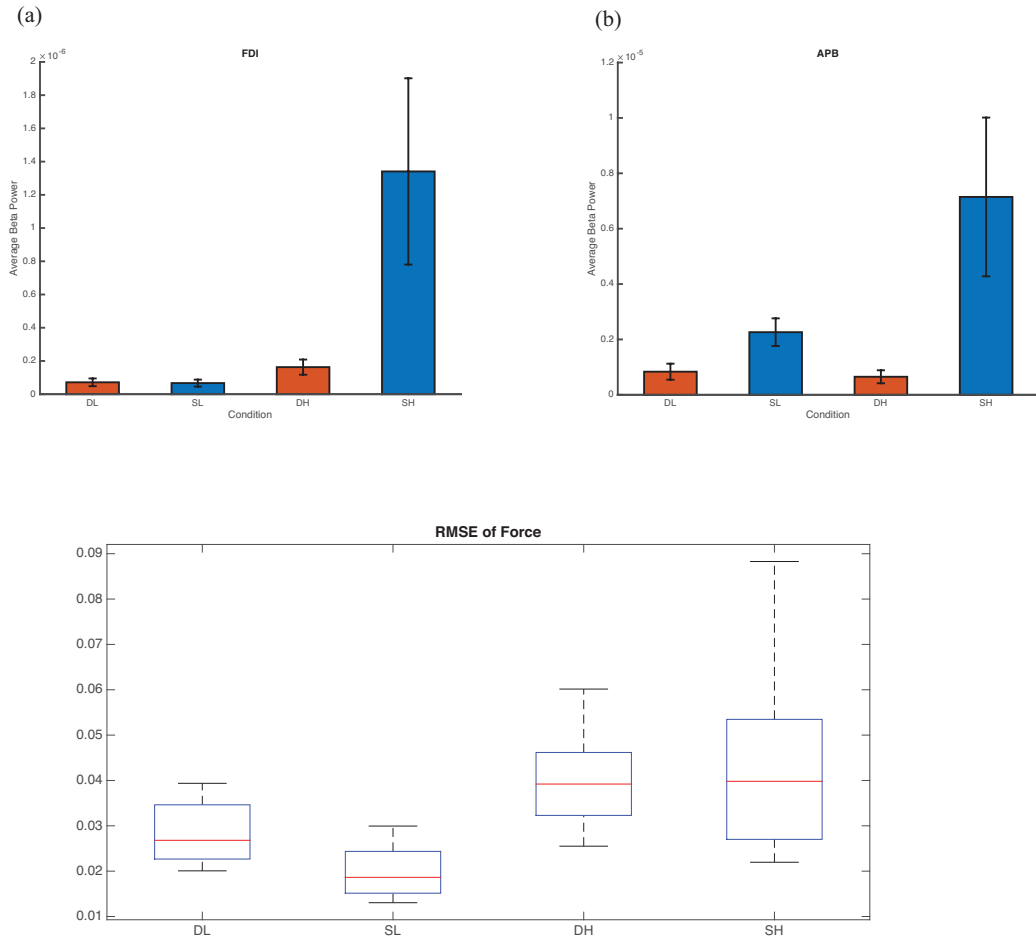
Figure 6.12: Average beta power for the FDI and APB muscles for the DL, SL, DH and SH conditions. (a) FDI power for all four conditions. The largest beta power for the FDI was apparent during the SH task. The power during the SH was significantly higher than for all other conditions. (b)

Additionally, we explored beta power for each condition in the four scalp electrodes. Figure 6.13 show a representative example for electrode C3 since all other electrodes had a similar trend. The statistics for this electrode showed that there was no significant difference between the DH and SH conditions for C3 beta power, and in fact there there were no differences in effect for any condition.
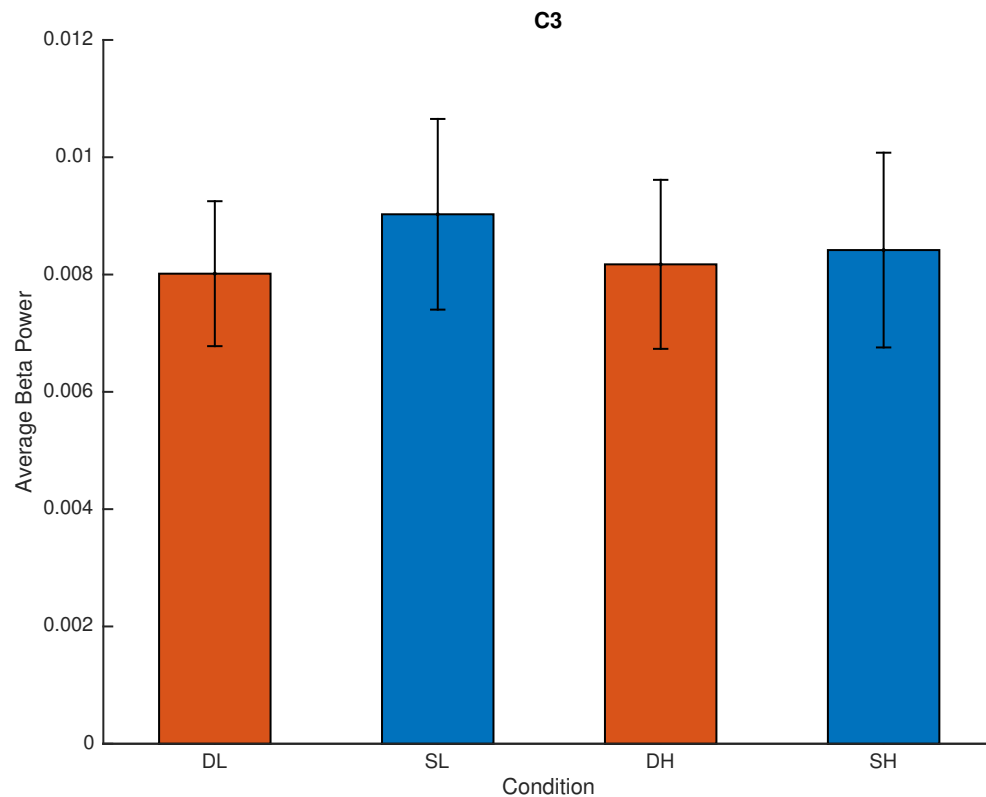
Figure 6.13: Average beta power for the EEG electrode C3 for the DL, SL, DH and SH conditions.

Based on literature findings, power does not necessarily have an effect on coherence. This has been demonstrated in studies which have used drugs to modify cortical power and

coherence. In one study diazepam was used to increase beta power in the motor cortex, however there was no change in beta corticomuscular coherence (Baker & Baker 2003). The second study, which used carbamazepine (CBZ) on epilepsy patients, showed that after taking CBZ there was an increase in coherence, however no significant change in EEG power (Riddle et al. 2004). This demonstrates a disconnect between spectral power and coherence.

6.3.6 Root Mean Square Error of Force

Lastly, we investigated the performance of the force variability in the tasks for all four conditions. Figure 6.14 shows the root mean square error (RMSE) of compression force to target force for all four conditions. As would be expected, force variability increased during higher force production. Furthermore, since there was no difference in force variability during high force compression for either object, hence this rules out force variability as the leading cause of the change in corticomuscular and inter muscular coherence.
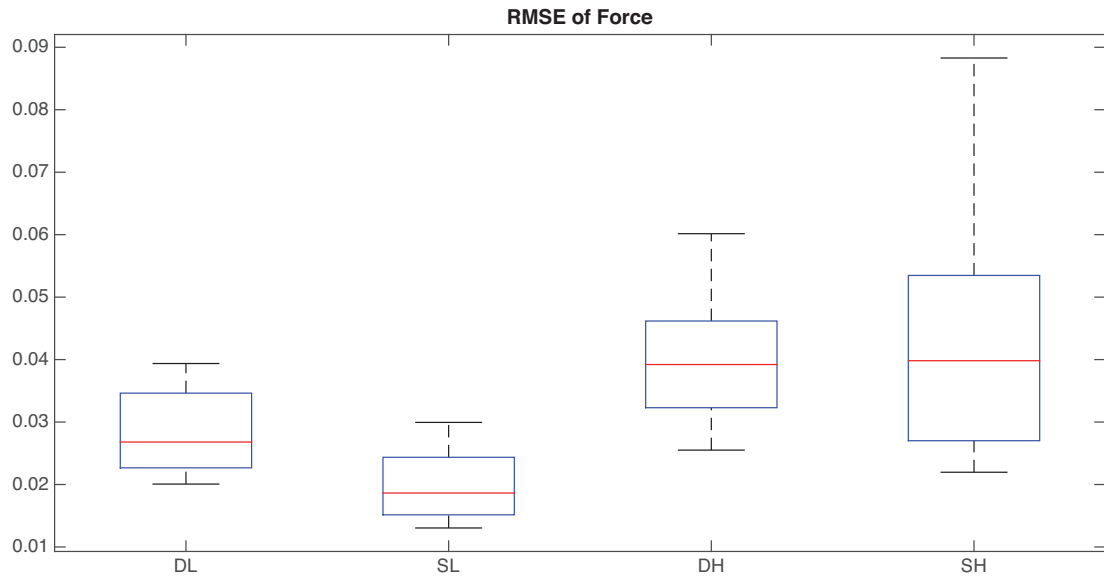
Figure 6.14: Root mean square error of compression force to target force.

6.4 Discussion

The role of the sensorimotor cortex during dexterous manipulation in humans is a topic of intense interest. In this study, we present for the first time, a measure of corticomuscular coherence during unstable and unpredictable dynamic manipulation. To our knowledge, the functional significance of cortico-muscular coupling under these conditions has never been unexplored. fMRI studies under these dexterously demanding conditions have shown a continuous and context-sensitive involvement of the brain, depending on the functional parameters of the task (Mosier et al. 2011). We have extended this approach to include cortical coupling to hand muscles and emphasize tasks where the level of instability can be regulated. Our results indicate that in the DL and DH conditions, significant corticomuscular coherence appeared in M1, however, their magnitudes were not significantly

different. The highest magnitude of beta CMC was recorded over M1 during the SL condition with coherence extension into the supplementary motor area (SMA). Prior studies have shown that object compliance affects coherence magnitude (Kilner et al. 2000, Riddle & Baker 2006). During fine manipulation, SMA coherence was also shown to be increased in the beta frequency range (Chen et al. 2013). However, no study has investigated CMC under unstable conditions.

Investigators have reported that the index finger and thumb are independently controlled (Schieber & Santello 2004). Based on this idea, the model in Fig. 6.15 demonstrates the possible underlying principles that may enable stable versus dexterous manipulation. When performing a task that requires minimal sensorimotor integration, such as the DL, DH and SL tasks, we speculate that the cortical representations of the FDI and APB operate in synchrony to perform a stabilizing task involving a predominantly co-contraction strategy of the muscles. This idea is depicted in Fig. 6.15a. The underlying neural oscillators controlling the FDI and APB are coupled during stable manipulation. In addition, there would be strong coupling in the FDI-APB coherence, representative of a common neural drive to both muscles. However, in the unstable SH condition, the index finger and thumb must operate more independently thereby disrupting the coupling between the FDI and APB cortical representations. Since the common drive between the FDI and APB would no longer exist, the coherence between FDI and APB would decrease.

(a) Stable Domain (b) Unstable Domain
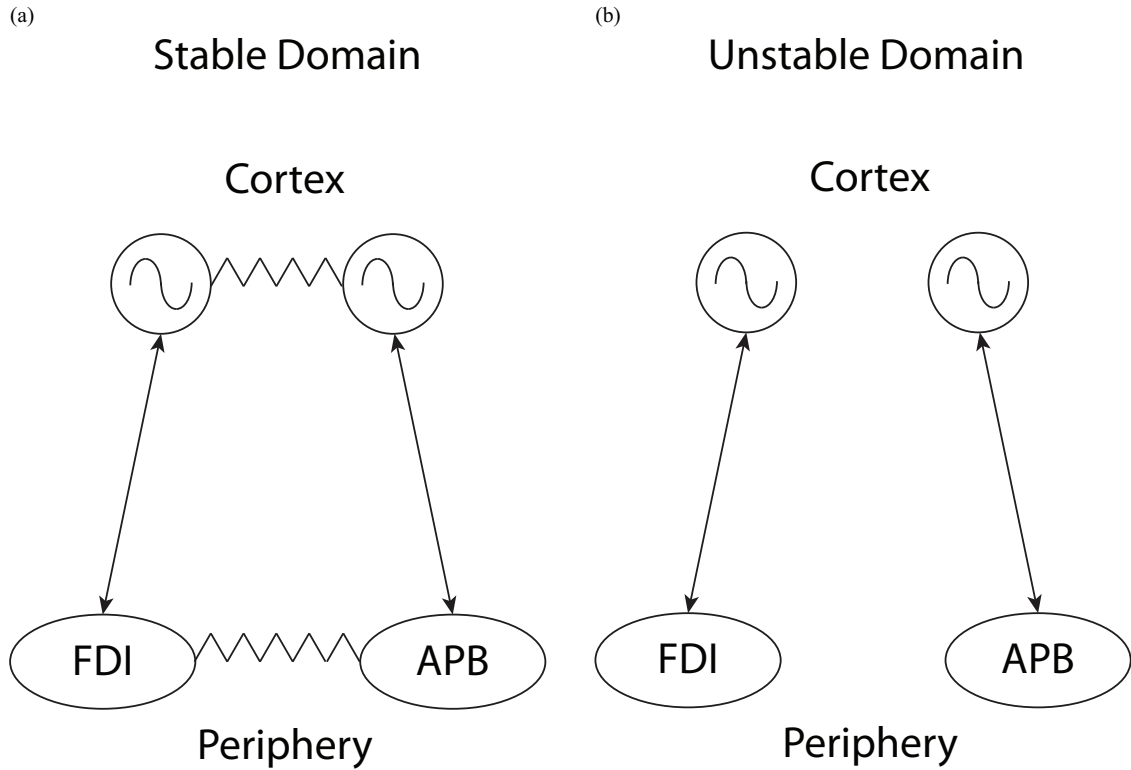
Figure 6.15: Model of cortical drive to hand muscles during stable and unstable tasks. In the stable domain, ares of the cortex representing the FDI and APB are driven by underlying neural oscillators.

Figure 6.16 shows the FDI-APB coherence across the low and high force production conditions. These muscles were chosen due to their critical involvement in the maintenance of the static force production. As expected, the peak Z-transformed coherence in all four conditions appeared in the beta range with the largest value existing in the SL condition at a frequency of 23.3 Hz and a coherence value of 10.5. Coherence spectra during compression tasks with the dowel were similar with the higher force level being slightly greater than that of the low force compression with the dowel. In the SH condition, the beta coherence was much lower than any of the other conditions and had a

peak value of 2.3 at 24.4 Hz. These EMG-EMG coherence spectra supports the idea that the cortical drive to the FDI and APB are more independently controlled in the presence of instability. To investigate the disruption in neural oscillatory coupling between the FDI and APB areas of the cortex, higher density cortical electrodes would be required. Nonetheless, the decrease in FDI-EEG, APB-EEG and FDI-APB coherence during the SH task help to support our model
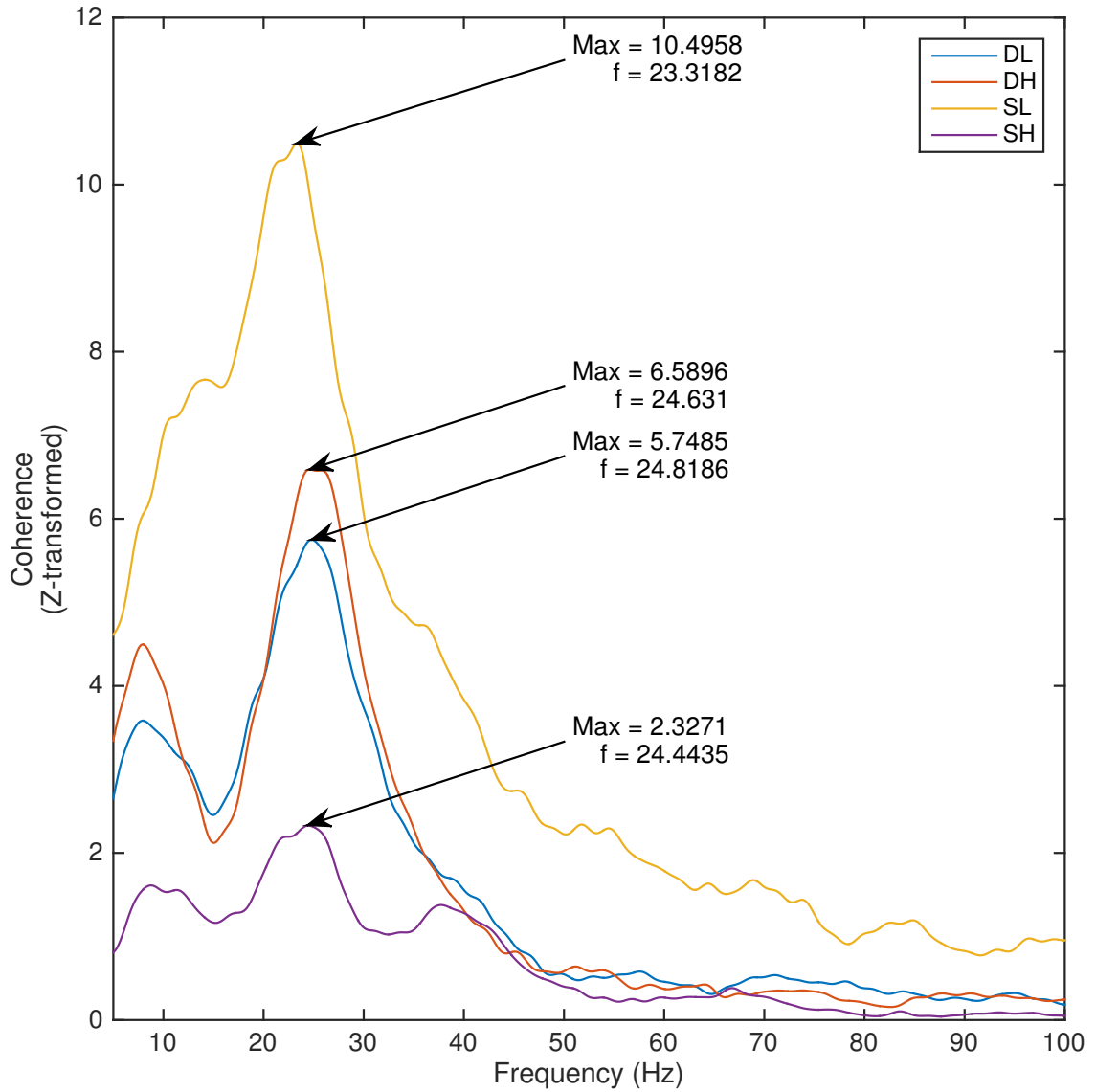
Figure 6.16: EMG to EMG coherence between the *first dorsal interosseous* and the *abductor pollicis brevis*. The SL condition is shown as the yellow trace with a peak coherence of 10.5 at 23.3 Hz. The DL (blue trace) and DH (red trace) have similar peak coherence values within the beta range at 5.7 and 6.6 at 24.8 and 24.6 Hz, respectively. The SH condition (purple trace) has the lowest overall beta range coherence with a max value of 2.3 at 24.4 Hz

We performed an additional analysis to investigate the changes in gamma frequency CMC in the task. Figure 6.17 shows non-thresholded head maps of the grand averages of the spatial Z-transformed corticomuscular coherence between the FDI and all EEG channels during the DL (Fig. 6.17a) and SL (Fig. 6.17b) conditions. For both low force tasks, a significant peak in beta coherence appears over the left primary motor cortex. The measured peak coherence values were 6.42 and 8.23 for the DL and SL condition, respectively. In the SL condition (Fig. 6.17b), coherence extends medially into electrodes Cz and FCz, over the supplementary motor area.
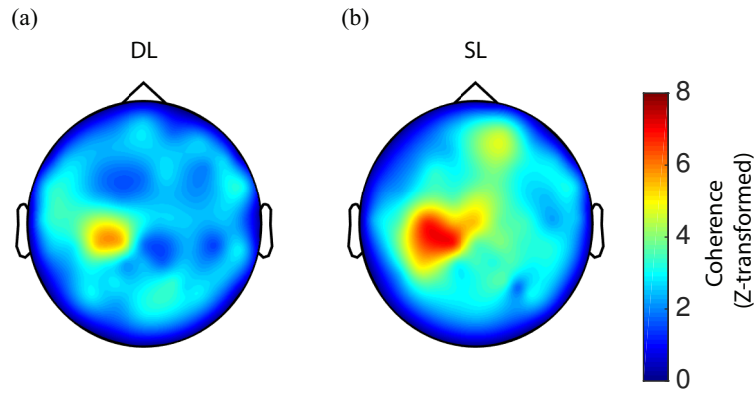
Figure 6.17: Grand average FDI-EEG beta coherence head maps during the low force conditions. (a) DL condition. Peak CMC appears over contralateral M1. (b) SL condition. Peak coherence exists over contralateral M1 with greater magnitude than in the DL condition. Coherence extends medially into the supplementary motor area (i.e. electrodes Cz and FCz).

Based on the spatial shift into the SMA in the SL task, we extended our investigation to include changes in gamma range CMC over electrode C3 (sensorimotor) and Cz (SMA). Figure 6.18 shows the change in average gamma coherence between objects at matched

force levels was calculated for each subject. A Wilcoxson rank sum test was used to show that the average gamma coherence significantly increased only in the SMA electrode (Cz) during the SH task as compared to the DH task ($p = 0.007$).

Given the unavoidable delays in the nervous system, it is poorly understood whether and how the cerebral cortex can contribute to the time-critical control of fingertip forces during dexterous dynamic manipulation. Corticomuscular coherence gives insight into how the brain communicates with the body. Given that our interaction with objects involves a multitude of complex force productions which dynamically change with task demands, it is necessary to not limit our analysis to the beta range coherence which is associated with static force. Furthermore, since strategic planning is involved, the investigation of CMC in cortical regions other than the M1 and S1 are imperative. In this study, we did not have any premonitions about what frequency range to investigate nor the cortical areas to include since this task varied drastically from previous literature. The goal of the tasks in this study was to maintain a constant level of force. From the perspective of the force recordings, there did not exist a noticeable difference in the force production during the SH and DH tasks. However, the nervous system was faced with the added challenge of interacting with an unstable object. As a result, we determined that the cortex communicates with the musculature in a far different manner when the need to exert a constant force on an unstable spring is required. This suggests that the neural strategies involved are not classified into a uni-dimensional goal directed objective, such as constant force production. Instead the cortex chooses to engage higher frequency ranges involving context-sensitive cortical circuits which are dependent on the temporal, dynamic and dexterity demands of the task. Lastly, it is likely that the cortex requires the

126
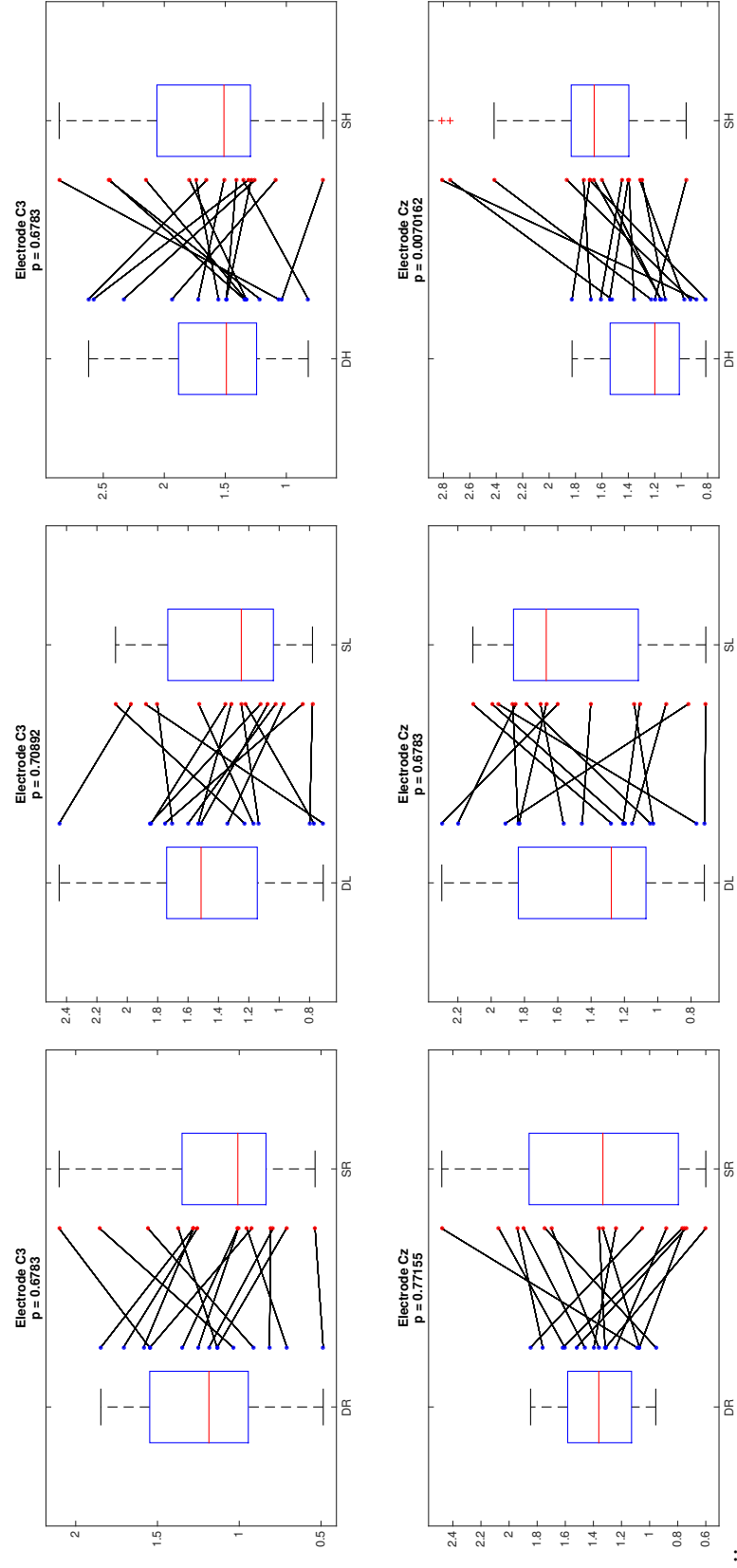
Figure 6.18: Change in gamma coherence across subjects and the rest, low and high conditions in electrodes C3 (over sensorimotor) and Cz (over SMA). Using a Wilcoxon rank sum test, it was determined that there was no statistical difference in the change in gamma coherence in any of the C3 electrodes for matched force conditions. However in the SMA, there existed a significant increase in the average gamma coherence for the spring-high task as compared to the dowel-high task.

use of higher frequency communication to account for the instabilities and uncertainties seen in everyday object manipulation.

Acknowledgements

Chapter 7

Conclusions and Future Work

The human hand is an amazingly complex and fascinating apparatus. There apparently seems to be no limit to its capabilities. Our hands have enabled humans to build skyscrapers that pierce the clouds, paint breathtaking sceneries, compose soothing music; it is strong and robust enough to grip a sledgehammer with immense strength to drive a spike into the ground, yet is nimble enough to thread a needle. However, the neural mechanisms that give us the ability to precisely control finger movements and forces is by no means a trivial one.

In this dissertation, one piece of the puzzle in the neural control of movement was presented. By investigating the temporal relationship two electrophysiological measurements, EEG and EMG, it is possible to gain insight into how cortical activity is transformed into motor precision fingertip control. Oscillations are an abundant phenomenon in the universe and are present in the nervous system as well. Therefore, the role of these oscillations under real-world conditions of dexterous manipulation are essential to our understanding our own bodies.

Continued research in this area and similar fields will undoubtedly lead to the advancement of brain-computer interfaces and robotic hands. It is my hope that, as technological advances are made, and it becomes possible to probe and track neural activity from cortex to muscles to endpoint force along each step of the way, we will come closer to the development of a truly dexterous prosthetic hand that is indistinguishable from the biological hand.

Bibliography

Alexander, R. M. (1997), 'A minimum energy cost hypothesis for human arm trajectories', *Biological cybernetics* **76**(2), 97–105.

Amjad, A., Halliday, D., Rosenberg, J. & Conway, B. (1997), 'An extended difference of coherence test for comparing and combining several independent coherence estimates: theory and application to the study of motor units and physiological tremor', *Journal of neuroscience methods* **73**(1), 69–79.

Andreasson, J., Ekstrom, M., Fard, A., Castao, J. & Johnson, T. (2002), 'Remote system for patient monitoring using bluetooth', **1**, 304–307.

Ashe, J. (1997), 'Force and the motor cortex', *Behavioural Brain Research* **87**(2), 255–269.

Baker, M. R. & Baker, S. N. (2003), 'The effect of diazepam on motor cortical oscillations and corticomuscular coherence studied in man', *The Journal of physiology* **546**(3), 931–942.

Baker, S. N. (2007), 'Oscillatory interactions between sensorimotor cortex and the periphery', *Current opinion in neurobiology* **17**(6), 649–655.

Baker, S. N., Chiu, M. & Fetz, E. E. (2006), 'Afferent encoding of central oscillations in the monkey arm', *Journal of Neurophysiology* **95**(6), 3904–3910.

Baker, S. N., Pinches, E. M. & Lemon, R. N. (2003), 'Synchronization in monkey motor cortex during a precision grip task. ii. effect of oscillatory activity on corticospinal output', *Journal of Neurophysiology* **89**(4), 1941–1953.

Baker, S., Olivier, E. & Lemon, R. (1997), 'Coherent oscillations in monkey motor cortex and hand muscle emg show taskdependent modulation', *The Journal of Physiology* **501**(1), 225–241.

Bear, M., Connors, B. W., Paradiso, M., Bear, M., Connors, B. & Neuroscience, M. (1996), 'Exploring the brain', *Neuroscience: Williams and Wilkins* .

Bennett, K. & Lemon, R. (1996), 'Corticomotoneuronal contribution to the fractionation of muscle activity during precision grip in the monkey', *Journal of Neurophysiology* **75**(5), 1826–1842.

Berger, H. (1929), 'ber das elektrenkephalogramm des menschen', *European Archives of Psychiatry and Clinical Neuroscience* **87**(1), 527–570.

Bernhard, C., Bohm, E. & Petersen, I. (1953), 'Investigations on the organization of the corticospinal system in monkeys', *Acta Physiologica Scandinavica* **29**(S106), 79–105.

Bernstein, N. A. (1967), 'The co-ordination and regulation of movements'.

Bertrand, O., Perrin, F. & Pernier, J. (1985), 'A theoretical justification of the average reference in topographic evoked potential studies', *Electroencephalography and Clinical Neurophysiology/Evoked Potentials Section* **62**(6), 462–464.

Blok, J. H., Stegeman, D. F. & van Oosterom, A. (2002), 'Three-layer volume conductor model and software package for applications in surface electromyography', *Annals of Biomedical Engineering* **30**(4), 566–577.

Boiten, F., Sergeant, J. & Geuze, R. (1992), 'Event-related desynchronization: the effects of energetic and computational demands', *Electroencephalography and clinical neurophysiology* **82**(4), 302–309.

Brown, P. (2000), 'Cortical drives to human muscle: the piper and related rhythms', *Progress in neurobiology* **60**(1), 97–108.

Brown, P., Salenius, S., Rothwell, J. C. & Hari, R. (1998), 'Cortical correlate of the piper rhythm in humans', *J Neurophysiol* **80**(6), 2911–2917.

Burgar, C. G., Valero-Cuevas, F. J. & Hentz, V. R. (1997), 'Fine-wire electromyographic recording during force generation: Application to index finger kinesiologic studies1', *American journal of physical medicine and rehabilitation* **76**(6), 494–501.

Chakarov, V., Naranjo, J. R., Schulte-Mnting, J., Omlor, W., Huethe, F. & Kristeva, R. (2009), 'Beta-range eeg-emg coherence with isometric compensation for increasing modulated low-level forces', *Journal of neurophysiology* **102**(2), 1115–1120.

Chatrian, G. E., Petersen, M. C. & Lazarte, J. A. (1959), 'The blocking of the rolandic wicket rhythm and some central changes related to movement', *Electroencephalography and clinical neurophysiology* **11**(3), 497–510.

Chen, S., Entakli, J., Bonnard, M., Berton, E. & De Graaf, J. B. (2013), 'Functional corticospinal projections from human supplementary motor area revealed by corticomuscular coherence during precise grip force control', *Plos One* **8**(3).

Cianchetti, F. A. & Valero-Cuevas, F. J. (2010), 'Anticipatory control of motion-to-force transitions with the fingertips adapts optimally to task difficulty', *J Neurophysiol* **103**(1), 108–16. Cianchetti, Flor A Valero-Cuevas, Francisco J AR-050520/AR/NIAMS NIH HHS/ AR-052345/AR/NIAMS NIH HHS/ J Neurophysiol. 2010 Jan;103(1):108-16. Epub 2009 Nov 4.

Conway, B., Halliday, D., Farmer, S., Shahani, U., Maas, P., Weir, A. & Rosenberg, J. (1995), 'Synchronization between motor cortex and spinal motoneuronal pool during the performance of a maintained motor task in man', *The Journal of physiology* **489**(Pt 3), 917–924.

Cosmanescu, A., Miller, B., Magno, T., Ahmed, A. & Kremenic, I. (2006), 'Design and implementation of a wireless (bluetooth) four channel bio-instrumentation amplifier and digital data acquisition device with user-selectable gain, frequency, and driven reference', pp. 2053–2056.

Crone, N. E., Miglioretti, D. L., Gordon, B., Sieracki, J. M., Wilson, M. T., Uematsu, S. & Lesser, R. P. (1998), 'Functional mapping of human sensorimotor cortex with electrocorticographic spectral analysis. i. alpha and beta event-related desynchronization', *Brain* **121**(12), 2271–2299.

Da Silva, F. L. & Pfurtscheller, G. (1999), 'Basic concepts on eeg synchronization and desynchronization'.

Davare, M., Lemon, R. & Olivier, E. (2008), 'Selective modulation of interactions between ventral premotor cortex and primary motor cortex during precision grasping in humans', *The Journal of physiology* **586**(11), 2735–2742.

Day, S. J. (1997), *The properties of electromyogram and force in experimental and computer simulations of isometric muscle contraction: data from an acute cat preparation*, University of Calgary.

Dayanidhi, S., Hedberg, ., Valero-Cuevas, F. J. & Forssberg, H. (2013), 'Developmental improvements in dynamic control of fingertip forces last throughout childhood and into adolescence', *Journal of neurophysiology* **110**(7), 1583–1592.

Deiber, M.-P., Honda, M., Ibaez, V., Sadato, N. & Hallett, M. (1999), 'Mesial motor areas in self-initiated versus externally triggered movements examined with fmri: effect of movement type and rate', *Journal of neurophysiology* **81**(6), 3065–3077.

Delorme, A. & Makeig, S. (2004), 'Eeglab: an open source toolbox for analysis of single-trial eeg dynamics including independent component analysis', *Journal of neuroscience methods* **134**(1), 9–21.

Desmurget, M. & Grafton, S. (2000), 'Forward modeling allows feedback control for fast reaching movements', *Trends in cognitive sciences* **4**(11), 423–431.

Donoghue, J. P., Sanes, J. N., Hatsopoulos, N. G. & Gal, G. (1998), 'Neural discharge and local field potential oscillations in primate motor cortex during voluntary movements', *Journal of Neurophysiology* **79**, 159–173.

Dujardin, K., Derambure, P., Defebvre, L., Bourriez, J., Jacquesson, J. & Guieu, J. (1993), 'Evaluation of event-related desynchronization (erd) during a recognition task: effect of attention', *Electroencephalography and clinical neurophysiology* **86**(5), 353–356.

Dum, R. P. & Strick, P. L. (1991), 'The origin of corticospinal projections from the premotor areas in the frontal lobe', *J Neurosci* **11**(3), 667–689.

Dum, R. P. & Strick, P. L. (2005), 'Frontal lobe inputs to the digit representations of the motor areas on the lateral surface of the hemisphere', *The Journal of neuroscience* **25**(6), 1375–1386.

Duncan, P. W., Propst, M. & Nelson, S. G. (1983), 'Reliability of the fugl-meyer assessment of sensorimotor recovery following cerebrovascular accident', *Physical therapy* **63**(10), 1606–1610.

Ehrsson, H. H., Fagergren, A., Jonsson, T., Westling, G., Johansson, R. S. & Forssberg, H. (2000), 'Cortical activity in precision-versus power-grip tasks: an fmri study', *Journal of neurophysiology* **83**(1), 528–536.

Faisal, A., Stout, D., Apel, J. & Bradley, B. (2010), 'The manipulative complexity of lower paleolithic stone toolmaking', *PloS one* **5**(11), e13718.

Farina, D., Arendt-Nielsen, L., Merletti, R. & Graven-Nielsen, T. (2002), 'Assessment of single motor unit conduction velocity during sustained contractions of the tibialis anterior muscle with advanced spike triggered averaging', *J Neurosci Methods* **115**(1), 1–12.

Farina, D., Mesin, L., Martina, S. & Merletti, R. (2004), 'A surface emg generation model with multilayer cylindrical description of the volume conductor', *Biomedical Engineering, IEEE Transactions on* **51**(3), 415–426.

Farina, Dario; Merletti, R. (2001), 'A novel approach for precise simulation of emg signal detected by surface electrodes'.

Farmer, S., Bremner, F., Halliday, D., Rosenberg, J. & Stephens, J. (1993), 'The frequency content of common synaptic inputs to motoneurones studied during voluntary isometric contraction in man', *The Journal of physiology* **470**(1), 127–155.

Feige, B., Aertsen, A. & Kristeva-Feige, R. (2000), 'Dynamic synchronization between multiple cortical motor areas and muscle activity in phasic voluntary movements', *Journal of Neurophysiology* **84**(5), 2622–2629.

Fetz, E. E. & Cheney, P. D. (1980), 'Postspike facilitation of forelimb muscle activity by primate corticomotoneuronal cells', *J Neurophysiol* **44**(4), 751–772.

Fisher, R. J., Galea, M. P., Brown, P. & Lemon, R. N. (2002), 'Digital nerve anaesthesia decreases emg-emg coherence in a human precision grip task', *Exp Brain Res* **145**(2), 207–14.

Flash, T. & Hogan, N. (1985), 'The coordination of arm movements: an experimentally confirmed mathematical model', *The journal of Neuroscience* **5**(7), 1688–1703.

Fuglevand, A. J., Winter, D. A., Patla, A. E. & Stashuk, D. (1992), 'Detection of motor unit action potentials with surface electrodes: influence of electrode size and spacing', *Biological Cybernetics* **67**(2), 143–153.

Galla, C., de Graaf, J. B., Bonnard, M. & Pailhous, J. (2005), 'High level of dexterity: differential contributions of frontal and parietal areas', *Neuroreport* **16**(12), 1271–1274.

Gootzen, T., Stegeman, D. & Van Oosterom, A. (1991), 'Finite limb dimensions and finite muscle length in a model for the generation of electromyographic signals', *Electroencephalography and Clinical Neurophysiology/Evoked Potentials Section* **81**(2), 152–162.

Gross, J., Pollok, B., Dirks, M., Timmermann, L., Butz, M. & Schnitzler, A. (2005), 'Task-dependent oscillations during unimanual and bimanual movements in the human primary motor cortex and sma studied with magnetoencephalography', *Neuroimage* **26**(1), 91–98.
URL: *http://www.sciencedirect.com/science/article/pii/S1053811905000480*

Grosse, P. & Brown, P. (2003), 'Acoustic startle evokes bilaterally synchronous oscillatory emg activity in the healthy human', *Journal of neurophysiology* **90**(3), 1654–1661.

Haller, S., Chapuis, D., Gassert, R., Burdet, E. & Klarhfer, M. (2009), 'Supplementary motor area and anterior intraparietal area integrate finegraded timing and force control during precision grip', *European Journal of Neuroscience* **30**(12), 2401–2406.

Halliday, D. M., Conway, B. A., Farmer, S. F. & Rosenberg, J. R. (1998), 'Using electroencephalography to study functional coupling between cortical activity and electromyograms during voluntary contractions in humans', *Neuroscience letters* **241**(1), 5–8.

Halliday, D. & Rosenberg, J. (2000), 'On the application, estimation and interpretation of coherence and pooled coherence', *Journal of neuroscience methods* **100**(1), 173–174.

Halliday, D., Rosenberg, J., Amjad, A., Breeze, P., Conway, B. & Farmer, S. (1995), 'A framework for the analysis of mixed time series/point process datatheory and application to the study of physiological tremor, single motor unit discharges and electromyograms', *Progress in biophysics and molecular biology* **64**(2), 237–278.

Hari, R. & Salenius, S. (1999), 'Rhythmical corticomotor communication', *Neuroreport* **10**(2), R1–10.

He, S.-Q., Dum, R. P. & Strick, P. (1995), 'Topographic organization of corticospinal projections from the frontal lobe: motor areas on the medial surface of the hemisphere', *Journal of Neuroscience* **15**(5), 3284–3306.

Hjorth, B. (1975), 'An on-line transformation of eeg scalp potentials into orthogonal source derivations', *Electroencephalography and clinical neurophysiology* **39**(5), 526–530.

Hjorth, B. (1980), 'Source derivation simplifies topographical eeg interpretation', *American Journal of EEG Technology* **20**(3), 121–132.

Holmstrom, L., de Manzano, O., Vollmer, B., Forsman, L., Valero-Cuevas, F. J., Ullen, F. & Forssberg, H. (2011), 'Dissociation of brain areas associated with force production and stabilization during manipulation of unstable objects', *Exp Brain Res* **215**(3-4), 359–67.

Huesler, E. J., Maier, M. A. & Hepp-Reymond, M.-C. (2000), 'Emg activation patterns during force production in precision grip. iii. synchronisation of single motor units', *Experimental brain research* **134**(4), 441–455.

Humphrey, D. R., Schmidt, E. & Thompson, W. (1970), 'Predicting measures of motor performance from multiple cortical spike trains', *Science* **170**(3959), 758–762.

Hutcheon, B. & Yarom, Y. (2000), 'Resonance, oscillation and the intrinsic frequency preferences of neurons', *Trends in neurosciences* **23**(5), 216–222.

James, L. M., Halliday, D. M., Stephens, J. A. & Farmer, S. F. (2008), 'On the development of human corticospinal oscillations: agerelated changes in eegemg coherence and cumulant', *European Journal of Neuroscience* **27**(12), 3369–3379.

Jancke, L., Specht, K., Mirzazade, S., Loose, R., Himmelbach, M., Lutz, K. & Shah, N. J. (1998), 'A parametric analysis of the rate effect in the sensorimotor cortex: a functional magnetic resonance imaging analysis in human subjects', *Neuroscience letters* **252**(1), 37–40.

Jasper, H. & Andrews, H. (1938), 'Brain potentials and voluntary muscle activity in man', *Journal of neurophysiology* .

Jasper, H. & Stefanis, C. (1965), 'Intracellular oscillatory rhythms in pyramidal tract neurones in the cat', *Electroencephalography and clinical neurophysiology* **18**(6), 541–553.

Jebsen, R. H., Taylor, N., Trieschmann, R., Trotter, M. J. & Howard, L. A. (1969), 'An objective and standardized test of hand function', *Archives of physical medicine and rehabilitation* **50**(6), 311.

Johansson, R. S. & Flanagan, J. R. (2009), 'Coding and use of tactile signals from the fingertips in object manipulation tasks', *Nature Reviews Neuroscience* **10**(5), 345–359.

Johansson, R. & Westling, G. (1984), 'Roles of glabrous skin receptors and sensorimotor memory in automatic control of precision grip when lifting rougher or more slippery objects', *Experimental brain research* **56**(3), 550–564.

Jonsson, B., Omfeldt, M. & Rundgren, A. (1967), 'Discomfort from the use of wire electrodes for electromyography', *Electromyography* **8**(1), 5–17.

Kawato, M. (1999), 'Internal models for motor control and trajectory planning', *Current opinion in neurobiology* **9**(6), 718–727.

Kilner, J., Baker, S., Salenius, S., Jousmki, V., Hari, R. & Lemon, R. (1999), 'Task-dependent modulation of 15-30 hz coherence between rectified emgs from human hand and forearm muscles', *The Journal of Physiology* **516**(2), 559–570.

Kilner, J. M., Baker, S. N., Salenius, S., Hari, R. & Lemon, R. N. (2000), 'Human cortical muscle coherence is directly related to specific motor parameters', *The Journal of neuroscience* **20**(23), 8838–8845.

Kilner, J. M., Fisher, R. J. & Lemon, R. N. (2004), 'Coupling of oscillatory activity between muscles is strikingly reduced in a deafferented subject compared with normal controls', *Journal of neurophysiology* **92**(2), 790–796.

Kristeva-Feige, R., Fritsch, C., Timmer, J. & Lcking, C.-H. (2002), 'Effects of attention and precision of exerted force on beta range eeg-emg synchronization during a maintained motor contraction task', *Clinical Neurophysiology* **113**(1), 124–131.

Kristeva, R., Patino, L. & Omlor, W. (2007), 'Beta-range cortical motor spectral power and corticomuscular coherence as a mechanism for effective corticospinal interaction during steady-state motor output', *Neuroimage* **36**(3), 785–792.

KuhtzBuschbeck, J. P., Ehrsson, H. H. & Forssberg, H. (2001), 'Human brain activity in the control of fine static precision grip forces: an fmri study', *European Journal of Neuroscience* **14**(2), 382–390.

Kuypers, H. (1960), 'Central cortical projections to motor and somato-sensory cell groups', *Brain* **83**(1), 161–184.

Laine, C. M., Negro, F. & Farina, D. (2013), 'Neural correlates of task-related changes in physiological tremor', *Journal of neurophysiology* **110**(1), 170–176.

Laine, C. M., Yavuz, . U. & Farina, D. (2014), 'Taskrelated changes in sensorimotor integration influence the common synaptic input to motor neurones', *Acta Physiologica* **211**(1), 229–239.

Lebedev, M. & Wise, S. (2000), 'Oscillations in the premotor cortex: single-unit activity from awake, behaving monkeys', *Experimental brain research* **130**(2), 195–215.

Lemon, R., Baker, S., Davis, J., Kirkwood, P., Maier, M. & Yang, H. (1998), The importance of the cortico-motoneuronal system for control of grasp, *in* 'Novartis Found Symp', Vol. 218, pp. 202–215.

Lemon, R. & Mantel, G. (1989), 'The influence of changes in discharge frequency of corticospinal neurones on hand muscles in the monkey', *The Journal of physiology* **413**(1), 351–378.

Lemon, R. N. (2008), 'Descending pathways in motor control', *Annu. Rev. Neurosci.* **31**, 195–218.

Lemon, R. N., Johansson, R. & Westling, G. (1995), 'Corticospinal control during reach, grasp, and precision lift in man', *the Journal of Neuroscience* **15**(9), 6145–6156.

Leocani, L., Toro, C., Manganotti, P., Zhuang, P. & Hallett, M. (1997), 'Event-related coherence and event-related desynchronization/synchronization in the 10 hz and 20 hz eeg during self-paced movements', *Electroencephalography and Clinical Neurophysiology/Evoked Potentials Section* **104**(3), 199–206.

Llins, R. R. (1988), 'The intrinsic electrophysiological properties of mammalian neurons: insights into central nervous system function', *Science* **242**(4886), 1654–1664.

Loeb, G., Brown, I. & Cheng, E. (1999), 'A hierarchical foundation for models of sensorimotor control', *Experimental brain research* **126**(1), 1–18.

Lowery, M. M., Stoykov, N. S., Dewald, J. & Kuiken, T. (2004), 'Volume conduction in an anatomically based surface emg model', *Biomedical Engineering, IEEE Transactions on* **51**(12), 2138–2147.

Lowery, M. M., Stoykov, N. S., Taflove, A. & Kuiken, T. A. (2002), 'A multiple-layer finite-element model of the surface emg signal', *IEEE Transactions on Biomedical Engineering* **49**(5).

MacKay, W. A. (2005), 'Wheels of motion: oscillatory potentials in the motor cortex', *Motor Cortex in Voluntary Movements: A Distributed System for Distributed Functions* pp. 181–211.

Maier, M. A. & Hepp-Reymond, M.-C. (1995), 'Emg activation patterns during force production in precision grip', *Experimental Brain Research* **103**(1), 108–122.

Maier, M. & Hepp-Reymond, M. (1994), 'Emg activation patterns during force production in precision grip. ii. muscular synergies in the spatial and temporal domain', *Experimental brain research* **103**(1), 123–136.

Maris, E., Schoffelen, J.-M. & Fries, P. (2007), 'Nonparametric statistical testing of coherence differences', *Journal of neuroscience methods* **163**(1), 161–175.

Marsden, J., Werhahn, K., Ashby, P., Rothwell, J., Noachtar, S. & Brown, P. (2000), 'Organization of cortical activities related to movement in humans', *The Journal of Neuroscience* **20**(6), 2307–2314.

Martin, J. H. (2003), *Neuroanatomy: text and atlas 3rd Ed.*, McGraw Hill.

Mathiowetz, V., Volland, G., Kashman, N. & Weber, K. (1985), 'Adult norms for the box and block test of manual dexterity', *American Journal of Occupational Therapy* **39**(6), 386–391.

Mathiowetz, V., Weber, K., Kashman, N. & Volland, G. (1985), 'Adult norms for the nine hole peg test of finger dexterity', *OTJR: Occupation, Participation and Health* **5**(1), 24–38.

McClelland, V. M., Cvetkovic, Z. & Mills, K. R. (2012), 'Rectification of the emg is an unnecessary and inappropriate step in the calculation of corticomuscular coherence', *Journal of neuroscience methods* **205**(1), 190–201.

McDonnell, M. N., Ridding, M. C., Flavel, S. C. & Miles, T. S. (2005), 'Effect of human grip strategy on force control in precision tasks', *Experimental brain research* **161**(3), 368–373.

McFarland, D. J., McCane, L. M., David, S. V. & Wolpaw, J. R. (1997), 'Spatial filter selection for eeg-based communication', *Electroencephalography and Clinical Neurophysiology* **103**(3), 386–394.

Mendez-Balbuena, I., Huethe, F., Schulte-Mnting, J., Leonhart, R., Manjarrez, E. & Kristeva, R. (2011), 'Corticomuscular coherence reflects interindividual differences in the state of the corticomuscular network during low-level static and dynamic forces', *Cerebral Cortex* p. bhr147.

Mima, T. & Hallett, M. (1999), 'Corticomuscular coherence: a review', *Journal of Clinical Neurophysiology* **16**(6), 501.

Mima, T., Simpkins, N., Oluwatimilehin, T. & Hallett, M. (1999), 'Force level modulates human cortical oscillatory activities', *Neuroscience letters* **275**(2), 77–80.

Mosier, K., Lau, C., Wang, Y., Venkadesan, M. & Valero-Cuevas, F. J. (2011), 'Controlling instabilities in manipulation requires specific cortical-striatal-cerebellar networks', *J Neurophysiol* **105**(3), 1295–305.

Muir, R. & Lemon, R. (1983), 'Corticospinal neurons with a special role in precision grip', *Brain research* **261**(2), 312–316.

Murthy, V. N. & Fetz, E. E. (1992), 'Coherent 25-to 35-hz oscillations in the sensorimotor cortex of awake behaving monkeys', *Proceedings of the National Academy of Sciences* **89**(12), 5670–5674.

Murthy, V. N. & Fetz, E. E. (1996*a*), 'Oscillatory activity in sensorimotor cortex of awake monkeys: synchronization of local field potentials and relation to behavior', *Journal of Neurophysiology* **76**(6), 3949–3967.

Murthy, V. N. & Fetz, E. E. (1996*b*), 'Synchronization of neurons during local field potential oscillations in sensorimotor cortex of awake monkeys', *Journal of Neurophysiology* **76**(6), 3968–3982.

Myers, L., Lowery, M., O'malley, M., Vaughan, C., Heneghan, C., Gibson, A. S. C., Harley, Y. & Sreenivasan, R. (2003), 'Rectification and non-linear pre-processing of emg signals for cortico-muscular analysis', *Journal of neuroscience methods* **124**(2), 157–165.
URL: *http://www.sciencedirect.com/science/article/pii/S0165027003000049*

Nashmi, R., Mendona, A. J. & MacKay, W. A. (1994), 'Eeg rhythms of the sensorimotor region during hand movements', *Electroencephalography and clinical neurophysiology* **91**(6), 456–467.

Nunez, P. L., Srinivasan, R., Westdorp, A. F., Wijesinghe, R. S., Tucker, D. M., Silberstein, R. B. & Cadusch, P. J. (1997), 'Eeg coherency: I: statistics, reference electrode, volume conduction, laplacians, cortical imaging, and interpretation at multiple scales', *Electroencephalography and clinical neurophysiology* **103**(5), 499–515.

Nunez, P., Silberstein, R., Cadusch, P., Wijesinghe, R., Westdorp, A. & Srinivasan, R. (1994), 'A theoretical and experimental study of high resolution eeg based on surface laplacians and cortical imaging', *Electroencephalography and clinical neurophysiology* **90**(1), 40–57.

Oaube, J. R. (1991), 'Aaem minimonograph 11: needle examination in clinical electromyography', *Muscle and nerve* **14**(8), 685–700.

Ohara, S., Mima, T., Baba, K., Ikeda, A., Kunieda, T., Matsumoto, R., Yamamoto, J., Matsuhashi, M., Nagamine, T. & Hirasawa, K. (2001), 'Increased synchronization of cortical oscillatory activities between human supplementary motor and primary sensorimotor areas during voluntary movements', *The Journal of Neuroscience* **21**(23), 9377–9386.

Omlor, W., Patino, L., Hepp-Reymond, M.-C. & Kristeva, R. (2007), 'Gamma-range corticomuscular coherence during dynamic force output', *Neuroimage* **34**(3), 1191–1198.

Omlor, W., Patino, L., Mendez-Balbuena, I., Schulte-Mnting, J. & Kristeva, R. (2011), 'Corticospinal beta-range coherence is highly dependent on the pre-stationary motor state', *The Journal of Neuroscience* **31**(22), 8037–8045.

Oostenveld, R., Fries, P., Maris, E. & Schoffelen, J.-M. (2011), 'Fieldtrip: open source software for advanced analysis of meg, eeg, and invasive electrophysiological data', *Computational intelligence and neuroscience* **2011**, 1.

Patino, L., Omlor, W., Chakarov, V., Hepp-Reymond, M.-C. & Kristeva, R. (2008), 'Absence of gamma-range corticomuscular coherence during dynamic force in a deafferented patient', *Journal of neurophysiology* **99**(4), 1906–1916.

Pauluis, Q., Baker, S. N. & Olivier, E. (1999), 'Emergent oscillations in a realistic network: the role of inhibition and the effect of the spatiotemporal distribution of the input', *Journal of computational neuroscience* **6**(1), 27–48.

Percival, D. & Walden, A. (1993), 'Spectral analysis for physical applications: Multitaper and conventional univariate techniques (cambridge', *Press, New York* .

Pesaran, B. (2008), 'Spectral analysis for neural signals', *Short Course III* p. 1.

Peters, B. O., Pfurtscheller, G. & Flyvbjerg, H. (2001), 'Automatic differentiation of multichannel eeg signals', *Biomedical Engineering, IEEE Transactions on* **48**(1), 111–116.

Pfurtscheller, G. & Lopes da Silva, F. H. (1999), 'Event-related eeg/meg synchronization and desynchronization: basic principles', *Clinical neurophysiology* **110**(11), 1842–1857.

Pfurtscheller, G. & Neuper, C. (1994), 'Event-related synchronization of mu rhythm in the eeg over the cortical hand area in man', *Neuroscience letters* **174**(1), 93–96.

Plonsey, R. (1974), 'The active fiber in a volume conductor', *Biomedical Engineering, IEEE Transactions on* **21**(5), 371–381.

Popivanov, D., Mineva, A. & Krekule, I. (1999), 'Eeg patterns in theta and gamma frequency range and their probable relation to human voluntary movement organization', *Neuroscience letters* **267**(1), 5–8.

Proulx, J., Clifford, R., Sorensen, S., Lee, D. & Archibald, J. (2006), 'Development and evaluation of a bluetooth ekg monitoring sensor', pp. 507–511.

Rajaratnam, B. (2014), 'Ch goh j, kumar vp (2014) a comparison of emg signals from surface and fine-wire electrodes during shoulder abduction', *Int J Phys Med Rehabil* **2**(206), 2.

Rash, G. S. & Quesada, P. (2003), 'Electromyography fundamentals', *Retrieved February 4*.

Reyes, A. & Valero-Cuevas, F. J. (2013), 'Inexpensive, wearable, wireless, multi-channel, and multi-sensor data acquisition system', pp. 216–219.

Riddle, C. N., Baker, M. R. & Baker, S. N. (2004), 'The effect of carbamazepine on human corticomuscular coherence', *Neuroimage* **22**(1), 333–340.

Riddle, C. N. & Baker, S. N. (2005), 'Manipulation of peripheral neural feedback loops alters human corticomuscular coherence', *The Journal of physiology* **566**(2), 625–639.

Riddle, C. N. & Baker, S. N. (2006), 'Digit displacement, not object compliance, underlies task dependent modulations in human corticomuscular coherence', *Neuroimage* **33**(2), 618–627.

Roeleveld, K., Blok, J., Stegeman, D. & Van Oosterom, A. (1997), 'Volume conduction models for surface emg; confrontation with measurements', *Journal of Electromyography and Kinesiology* **7**(4), 221–232.

Roland, P., Larsen, B., Lassen, N. & Skinhoj, E. (1980), 'Supplementary motor area and other cortical areas in organization of voluntary movements in man', *J Neurophysiol* **43**(1), 118–136.

Rosenberg, J., Amjad, A., Breeze, P., Brillinger, D. & Halliday, D. (1989), 'The fourier approach to the identification of functional coupling between neuronal spike trains', *Progress in biophysics and molecular biology* **53**(1), 1–31.

Roth, B. J., Gielen, F. L. & Wikswo, J. P. (1988), 'Spatial and temporal frequency-dependent conductivities in volume-conduction calculations for skeletal muscle', *Mathematical Biosciences* **88**(2), 159–189.

Rougeul-Buser, A. & Buser, P. (1997), 'Rhythms in the alpha band in cats and their behavioural correlates', *International Journal of Psychophysiology* **26**(1-3), 191–203.

Safri, N. M., Murayama, N., Hayashida, Y. & Igasaki, T. (2007), 'Effects of concurrent visual tasks on cortico-muscular synchronization in humans', *Brain research* **1155**, 81–92.

Safri, N. M., Murayama, N., Igasaki, T. & Hayashida, Y. (2006), 'Effects of visual stimulation on cortico-spinal coherence during isometric hand contraction in humans', *International journal of psychophysiology* **61**(2), 288–293.

Salenius, S., Portin, K., Kajola, M., Salmelin, R. & Hari, R. (1997), 'Cortical control of human motoneuron firing during isometric contraction', *Journal of Neurophysiology* **77**(6), 3401–3405.

Sanes, J. N. & Donoghue, J. P. (1993), 'Oscillations in local field potentials of the primate motor cortex during voluntary movement', *Proceedings of the National Academy of Sciences* **90**(10), 4470–4474.

Schieber, M. H. & Santello, M. (2004), 'Hand function: peripheral and central constraints on performance', *Journal of Applied Physiology* **96**(6), 2293–2300.

Schoffelen, J. M., Oostenveld, R. & Fries, P. (2005), 'Neuronal coherence as a mechanism of effective corticospinal interaction', *Science* **308**(5718), 111–113.

Schoffelen, J.-M., Poort, J., Oostenveld, R. & Fries, P. (2011), 'Selective movement preparation is subserved by selective increases in corticomuscular gamma-band coherence', *The Journal of Neuroscience* **31**(18), 6750–6758.

Semciw, A. I., Neate, R. & Pizzari, T. (2014), 'A comparison of surface and fine wire emg recordings of gluteus medius during selected maximum isometric voluntary contractions of the hip', *Journal of Electromyography and Kinesiology* **24**(6), 835–840.

Shinoda, Y., Yokota, J.-I. & Futami, T. (1981), 'Divergent projection of individual corticospinal axons to motoneurons of multiple muscles in the monkey', *Neuroscience letters* **23**(1), 7–12.

Sirin, A. & Patla, A. (1987), 'Myoelectric changes in the triceps surae muscles under sustained contractions', *European journal of applied physiology and occupational physiology* **56**(2), 238–244.

Slepian, D. & Pollack, H. O. (1961), 'Prolate spheroidal wavefunctions: Fourier analysis and uncertainty i', *Bell System Tech Journal* **40**, 43–63.

Slock, D. T. & Kailath, T. (1991), 'Numerically stable fast transversal filters for recursive least squares adaptive filtering', *Signal Processing, IEEE Transactions on* **39**(1), 92–114.

Smith, A. M. (1981), 'The coactivation of antagonist muscles', *Canadian journal of physiology and pharmacology* **59**(7), 733–747.

Stanck Jr, A. & Pfurtscheller, G. (1996), 'Event-related desynchronisation of central beta-rhythms during brisk and slow self-paced finger movements of dominant and nondominant hand', *Cognitive Brain Research* **4**(3), 171–183.

Stefan, H., Quesney, L., AbouKhalil, B. & Olivier, A. (1991), 'Electrocorticography in temporal lobe epilepsy surgery', *Acta neurologica scandinavica* **83**(2), 65–72.

Steriade, M. (1997), 'Synchronized activities of coupled oscillators in the cerebral cortex and thalamus at different levels of vigilance', *Cerebral Cortex* **7**(6), 583–604.
URL: *http://cercor.oxfordjournals.org/content/7/6/583.full.pdf*

Talati, A., Valero-Cuevas, F. J. & Hirsch, J. (2005), 'Visual and tactile guidance of dexterous manipulation tasks: An fmri study 1, 2', *Perceptual and motor skills* **101**(1), 317–334.

Tecchio, F., Porcaro, C., Zappasodi, F., Pesenti, A., Ercolani, M. & Rossini, P. M. (2006), 'Cortical short-term fatigue effects assessed via rhythmic brainmuscle coherence', *Experimental brain research* **174**(1), 144–151.

Thickbroom, G., Phillips, B., Morris, I., Byrnes, M. & Mastaglia, F. (1998), 'Isometric force-related activity in sensorimotor cortex measured with functional mri', *Experimental brain research* **121**(1), 59–64.

Thomson, D. J. (1982), 'Spectrum estimation and harmonic analysis', *Proceedings of the IEEE* **70**(9), 1055–1096.

Toma, K., Mima, T., Matsuoka, T., Gerloff, C., Ohnishi, T., Koshy, B., Andres, F. & Hallett, M. (2002), 'Movement rate effect on activation and functional coupling of motor cortical areas', *Journal of neurophysiology* **88**(6), 3377–3385.

Turak, B., Louvel, J., Buser, P. & Lamarche, M. (2001), 'Parieto-temporal rhythms in the 69 hz band recorded in epileptic patients with depth electrodes in a self-paced movement protocol', *Clinical neurophysiology* **112**(11), 2069–2074.

Uno, Y., Kawato, M. & Suzuki, R. (1989), 'Formation and control of optimal trajectory in human multijoint arm movement', *Biological cybernetics* **61**(2), 89–101.

Valero-Cuevas, F. J., Smaby, N., Venkadesan, M., Peterson, M. & Wright, T. (2003), 'The strength-dexterity test as a measure of dynamic pinch performance', *Journal of biomechanics* **36**(2), 265–270.

Weinand, M., Wyler, A., Richey, E., Phillips, B. & Somes, G. (1992), 'Long-term ictal monitoring with subdural strip electrodes: prognostic factors for selecting temporal lobectomy candidates', *Journal of neurosurgery* **77**(1), 20–28.

Westling, G. & Johansson, R. (1984), 'Factors influencing the force control during precision grip', *Experimental Brain Research* **53**(2), 277–284.

Westling, G. & Johansson, R. S. (1987), 'Responses in glabrous skin mechanoreceptors during precision grip in humans', *Experimental Brain Research* **66**(1), 128–140.

Winstein, C. J., Grafton, S. T. & Pohl, P. S. (1997), 'Motor task difficulty and brain activity: investigation of goal-directed reciprocal aiming using positron emission tomography', *Journal of Neurophysiology* **77**(3), 1581–1594.

Winter, B. (2013*a*), 'Linear models and linear mixed effects models in r: Tutorial 11', *arXiv preprint arXiv:1308.5499* .

Winter, B. (2013*b*), 'A very basic tutorial for performing linear mixed effects analyses', *arXiv preprint arXiv:1308.5499* .

Witham, C. L., Wang, M. & Baker, S. N. (2010), 'Corticomuscular coherence between motor cortex, somatosensory areas and forearm muscles in the monkey', *Front Syst Neurosci* **4**.

Witte, M., Patino, L., Andrykiewicz, A., HeppReymond, M. & Kristeva, R. (2007), 'Modulation of human corticomuscular betarange coherence with lowlevel static forces', *European Journal of Neuroscience* **26**(12), 3564–3570.

Wyler, A., Ojemann, G., Lettich, E. & Ward Jr, A. (1984), 'Subdural strip electrodes for localizing epileptogenic foci', *Journal of neurosurgery* **60**(6), 1195–1200.

Yao, B., Salenius, S., Yue, G. H., Brown, R. W. & Liu, J. Z. (2007), 'Effects of surface emg rectification on power and coherence analyses: an eeg and meg study', *Journal of neuroscience methods* **159**(2), 215–223.

Zhou, P.-b. (2012), *Numerical analysis of electromagnetic fields*, Springer Science and Business Media.